168
36

To the Graduate Council:

I am submitting herewith a thesis written by Hugh Curtis Monger entitled "Geochemical and Mineralogical Properties of Copper Ridge and Chepultepec Regolith at the Oak Ridge National Laboratory Reservation-West Chestnut Ridge Site." I have examined the final copy of the thesis for form and content and recommend that it be accepted in partial fulfillment of the requirements for the degree of Master of Science, with a major in Geology.

Richard W. Arnseth
Richard W. Arnseth, Major Professor

We have read this thesis
and recommend its acceptance:

Wm W. Byerly

D. A. Liethe

Otto C. Kopp

Accepted for the Council:

Lewis Winkel
Vice Provost
and Dean of the Graduate School

STATEMENT OF PERMISSION TO USE

In presenting this thesis in partial fulfillment of the requirements for a Master's degree at The University of Tennessee, Knoxville, I agree that the Library shall make it available to borrowers under rules of the Library. Brief quotations from this thesis are allowable without special permission, provided that accurate acknowledgment of the source is made.

Permission for extensive quotation from or reproduction of this thesis may be granted by my major professor, or in his absence, by the Head of Interlibrary Services when, in the opinion of either, the proposed use of the material is for scholarly purposes. Any copying or use of the material in this thesis for financial gain shall not be allowed without my written permission.

Signature Hugh Curtis Monger

Date 5/19/86

GEOCHEMICAL AND MINERALOGICAL PROPERTIES OF COPPER RIDGE AND CHEPULTEPEC REGOLITH AT THE OAK RIDGE NATIONAL LABORATORY RESERVATION-WEST CHESTNUT RIDGE SITE

A Thesis

Presented for the

Master of Science

Degree

The University of Tennessee, Knoxville

Hugh Curtis Monger

June 1986

ACKNOWLEDGMENTS

In the course of this project, a number of people have assisted me generously. In particular, I am indebted to Dr. Richard W. Arnseth, Dr. O.C. Kopp, Dr. Don W. Byerly, and Dr. D.A. Lietzke, who served as my director and committee, respectively.

I hereby acknowledge with thanks James Coleman and the Amoco Foundation for their financial assistance.

Other assistance was provided by R.H. Ketelle and S.Y. Lee of the Oak Ridge National Laboratory; Dennis Owen and Eric Johnson of the Department of Geological Sciences, University of Tennessee; Dr. R.J. Lewis of the Plant and Soil Science Department, University of Tennessee; Chemistry Department, University of Tennessee; and the Oak Ridge National Laboratory, operated by Martin Marietta Energy Systems, Inc., which provided the samples.

I would also like to express gratitude to my family, especially my wife Sue Ann.

ABSTRACT

The nature and properties of regolith overlying the Copper Ridge and Chepultepec formations of the Knox Group at the Oak Ridge National Laboratory Reservation-West Chestnut Ridge Site (WCRS) were investigated to determine (a) their natural ability to adsorb dissolved waste, (b) the weathering products of siliceous carbonates, and (c) processes leading to pedogenic horizonation.

With the exception of ion exchange capacity, standard soil methods were used to determine particle size distribution; pH and salt pH; bulk chemical composition (<2mm) using XRF; mineralogical composition using XRD of <2mm size-fraction, <2μm size-fraction, and magnetic nodules; and extractable amorphous oxyhydroxides of Fe, Mn, Si, and Al analyzed by AA and colorimetric techniques.

The results of this study include identification of a maximum clay concentration at approximately 3 meters, a relatively high concentration of sand and silt near the surface, and deeper, variable concentrations of sand, silt, and gravel layers inherited from the parent rock. The pH values ranged from 4.5 to 5.7. Bulk mineralogy (<2mm) was predominately quartz with minor amounts of kaolinite, illite, and aluminum hydroxy-interlayered vermiculite (HIV). Clay fraction mineralogy, in order of abundance, was kaolinite, quartz, illite, and HIV. The magnetic sand-sized nodules were most concentrated in the upper soil horizons and were composed of maghemite, hematite, and quartz. Bulk chemical

composition revealed relatively high concentrations of the soluble cations Mg^{++}, K^{+}, Ca^{++}, and Rb^{+} at the surface; concentrations decreased with depth until below 2 meters where they became highly variable. Iron trends were similar to Ti trends; Al trends were inversely related to Si trends; and Al closely correlated to clay content. Cation exchange capacities ranged from 30 to 200 mmol $(\frac{1}{2}\ Ba^{2+})\cdot kg^{-1}$ or 3 to 20 meq/100g; anion exchange capacities were very low, below the detection sensitivity of the XRF method. Amorphous oxyhydroxides were most concentrated near the surface with highly variable concentrations below 2 meters.

The adsorption capacity of the regolith, dependent upon amorphous oxyhydroxides and clay content, is likely to change once it has been subjected to chemical waste due to the chemical vulnerability of oxyhydroxides of Fe, Mn, Si, and Al. Anionic species are not significantly adsorbed by the regolith at WCRS. Detrital illite is converted into HIV by weathering which results in the stripping-out of the K^{+} ion, exemplified by high concentrations of HIV in the upper soil horizons which decrease with depth while correspondingly low concentrations of illite in the upper soil horizons increase with depth. Soluble cations of Mg^{++}, K^{+}, Ca^{++}, and Rb^{+} are concentrated near the surface due to biocycling by plants and recent agricultural practices.

TABLE OF CONTENTS

TABLE OF CONTENTS (continued)

LIST OF TABLES

LIST OF FIGURES

LIST OF FIGURES (Continued)

LIST OF FIGURES (Continued)

CHAPTER I

INTRODUCTION

Purpose of the Study

The purpose of this study is to characterize the upper 7.6 meters (25 ft.) of regolith overlying the Copper Ridge and Chepultepec members of the Knox Group at the West Chestnut Ridge Site (WCRS). Analyses were performed at various depths on seven cores. Investigations of the regolith focus on (a) their natural ability to absorb dissolved waste, (b) the weathering products of siliceous carbonates, and (c) processes leading to pedogenic horizonation. The term regolith is used throughout to encompass both soils and the less-weathered residua and is defined as the unconsolidated material lying on top of bedrock which includes soil, alluvium, and rock fragments weathered from the bedrock.

Regolith properties which relate to waste disposal were analyzed in case surficial regolith should be used in the construction of a shallow burial facility. Properties pertinent to use of the site for shallow burial are ion exchange capacities, mineralogical composition, distribution of amorphous phases of Fe, Mn, Si, and Al oxyhydroxides, pH and salt pH, and particle size distribution. Also included is a brief discussion on the nature and importance of macropores.

The weathering products of siliceous carbonates are documented by mineralogical composition as a function of depth, the bulk chemical composition, particle size distribution, and the

distribution of amorphous phases of Fe, Mn, Si, and Al oxyhydroxides. Also, physical descriptions of color, soil texture, soil structure, soil consistency, root abundance, and clay coatings were made for regolith samples and are presented in Appendix E.

Two aspects of pedogenic horizonation were examined: formation of the clay-enriched argillic horizon and distribution of soluble cations due to biocycling.

Related Research

Research in the three areas of interest of this study (i.e., waste disposal, weathering products of siliceous carbonates, and pedogenic horizonation) has been conducted by several investigators on regolith at the WCRS or similar regolith. Lee, Kopp, and Lietzke (1984) characterized the morphological, physicochemical, and mineralogical properties of selected samples of the soils and residua. Samples from four soil profiles and six residuum cores were analyzed and it was found that the gravel and sand fragments comprised various types of chert, iron/manganese oxide nodules, and quartz; the silt fraction mainly quartz; and the clay fraction varying amounts of kaolinite, mica, vermiculite, HIV, amorphous iron/aluminum oxides, gibbsite, and quartz.

Ketelle and Huff (1984) found that the residual soils at WCRS are predominately clays of low to high plasticity with very strong moisture-retention characteristics; even in late summer and autumn the saturation indices are generally greater than 90%

below depths of 3 meters. They also characterized the soils as being extensively leached, slightly acid, and very weakly buffered.

Seeley and Kelmers (1984) measured sorption ratios (Rs) of the regolith at WCRS. Sorption ratio, given by the equation:

$$Rs = [solid]/[solution],$$

is the ratio of the concentration of an index species which has been adsorbed by a solid divided by the concentration of the index species in the test solution after contact. Sorption ratios are similar to the distribution coefficient (Kd), but differ in that Kd is obtained under thermodynamic equilibrium conditions which are seldom met in most natural applications; therefore, Rs is used to express measurements of the distribution of radionuclides between groundwater and a solid adsorbent; Rs does not imply thermodynamic ideal behavior (Seeley and Kelmers, 1984, pp. 20-21). The numerator of Rs, expressed in moles per gram, is proportional to ion exchange capacity, expressed as millimoles per kilogram. Seeley and Kelmers (p. 11) found a range for Rs of 61,000 L/kg for the cation europium (Eu^{3+}) to 1.6 L/kg for the anionic technetium oxide (TcO_4^-).

Lee et al. (1984) measured cation exchange capacity values ranging from 40 mmol Ca/kg to 85 mmol Ca/kg which convert to 8 meq/100g and 17 meq/100g. Lee et al. measured a pH range of 4.1 to 6.7 and noted that the regolith samples have a low acidity buffering capacity which indicates a fragile chemical and

mineralogical equilibria which can easily be altered if extreme chemical conditions are imposed on the regolith.

Fuller (1978) studied the movement and retention of selected metals and found that in addition to porosity, the attenuation of metals was strongly dependent upon the amounts and types of clay, base saturation, and hydrous iron oxide present. Triegel (1980) discussed the fact that there are relationships between the mobility of selected metals and the amount of aluminum and manganese oxhydroxides, pH, redox conditions, organic matter content, and the types and concentrations of other ions or gases in the soil. Amorphous phases of iron, manganese, silicon, and aluminum which exist as coatings and nodules are recognized as having the ability to adsorb ionic specices. For certain trace elements, such amorphous phases may play a more important role as sinks than aluminosilicate clays (Jenne, 1977). Jenne states that, in general, the amorphous oxides of manganese and iron are more important as sinks than the amorphous oxides of aluminum and silicon because the former have greater sorption capacities, tend to dissolve as the redox potential decreases, and reprecipitate when the system becomes oxygenated; whereas amorphous oxides of aluminum and silicon are not susceptible to redox reactions unless they have co-precipitated with iron. Metals may be adsorbed on the large surface areas of the amorphous oxhydroxides as replacements for manganese, iron, or aluminum (Triegel, 1980).

Macroporosity of regolith is another important factor concerning waste disposal. A macropore, as defined by Beven and

Germann (1982), is a structure that permits nonequilbrium channeling flow, whatever the size. This allows rapid movement of water, solutes, and pollutants through regolith. Macropores at WCRS are mainly of two types: (a) biogenic related macropores such as tree rootcasts and animal burrows which are most prominent in the upper 2 m of the soil and (b) macropores due to soil structure and saprolitic structure, which are most prominent below 2 m. Movement of water in saturated macropores through otherwise unsaturated soil has been observed to take place over considerable distances and at high velocities (Aubertin, 1971; Beasley, 1976; Mosley, 1982). In order for water to move through the macropores it must be supplied to the macropores in excess to lateral absorption to the surrounding soil matrix. These conditions occur during storm rainfall (Beven and Germann, 1981). Flow through the bulk regolith (macropores plus adjacent matrix material) is dominant during non-storm rainfall conditions. Debate continues about whether it is mainly the macropore wall material that adsorbs ionic species or the entire bulk sample. Regardless, when cation and anion exchange capacities for regolith are routinely measured the results are of the highly disturbed, often crushed bulk sample, when in reality leachate may only contact macropore wall material and not the higher surface area of the crushed bulk sample. The difficulty of studying the properties of macropore wall material results from the problems of studying fluid movement through an undisturbed, intact regolith and the

difficulty of collecting the small film of macropore wall material for analysis.

In this thesis, macropores were not a main focus because the samples containing them were too small and too disturbed. However, macropores were observed in the samples as indicated by accumulations of layers of translocated clay (argillans) on macropore walls.

Research related to the weathering of siliceous carbonates has been conducted by Miller (1972). Miller examined the transformation undergone by carbonate rocks during weathering. One of the soils examined by Miller was Fullerton Cherty Silt Loam, which also occurs at WCRS. Miller dissolved the carbonate rock with HCl and analyzed the residue and found illite to be primarily the only phyllosilicate, meaning the other phyllosilicate clay minerals (kaolinite and HIV) are secondary minerals formed or altered in situ by weathering (p. 149). Miller observed a pH range from 5.0 in the B horizon to 8.2 next to the carbonate rock and a CEC range of 7.8 to 25.4 meq/100g (78 to 254 mmole($\frac{1}{2}Ba^{2+}$) $\cdot Kg^{-1}$) (p. 51). Miller measured the amount of free iron oxide and found a range of 2 to 6 wt. % with the largest amounts in the B horizon. Miller observed highest concentrations of HIV in the uppermost soil horizons which decreased with depth with a corresponding increase of illite.

Lee et al. (1984) also observed the highest concentration of HIV in the uppermost soil horizons which decreased with depth as illite concentration increased with depth. Other weathering

related findings by Lee et al. included relatively high concentrations of magnetic nodules in the upper soil horizons which decreased in concentration with depth. The magnetic nodules were composed of maghemite, hematite and quartz. Maghemite and magnetite have similar d-spacings. Lee confirmed the presence of maghemite by mixing maghemite and magnetite and performing XRD on the mixed sample (personal communication via O.C. Kopp). The result was double XRD peaks at 2.95 Å (maghemite) and 2.97 Å (magnetite), 2.51 Å (maghemite) and 2.10 Å (magnetite), 1.60 Å (maghemite) and 1.62 Å (magnetite). During pedogenesis, iron oxyhydroxides were converted to maghemite and hematite through dehydration and slow oxidation (Kopp and Lee, 1985). Kopp and Lee (1985) observed that maghemite was most abundant along grain surfaces and fractures which provided access for fluids and dissolved gases.

Buol et al. (1973) state that illite found in residuum is usually in the initial unweathered material and that moderate to low pH conditions cause instability and disappearance of illite as it is converted to a vermiculite-type mineral. Buol et al. also note that aluminum interlayered vermiculites are synthesized under conditions of moderate to low pH conditions and medium to high Al and Si concentrations. Interlayer spaces serve as sinks for the Al in solution (Jackson, 1963). Kaolinite is synthesized under conditions of approximately equal concentrations of Si and Al, low pH, and essentially an absence of Mg and other bases. The formation of kaolinite is aided by the presence of layer

silicates which serve as "templates" or patterns for the 1:1 sheet structures (Buol et al., 1973, p. 85).

Amorphous phases of Fe, Mn, Si, and Al are the products of weathering and represent the destruction of pre-existing minerals. Jenne (1977) states that amorphous oxyhydroxides exist as coatings and discrete particles. Jenne records a 11.2 wt. % amorphous Fe_2O_3 for one sample taken from limestone soils in the Appalachians. Lee et al. (1984) record an amorphous Fe_2O_3 range of 2.7 to 9.2 wt. % on the <2 μm size fraction. Lee used the citrate-bicarbonate-dithionite extraction method (Mehra and Jackson, 1960) which, according to Ristvet (1978, p. 261), dissolves 100% of amorphous Fe-oxide with one 15-minute treatment.

Amorphous iron oxide is considered to be microcrystalline goethite (Schwertmann, 1959) with variable amounts of water while, amorphous manganese oxyhydroxides are basically manganese dioxides with variable replacements for Mn^{4+}. Amorphous aluminum commonly occurs as hydroxy polymers (Tweneboah, 1967) which probably serve as nuclei for gibbsite precipitation. Silicon occurs in solution as undissociated H_4SiO_4 until it becomes a polymeric colloid at concentrations above its solubility limit (McKenzie and Cline, 1963).

The regolith of the Knox Group has been used to identify the different formations of the Knox Group for mapping purposes. Bridge (1956) describes the difference between the Copper Ridge

and Longview:[1] the Copper Ridge weathers to clays that are orange or red with chert that is dull, opaque, grayish-white and is stained yellow, red and black by iron and manganese oxides, whereas the Longview commonly weathers to a light-gray residual soil with abundant large irregular masses of chert. Milici (1973) states that because chert is more abundant in both the Copper Ridge and Longview than in the Chepultepec, the Chepultepec occupies a valley position between the low ridges underlain by the more siliceous Copper Ridge and Longview.

Swingle (1959) notes that in areas underlain by the Knox Group the residuum ranged in thickness from a few feet to well over 100 feet (30.5 m). Pinnacles of bedrock locally stand above the land surface, yet a few feet away the bedrock may be 100 feet (30.5 m) or more beneath the surface. Swingle noted that the residuum was composed of the insoluble constituents of the parent rock (i.e., chert, illite, kaolinite, and quartz) where massive chert ledges and sandstone beds reflect the attitude of the underlying rocks. The weathering of siliceous carbonates, as described by Swingle, is most effective in the zone of water-table fluctuation, which has been measured to be 50 feet (15.2 m) or more beneath hills and ridges in the Cleveland, Tennessee area. Chemical analyses of ground water indicate that leaching of the

---

[1] The Longview Dolomite was abandoned by Harris (1969, p. 8) in his revision of upper Knox stratigraphy. The boundaries of the Kingsport Formation and the Chepultepec Dolomite were readjusted to include the Longview Dolomite north of Knoxville, Tennessee (Milici, 1973, p. 24).

soluble constituents is currently taking place. Swingle observed alluvium in the Cleveland area on ridges as high as 1,350 feet (411 m) above sea level and stated that it could be distinguished from the residuum by its darker brown to red color (p. 35). Alluvial gravels of quartzite and sandstone, manganese and iron oxides, nodules and lumps of limonite and lithiophorite are present in shallow soils above chert and are probably associated with the Tertiary period.

Research concerning pedogenic horizonation is extensive. The research most closely related to this study is by Simonson (1949) who studied the formation of argillic horizons (clay-rich horizons roughly equivalent to the B horizon) in soils that are now classified as Ultisols. He observed that there was not enough A horizon to account for the massive build-up of clay in the argillic horizon. This fact induced Simonson to discount lessivage (the mechanical migration of small mineral particles from the A to B horizons) and place more emphasis on clay formation in situ in the B horizon. However, much of the overlying A horizon could have been removed in the geologic past (D.A. Lietzke, personal communication). Mass movement of the surface material may have occured during periglacial periods. More recently, large quantities of A horizon have been eroded due to agricultural practices.

Buol et al. (1973) observed that although forested Ultisols have been extensively leached, there is a paradoxically high concentration of base cations in the uppermost soil horizons.

They suggest that biocycling, whereby roots extract the base cations at depth and return them to the soil surface in plant tissues, is the responsible process.

Ultisols, the predominant soil type at WCRS, are low-base status soils with an argillic horizon and a mean annual soil temperature of 15-22°C. Dokuchaev (1883), a Russian geologist, recognized that soil formation is predictable, being dependent on five factors: parent material, climate, native vegetation, time, and topography. Ultisols are related to the five soil-forming factors in the following ways: Miller (1983) explains that Ultisols can form in any parent material that contains enough clay to form an argillic horizon or that contains enough weatherable minerals to form clays upon weathering. Very sandy materials with minute quantities of clays and weatherable minerals are the only common parent materials that fail to meet these requirements.

Ultisols can form in a variety of climates provided: a) evapotranspiration rates exceed precipitation during some season (this is essential for the formation of the argillic horizon), and b) precipitation exceeds the capacity of the soil to retain water during some season and water percolates through the profile (this is essential to maintain low-base status). Long periods of weathering and leaching can result in the formation of minerals such as kaolinite or gibbsite which were absent in the initial parent materials (Miller, 1983, p. 297).

Forest vegetation in both temperate and tropical climates is

characteristic of most natural Ultisol landscapes. Ultisols also occur in savanna landscapes of Africa and South America.
The shortest known time period required for Ultisol formation is 18,000-30,000 years B.P. on fluvial terraces of the Gulf Coastal Area (Gamble et al., 1970). Very old Ultisols have formed on surfaces that might exceed ten million years in parts of Missouri and Arkansas (Bretz, 1965).

Ultisols may occupy hillslopes, stream or marine terraces, or level upland areas. The position they occupy is controlled by relationships between geomorphology and other factors of formation (Miller, 1983).

Additional study of the regolith at the West Chestnut Ridge Site is being conducted by Anne Scales of the Department of Geological Sciences, University of Tennessee. Ms. Scales is documenting the bulk chemical composition of the regolith and the underlying bedrock, the mineralogical composition, the ion exchange capacities, the chert characteristics, and physical appearance of samples taken from cores which extend from the surface to bedrock, a depth up to approximately 30 m (100 ft.).

Field Area and Sampling Procedure

The West Chestnut Ridge Site (WCRS) is located near the southwest end of the Department of Energy's Oak Ridge Reservation, Oak Ridge, Tennessee, and is within the Valley and Ridge Province of the Appalachian Highland Physiographic region of the

Eastern United States (Figure 1). This region is characterized by parallel ridges alternating with valleys.

Stratigraphically, the site is underlain by the Knox Group which is Cambro-Ordovician in age. The Knox Group comprises carbonates with minor clastic interbedded strata, some of which are very cherty, which have been subdivided into (from the oldest to the youngest) the Copper Ridge, Chepultepec, Kingsport and Mascot formations (Harris, 1964). The residua weathered from these formations is commonly very deep, as much as twenty to thirty meters. In addition to residua on the site, ancient alluvium may also be present; supported by such evidence as an abrupt and pronounced absence of chert, deep red B horizons (2.5 YR 3/6), large manganese concretions, and abrupt changes in stratigraphy. Active geomorphic processes include sheet erosion, localized gully erosion, soil creep, subsidence related to carbonate dissolution, and subsurface sediment transport through open solution cavities (Ketelle et al., 1984).

The soils at the WCRS are predominately Ultisols (Typic, Rhodic, and Fragic Paleudults) with minor areas of Entisols and Inceptisols (Figure 2 and Table 1). Appendix A contains an explanation and key to soil mapping unit classification. Appendix B contains the description of soil mapping units from Figure 2.

Samples from the West Chestnut Ridge Site on the Oak Ridge National Laboratory Reservation were taken at various depths from seven cores which were drilled through three soil types: Dewey,

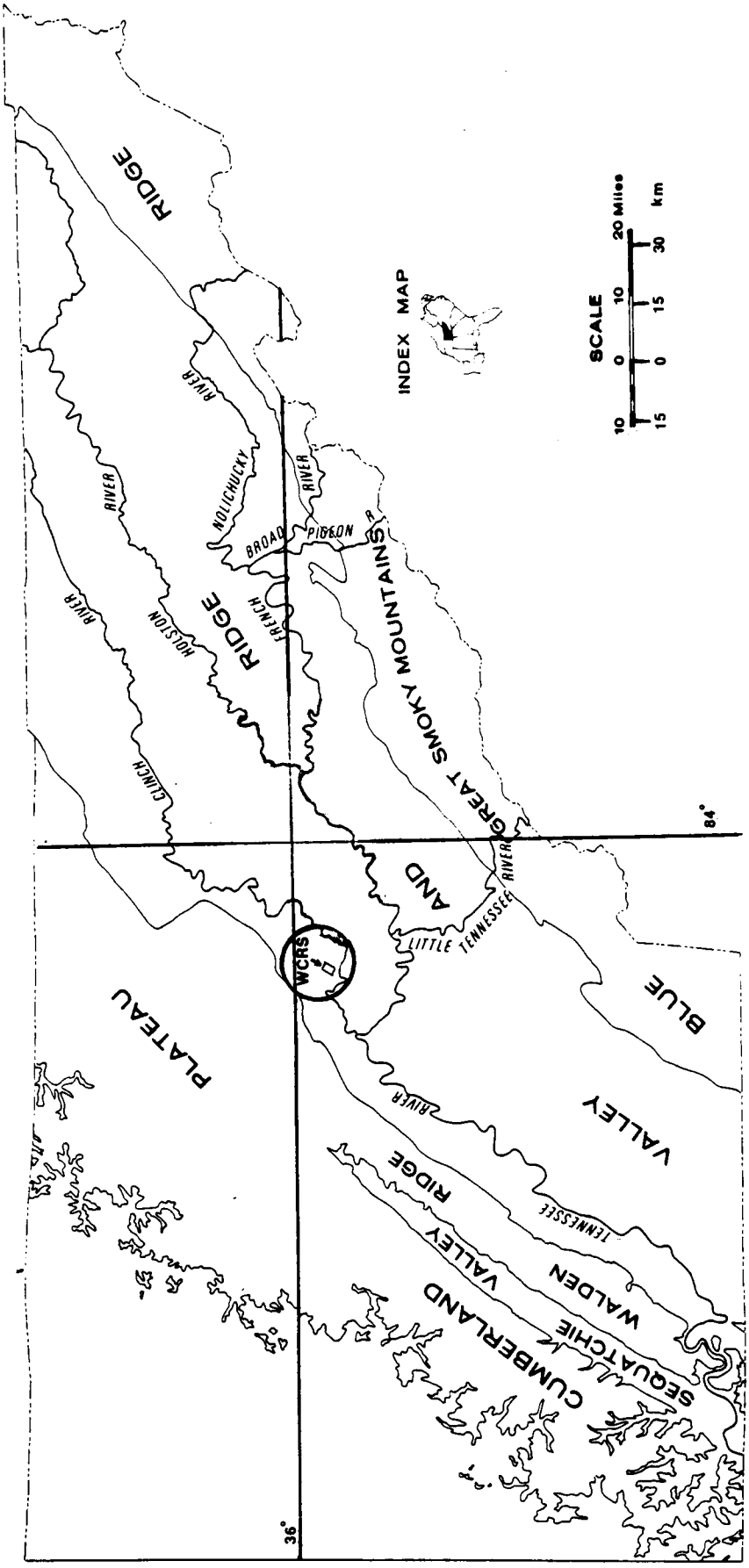

Figure 1. Location of the West Chestnut Ridge Site. (After Clark, 1973.)

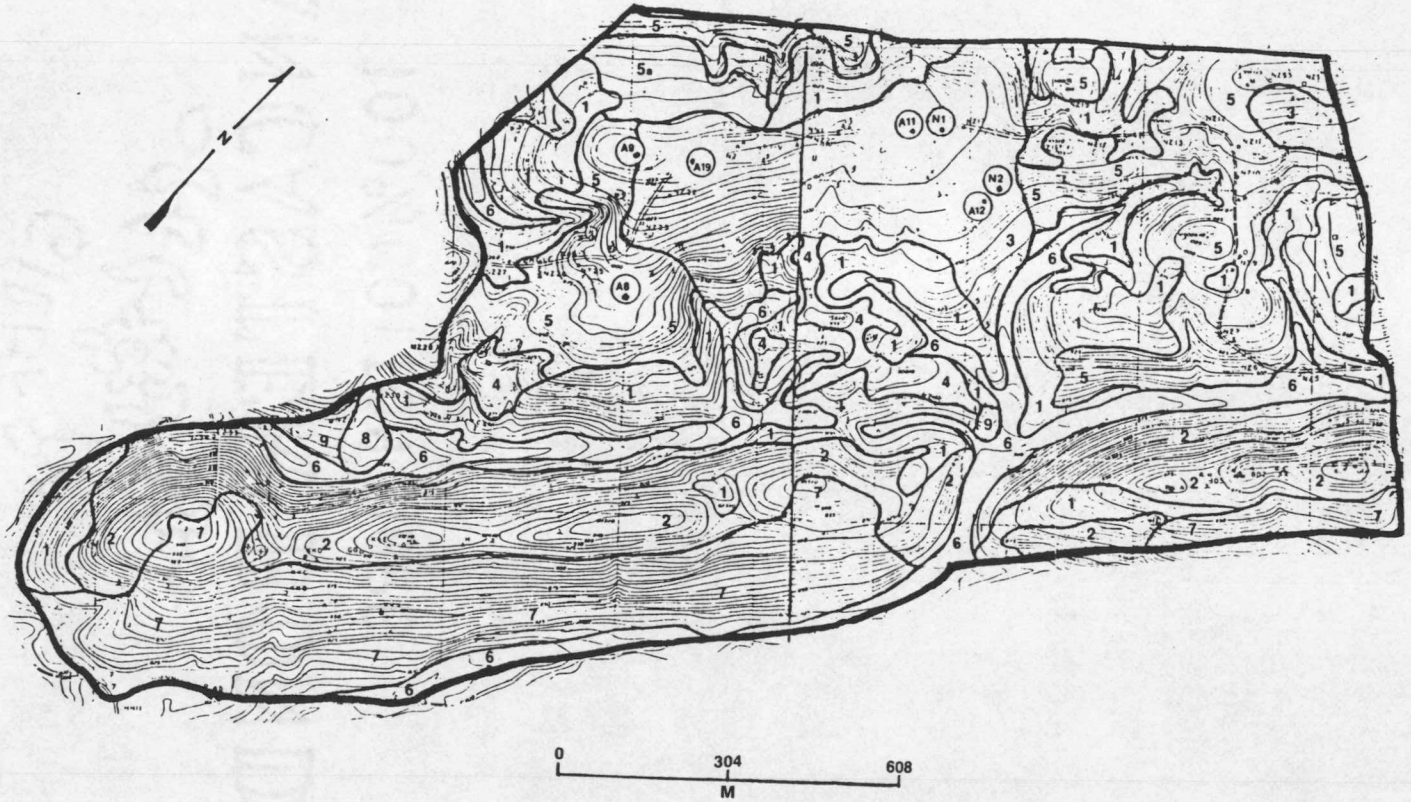

Figure 2. Soil Map with Locations of Cores. (After Lee et al., 1984) Core Drilling Sites Are Circled. Soil Mapping Units Are Numbered 1 Through 9. Refer to Table 1 and Appendix B. Mapped by H.C. Monger, 1984.

Table 1. Classification and Parent Materials of Soil Mapping Units.

Soil No.	Parent Material	Series	Classification
1	Colluvium	Shack	Fine-loamy, siliceous, thermic, Fragic Paleudult
2	"Longview" Residuum	Fullerton variant	Clayey- skeletal, mixed, thermic, Typic Paleudult
3	Ancient Alluvium	Dewey and Decatur variants	Fine-loamy, oxidic, thermic, Typic and Rhodic Paleudults
4	Chepultepec Residuum	Dunmore	Clayey, Mixed, thermic, Paleudults
5,5a	Copper Ridge Residuum	Colledgedale, Fullerton	Clayey, mixed, thermic, Paleudults
6	Holocene Alluvium	SND[a]	Entisols and Inceptisols - undifferentiated
7	Kingsport Residuum	Fullerton and Colledgedale	Fine-loamy, siliceous and clayey, kaolinitic Typic Paleudult
8	Pleistocene Alluvium	Holston	Fine-loamy, siliceous, thermic, Paleudults
9	Pleistocene Alluvium	Etowah	Fine-loamy, siliceous, thermic, Paleudults

[a] SND = Series is not determined.

Decatur, and Fullerton variants (Figure 2). Some cores have a more thorough vertical sample coverage, such as cores N1 and N2, due to the availability of samples recovered by the drilling rigs and unused by Woodward-Clyde Consultants. Figure 3 illustrates the depths from which the samples were taken. Samples were drilled into regolith overlying the Copper Ridge except core A8 which was drilled into regolith overlying Chepultepec. Spatially, the soil types display a complicated pattern due to a combination of geomorphic and pedogenic processes acting on tilted parent rock.

Samples were identified by combining the core symbol and the depth (in feet) at which the samples were taken. For example, sample N1-11.2 was taken from a 6-inch core section from core N1. The center depth of the core is 11.2 feet.

The samples were selected from core borings of the (A Series) type and Neutron Probe type. The A Series Borings were drilled using 8-inch (0.20m) outer diameter continuous fight hollow stem augers, and undisturbed sampling was accomplished by pushing a 3-inch (0.08m) diameter thin-walled Shelby tube 2-feet (0.62m) into the soils, or to refusal. The tube was then withdrawn and the top and bottom of the samples were sealed with wax (Woodward-Clyde Consultants, 1984). The Neutron Probe borings provided samples in Shelby tubes and were placed within a few meters of borings A12 and A11. The casings were installed by the application of downward pressure and rotary action (Woodward-Clyde Consultants, 1984).

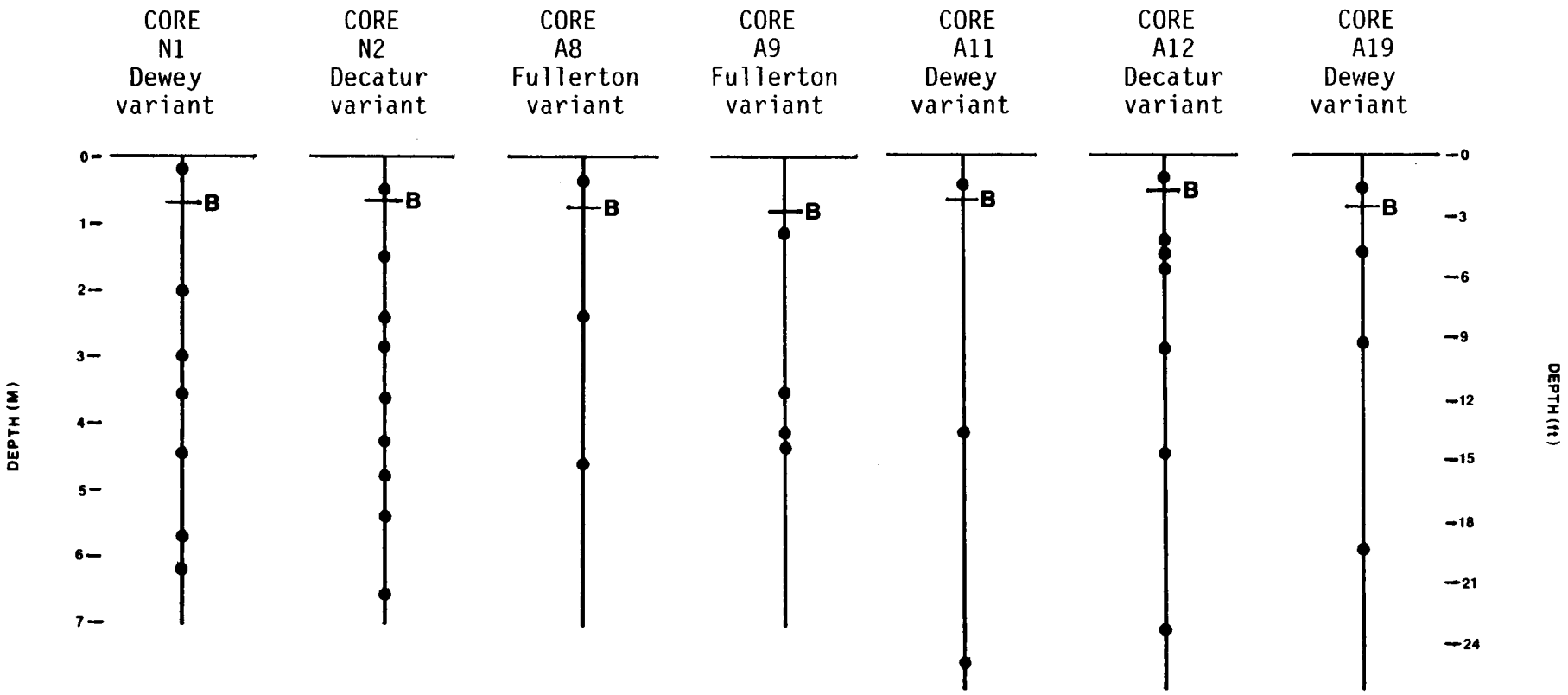

Figure 3. Sampling Depths of Cores and Corresponding Soil Types. Dots Indicate Sample Locations; Horizontal Bars Indicate the Approximate Upper B Horizon Boundary.

The samples were stored in Shelby tubes, glass jars, and plastic bags in a warehouse on the Oak Ridge National Laboratory Reservation for a few months until samples were selected labeled, and brought to the University of Tennessee.

CHAPTER II

METHODOLOGY

Introduction

The purpose of this chapter is to describe the general procedures and important instrumental and method specifications. References are supplied which present the details of each procedure.

Particle Size Fractionation

Samples were fractionated into gravel (>2 mm); sand (2 mm to 63 μm); silt (63 μm to 2 μm); and clay (<2 μm). The procedure involved the dispersion of 15 grams of oven-dry (80°C for 24 hours) <2 mm sample. This was accomplished by placing the sample into 250 ml centrifuge tubes, adding .01 N NH_4OH and shaking the sample with an automatic wrist shaker until Brownian Motion was observed under high power magnification (Allman and Lawrence, 1972). The slurry was then poured and washed with distilled water through the appropriate sieves. Separates were oven-dried at 80°C for 24 hours and weighed. The silt and clay fractions were separated by centrifugation at 1000 rpm for 1 minute and 28 seconds. The suspended clay was decanted into pre-weighed beakers as was the silt; both were oven-dried at 60°C for 24 hours and re-weighed. The weight of each size fraction was summed and subtracted from 15 grams to obtain a correction factor. Each size fraction was then multiplied by the correction factor

which then resulted in the summation of the size fraction totalling 100 %.

pH and Salt pH

Standard methods for the determination of pH were used (McLean, 1982).

For the determination of pH in distilled water, 5 ml of distilled water was added to 5 grams of air-dried sample (<2 mm) and shaken intermittently for 5 minutes and allowed to settle for a total of 10 minutes. A Beckman Electromate pH meter, which was standardized at pH 4 and pH 7, was used to determine pH by placing the electrode in the supernatant. The electrode was rinsed between each analysis with distilled water and re-standardized after every fourth analysis.

A salt pH was determined on the same samples by adding 0.050 ml of 1 M $CaCl_2$, shaking intermittently, and then inserting the electrode after 30 minutes.

X-Ray Diffraction Techniques

X-ray powder diffraction (XRD) was used to identify the mineralogical components of the <2 mm, <2 μm, and <0.2 μm size fractions. The specifications and setting conditions for a Norelco diffractometer were: CuK_α radiation, 1°2θ/minute, 35 kv and 17 ma, 100 cps at a time constant of 2 seconds. The d-spacings are reported in nanometers (nm). One nanometer is equal to ten angstroms (Å).

Diffractograms of the <2 mm size fraction were obtained from

packmounts of untreated, randomly selected samples. The size fraction was crushed to a fine powder using a porcelain mortar and pestle.

The <2 μm size fraction was analyzed from 3° to 30° 2θ after separation by centrifugation (Allman and Lawrence, 1972). This size fraction was mounted on glass slides using a smear mount method (Sledz, 1980) and was subjected to various treatments, including: potassium saturation at 25°C, potassium saturation and heated to 300°C, potassium saturation and heated to 550°C, magnesium saturation at 25°C, and vapor glycolation of magnesium saturated samples at 60°C.

The <0.2 μm size fraction was isolated by centrifugation, organics removed by H_2O_2 for upper soil horizon samples (Kunze, 1965), and mounted on glass slides using the smear mount technique.

Only qualitative XRD was used in the determination of relative mineral amounts. Relative concentrations of minerals is based on the presence or absence of peaks and corresponding peak heights. All samples were treated and mounted in the same manner. Peak height, however, is dependent on more than just the amount of a certain mineral; it is also dependent on the degree of mineral crystallinity and the amount of amorphous coating present on a mineral.

Magnetic Iron Nodule Distribution

Some of the particles of the sand-sized fraction are magnetic, being mainly composed of maghemite. The magnetic grains were isolated with a small hand magnet. Each sample was weighed before and after the removal of the magnetic grains, and the weight percent of magnetic grains was calculated.

X-Ray Fluorescence Techniques

The EG&G ORTEC X-ray fluorescence spectrometer, model 6110 TEFA-III X-probe was used to determine bulk chemical composition and ionic exchange capacities of the samples. This method involved the use of standards from the USGS, Canmet, National Bureau of Standards, British Chemical Standards, and Deutsche Demokratische Republik. Spiked samples of known barium and chlorine concentrations were also used as standards for the determination of ion exchange capacities.

The bulk chemistry was performed on the < 2 mm size fraction. The pressed pellet technique was used which involves grinding an oven-dry (60°C for 1 hour) sample in a shatter box for six minutes using liquid freon (Freon "TF") as a grinding agent. Three grams of powdered sample are then placed in a stainless steel mold, boric acid is added to hold the sample intact, and both are pressed at 30,000 psi.

The pressed pellets were analyzed using the ATAC program developed by EG&G ORTEC along with protocols for clays and ion exchange.

The standard error of calibration for each element analyzed is given in Appendix C, Table C1.

Ion Exchange Capacity Analysis by X-Ray Fluorescence Using $BaCl_2$

Measuring cation and anion exchange capacities using x-ray fluorescence (XRF) and Ba^{++} and Cl^- as index ions is a relatively fast and simple technique. It involves the saturation of a sample of known Ba and Cl composition with a $BaCl_2$ solution, the washing away of excess Ba and Cl which is not adsorbed, measuring the amount of entrained Ba and Cl, and then measuring adsorbed Ba and Cl by XRF.

More commonly used methods for determining ion exchange capacities include: (a) the summation method, (b) the direct displacement method, and (c) the radioactive tracer method (Rhoades, 1982). The XRF method is most related to (b) the direct displacement method which involves saturating a sample with an index cation and/or anion, displacing the adsorbed index ions by another salt solution, and determining the concentration of the index ions in the leachate. The XRF method eliminates the step which involves displacing the adsorbed index ion by measuring the adsorbed index ion on the solid.

The following is a discussion of the detailed procedure used to determine cation exchange using XRF on the <2 mm size fraction. The <2 mm size fraction was used because it is more representative of natural conditions as compared to the more commonly used

<2 μm size fraction. It was first necessary to know the amount of Ba in the untreated samples which was obtained during bulk chemical analysis. Five grams of homogenized <2 mm samples were placed in a pre-weighed Erlenmeyer flask. Subsamples of 2 grams were dried at 105°C for 2 hours to determine weight loss due to water evaporation. To the 5 gram samples in the Erlenmeyer flasks, 50 ml of 0.1 M $BaCl_2 \cdot 2H_2O$ solution was added. The flasks were shaken several times and allowed to sit for 24 hours. The supernatant was removed by pipetting, being careful not to remove any solids. Each sample was then rinsed three times with .002 M $BaCl_2 \cdot 2H_2O$ solution, pipetting off the clear supernatant between each rinse. The samples were then re-weighed to determine the amount of entrained .002 M $BaCl_2$ solution. The samples were then dried for 18 hours at 60°C and pressed in XRF pellets using the same procedure and specifications as the untreated samples.

The cation exchange capacity can be determined by comparing the amount of Ba in the treated samples to the amount of Ba originally in the sample once the entrained Ba is determined.

The mathematical procedure used to determine the cation exchange capacity (CEC) is given by working an example using sample N1-1.2:

Necessary Data:

wt. % Ba of untreated sample	=	0.03
wt. % Ba of treated sample	=	0.60
dehydrated sample wt.	=	4.99 grams
wt. of entrained .002 M $BaCl_2$	=	13.44 grams of solution

1) Actual wt. of Ba in untreated sample = 0.0015 grams

i.e., .0015 = 4.99 g sample x .03 wt. % Ba (untreated)

2) Actual wt. of Ba in treated sample = 0.0299 grams

i.e., .0299 = 4.99 g sample x .60 wt. % Ba (treated)

3) Entrained Ba = 0.003692 grams

i.e., $\frac{137.34 \text{ g Ba}}{1 \text{ mole Ba}} \quad \frac{1 \text{ mole Ba}}{1 \text{ mole } BaCl_2} \quad \frac{.002 \text{ mole } BaCl_2}{1000 \text{ ml solution}}$

$\frac{1 \text{ ml solution}}{1 \text{ g solution}} \times 13.44 \text{ g solution} = 0.0037 \text{ g Ba}$

4) Adsorbed Ba = 0.03 g Ba/4.99 g sample (rounding to two significant figures)

i.e., (.03 g Ba treated - .00g g Ba entrained) -

.00 g Ba untreated = 0.03 grams

5) Cation Exchange Capacity = 9 meq/100 g of sample

i.e., $\frac{1 \text{ meq}}{68.67 \text{ mg Ba}} \times \frac{1000 \text{ mg Ba}}{1 \text{ g Ba}} \times \frac{.003 \text{ g Ba}}{4.99 \text{ g sample}} =$

0.0875 meg/g sample = 9 meq/100 g sample (rounding to one whole number)

Extractable Fe, Mn, Si, and Al Oxyhydroxides of the <63 μm Size Fraction from Cores N1, N2, A8, A9, and A19

X-ray amorphous phases are difficult to characterize. However, a series of wet chemical dissolution steps have been shown to be relatively selective in extracting oxyhydroxide phases of Fe, Mn, Si, and Al.

Amorphous coatings and particles of iron and manganese were removed with two treatments of citrate-bicarbonate-dithionite (CBD) at 60°C. Mehra and Jackson (1960) and Follet et al. (1965)

developed and modified this method, respectively, which involves the reduction of iron and manganese by dithionite, followed by citrate chelation of dissolved iron and manganese while sodium bicarbonate acts to buffer the solution's pH. Ristvet (1978, p. 261) demonstrated that 100% of amorphous Fe oxide is removed with one CBD treatment, whereas only 0.4 wt. % of kaolinite is destroyed by one CBD treatment. Silicon and aluminum are also common components of the CBD extract and are throught to be contributed primarily by the amorphous and poorly crystalline aluminosilicate fractions which are associated with Fe and Mn (Kunze, 1965, p. 575).

Amorphous phases of silicon and aluminum oxyhydroxides form soluble sodium silicates and sodium aluminates in NaOH solutions at elevated temperatures. After the samples were subjected to two CBD treatments, they were then subjected to two 0.5 N NaOH treatments (25 ml per gram of sample) at 80°C as described by Hashimoto and Jackson (1960) and Follet et al. (1965).

The extracts were placed in plastic bottles and were analyzed for Fe, Mn, Al, and Si, using atomic absorption spectrometry and colorimetric techniques. An example, using sample N1-1.2, illustrates the mathematical treatment which enables the wt. % Fe_2O_3 to be calculated from the ppm of Fe in the CBD extract.

Necessary Data:

168 ppm of Fe in CBD extract

45 ml of CBD solution per gram of sample

$$\frac{168\ \mu g\ Fe}{1\ ml\ solution} \times \frac{45.0\ ml\ solution}{1\ g\ sample} \times \frac{1\ mole\ Fe}{55.847 \times 10^{6}\ \mu g Fe} \times \frac{1\ mole\ Fe_2O_3}{2\ mole\ Fe} \times$$

$$\frac{159.6922\ g\ Fe_2O_3}{1\ mole\ Fe_2O_3} \times 100 = 1.08\ wt.\ \%\ Fe_2O_3$$

Atomic Absorption Spectrometry and Colorimetric Determination of Extractable Fe, Mn, Si, and Al

A Varian atomic absorption spectrometer, model AA475 was used to determine the concentrations of iron and manganese in both the CBD and NaOH extracts. Iron was analyzed using a wavelength of 248.3 nm, a slit width of 0.2 nm, and an oxidizing flame. Manganese was analyzed using a wavelength of 279.5 nm, a slit width of 0.2 nm, and an oxidizing flame. Both were analyzed using air-acetylene. The iron concentration in the CBD extract was high and the solutions had to be diluted 200:1 for four samples and 100:1 for the other twenty-two. Iron in the NaOH extracts required no dilution. Nine out of the twenty-six CBD samples needed a 10:1 dilution for Mn. Manganese in the NaOH extract needed no dilution.

Due to the high salt content of the extracts, the burner, the nebulizer, and the aspiration tube of the atomic absorption spectrometer (AA) became progressively clogged. Frequent cleaning, aspirating distilled water between each sample, and the re-analysis of standards after every four samples was employed to reduce

the error introduced by the salting-up effect. Each iron and manganese sample of both extracts was analyzed four times; the standard deviation, mean absorbancy, and sample weights are given in Appendix D.

Extractable silicon and aluminum were measured using a Bausch and Lomb Spectronic 20 colorimeter. Silicon in both CBD and NaOH extracts was measured using the silicomolybic acid procedure developed by Grovett (1961). The aluminum in both extracts was measured using the Aluminon method of Hsu (1963) and Jayman and Sivasubramaniam (1974).

Insoluble Rust-Colored Precipitate in the NaOH Extracts

Six of the twenty-four samples developed a rust-colored precipitate in the NaOH extracts. The precipitate appeared iron-rich and was not subject to analysis by the AA due to its insolubility.

To get an idea of how much "iron-rich" material was in the six samples, the extracts were poured into separatory funnels, the precipitates allowed to settle, and then released into pre-weighed beakers. Three rinsings with distilled water were performed to remove the soluble salts which might be present. The supernatant was removed each time by pipetting. The samples were dried in an oven at 105°C for one hour and then weighed. The results are presented in Chapter III.

CHAPTER III

RESULTS AND DISCUSSION

Particle Size Distribution

Particle size distribution in the uppermost regolith at WCRS has mainly been influenced by pedogenic processes; namely, the downward translocation of fine particles, *in situ* clay mineral formation, and the accumulation of coarse fragments in the uppermost horizons. In addition, the particle size distribution is dependent upon the attitude of the titled saprolitic layers which contain various amounts of chert, sand, and clay (Figure 4). This accounts for the erratic distribution of the particle size classes (Table 2).

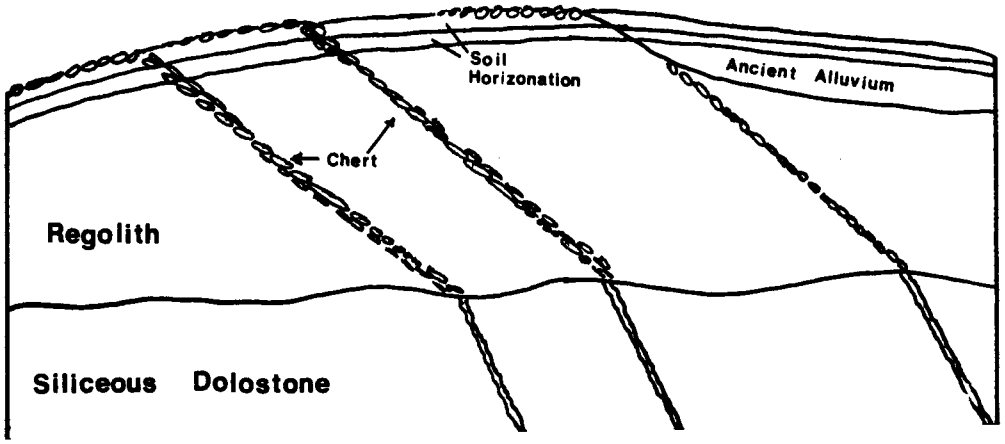

Figure 4. Particle Size Distribution and Its Dependence on Saprolitic Attitudes.

The clay particle size concentration generally reaches a maximum around a depth of 3 meters (Figures 5 & 6). This clay

Table 2. Particle Size Distribution of >2mm (gravel), 2mm-63μm (sand), 63μm-2μm (silt), and <2μm (clay).

Sample	Gravel[a] %	Sand[b] %	Silt[b] %	Clay[b] %
N1-1.2	11	9	83	8
N1-6.25	32	50	23	27
N1-9.2	1	1	90	9
N1-11.25	1	2	31	67
N1-14.2	1	4	73	23
N1-18.2	4	4	49	47
N1-20.25	26	13	41	46
N2-1.8	10	18	62	20
N2-4.5	1	23	48	29
N2-7.4	34	11	42	47
N2-9.4	18	10	39	51
N2-11.7	5	16	41	43
N2-13.8	22	10	50	40
N2-15.2	10	12	56	32
N2-17.4	44	32	42	26
N2-21.7	25	14	59	27
A8-1.25	3	31	61	8
A8-7.3	43	34	23	43
A8-14.5	22	11	45	44
A9-3.9	5	11	73	15
A9-11.25	39	5	43	52
A9-13.4	2	5	44	51
A9-13.7	4	7	46	47
A11-1.25	6	14	81	5
A11-13.25	1	1	61	38
A11-24.75	1	6	67	27
A12-1.25	1	18	75	7
A12-4.1	1	18	81	1
A12-4.7	9	24	51	25
A12-5.2	8	27	50	23
A12-9.25	12	16	39	45
A12-14.7	17	16	59	25
A12-23.5	13	15	55	30
A19-1.25	2	15	83	2
A19-4.5	11	16	70	14
A19-9.25	5	37	35	28
A19-19.25	19	3	72	25

[a] Weight percent total sample.

[b] Weight percent gravel-free sample.

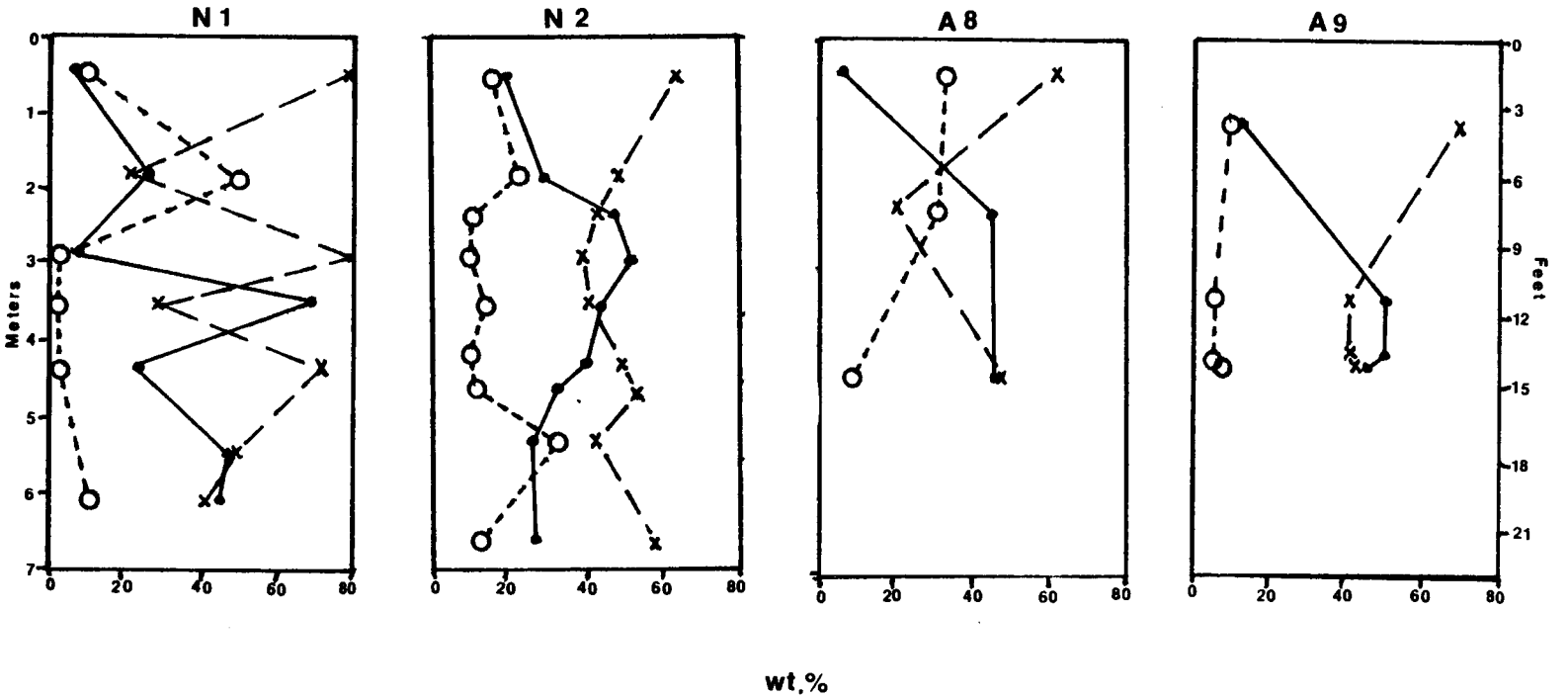

Figure 5. Clay, Silt, and Sand Concentration Versus Depth, Cores N1, N2, A8, and A9.

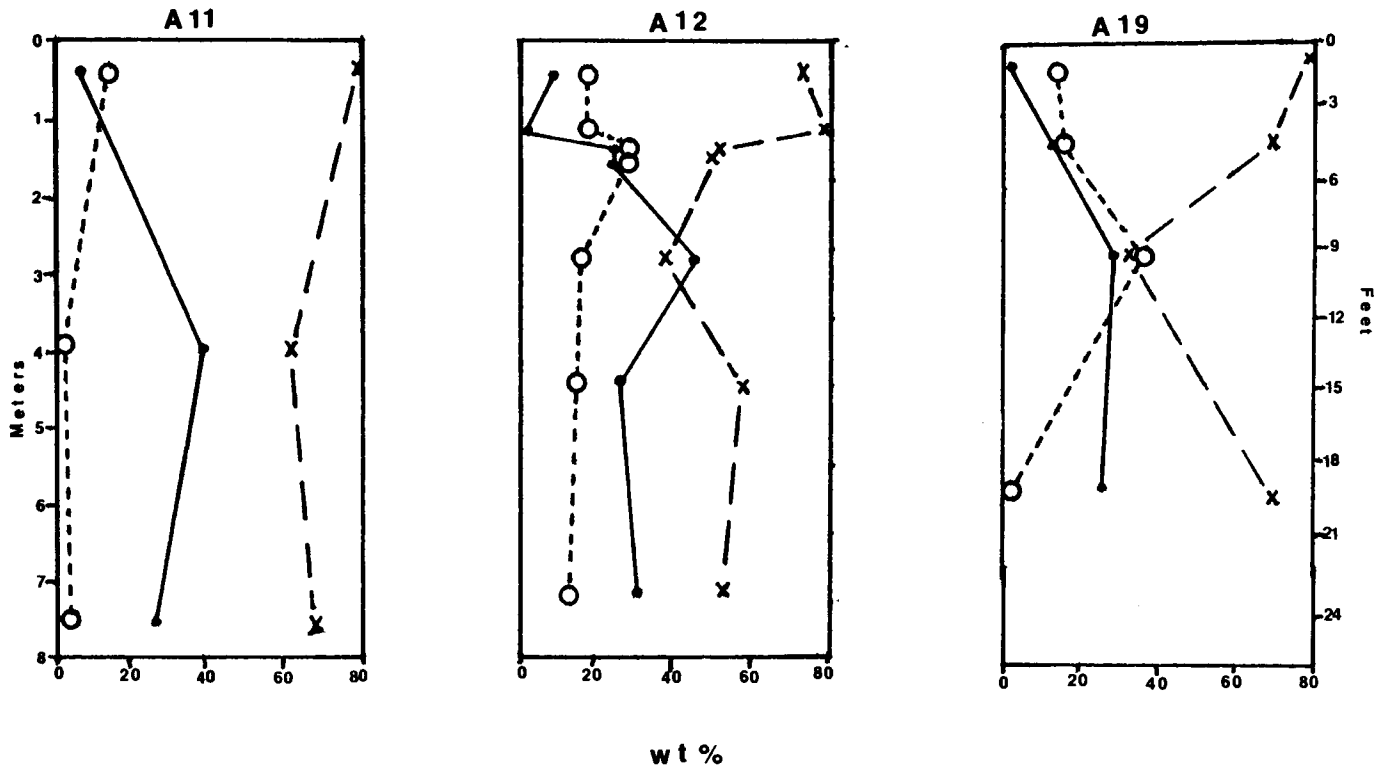

Figure 6. Clay, Silt, and Sand Concentration Versus Depth, Cores A11, A12, and A19.

"bulge" represents the section of the soil profile where water most readily translocates and deposits silicate clay minerals. In addition, this zone is most favorable for secondary kaolinite formation. Meteoric water carries dissolved elements from weathered pre-existing minerals downward into the clay bulge zone which is most commonly the maximum depth of rainfall penetration. Under acidic conditions, kaolinite has been observed to crystallize from water containing dissolved SiO_2 and Al_2O_3 (Grim, 1968, p. 486). Well-defined pseudo-hexagonal kaolinite was observed by Lee et al. (1984) at depths as shallow as 1 meter.

The silt-size fraction was larger than the clay or sand-size fractions, tending to be greatest in the upper soil horizons and decreasing with depth (Figure 5 & 6). The concentration of silt in the upper horizons is most probably due to selective downward translocation of clay-sized particles and wind-blown additions of silt-sized particles to the soil surface during the Pliestocene (D.A. Lietzke, personal communication). However, uppermost samples in each core show unusually high silt concentrations and low clay concentrations. This is because the organic matter was not removed prior to size separation. Polysaccharide constituents of the soil organic matter tend to glue clay particles together into silt-size aggregates. Only the uppermost samples, where organic matter is present, seem unusually high, the other samples are in fair agreement with Lee et al. (1984) who also measured particle size distribution on soils and residuum at WCRS.

The sand-size fraction has accumulated in the upper horizons and decreases with depth (Figure 5 & 6). An exception is found in Core N2 at 5.3 meters (17.4 ft.) and Core A19 at 2.8 meters (9.25 ft.). These cases are thought to be due to saprolitic layers rich in sand.

The gravel-size fraction displays the most variable distribution (Table 2). Gravel is less mobile than the smaller particles due to its relatively large size. Tilted layers of gravel-size chert were observed in a railroad cut in regolith overlying the Knox Group which is located up strike from WCRS near Bull Run Steam Plant (see Figure 4, p. 30). Field observations at WCRS reveal high concentrations of gravel and larger material, such as cobbles and boulders, which have accumulated on the ground surface as "float."

pH and Salt pH

Although the bedrock from which the regolith weathered is calcareous, the regolith is acidic due to long periods of intense leaching. The pH and salt pH were determined on samples from Cores N1, N2, A8, and A9. Water pH measurements ranged from 5.7 to 4.5

The salt pH was determined after 0.050 ml of 1 M CaCl was added, shaken intermittently, and an electrode inserted after 30 minutes. In general, the pH dropped about one pH unit except for the near-surface samples which only dropped a few tenths of a pH unit due to the higher organic matter content which serves as a

buffer. The results for both water pH and salt pH are given in Table 3.

There is essentially no residual dolomite or calcite present in the regolith, thus the regolith displays very little ability to buffer its acidity (Seeley and Kelmers, 1984). Soil pH changes are important because kaolinite and the amorphous phases are amphoteric, i.e., surface charge characteristics and thus exchange characteristics are altered by changes in pH. Cation exchange capacities decrease as pH is lowered, while anion exchange capacities increase as pH is lowered.

Mineralogy: Bulk (<2 mm)

XRD was performed on the <2 mm-size fraction of 16 randomly chosen samples with at least one sample from each core. XRD revealed mainly quartz in all samples with some minor clay peaks of kaolinite, illite, and aluminum hydroxy-interlayered vermiculite (HIV). There is little variability among the 16 samples and therefore only six diffractograms are presented as examples (Figure 7).

Sample A19-4.5 has an unusual peak at .383 nm. Although Miller (1972) observed feldspars in similar soils, this mineral did not match with any feldspars. The synthetic mineral Farringtonite, with the formula $Mg_3(PO_4)_2$, has its largest peak at .384 nm; its second largest peak at .334 nm, which in this case is obscured by a quartz peak; its third largest peak at .239 nm, which is barely discernible. One peak is not strong evidence for the presence of a mineral. However, since both phosphorus and

Table 3. Measurements of pH and Salt pH of Cores N1, N2, A8, and A9.

Sample	pHw[a]	pHs[b]
N1-1.2	5.7	4.5
N1-9.2	5.7	4.0
N1-11.25	5.5	4.4
N1-14.2	5.3	3.8
N1-18.2	5.0	3.7
N1-20.25	5.4	4.4
N2-1.8	5.5	4.5
N2-4.5	5.7	4.3
N2-7.4	4.9	4.0
N2-9.4	5.2	3.9
N2-11.7	4.5	3.7
N2-13.8	4.5	3.1
N2-15.2	5.2	3.6
N2-21.7	5.0	3.4
A8-1.25	5.4	4.0
A8-7.3	5.1	3.9
A8-14.3	5.4	3.5
A9-3.9	5.6	4.0
A9-13.4	4.8	4.0
A9-13.7	4.5	3.0

[a] pH in distilled water (10ml H_2O per 5 grams of <2mm sample).

[b] Salt pH (0.050 ml of 1 M $CaCl_2$ added to pHw).

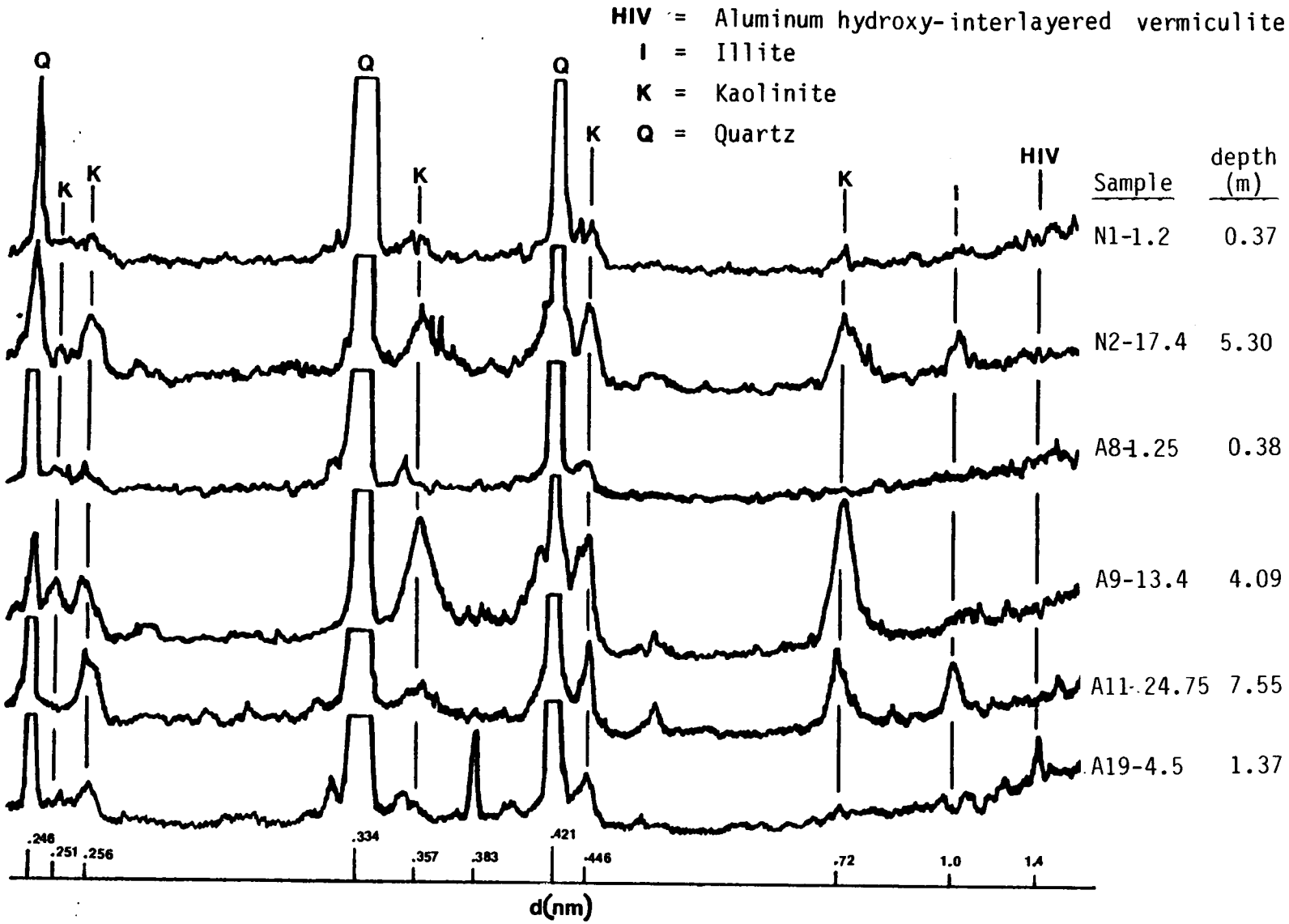

Figure 7. XRD Patterns of <2mm-Size Fraction of Random Samples.

magnesium are used as fertilizers and since this sample came from land which was once used for agriculture, one possible explanation is this mineral is an artifact of agriculture. This assumption, however, is complicated by the fact that the mineral was deeper in the soil (4.5 ft.) than one would expect a remnant fertilizer grain to be, making the possibility of the mineral being a secondary precipitate more probable.

Mineralogy: Clay Fraction (<2 μm)

The minerals which comprise the clay fraction, as revealed by XRD, are kaolinite, quartz, illite (also known as hydrous mica or soil mica), and HIV. Two samples, one representative of the upper soil horizons (shallower than 2 m) and one representative of the deeper, less weathered regolith were subjected to the various treatments described in the X-ray Diffraction Techniques section of Chapter II. The results are presented in Figure 8 (the upper soil horizon sample) and Figure 9 (the deeper, less weathered sample). Kaolinite is identified by peaks at 0.72, 0.446, and 0.357 nm (K saturated) which are destroyed at temperatures above 550°C. Quartz is identified by peaks at 0.421 and 0.334 nm (K saturated) which are not affected by any of the treatments. Illite is identified by peaks at 1.0, 0.5, and 0.33 nm (K saturated) which are not affected by the treatments. HIV is identified by peaks at 1.4 and 0.46 nm (K saturated). The 1.4 nm peak partially collapses toward 1.0 nm when heated to 300°C and 500°C (Figure 8).

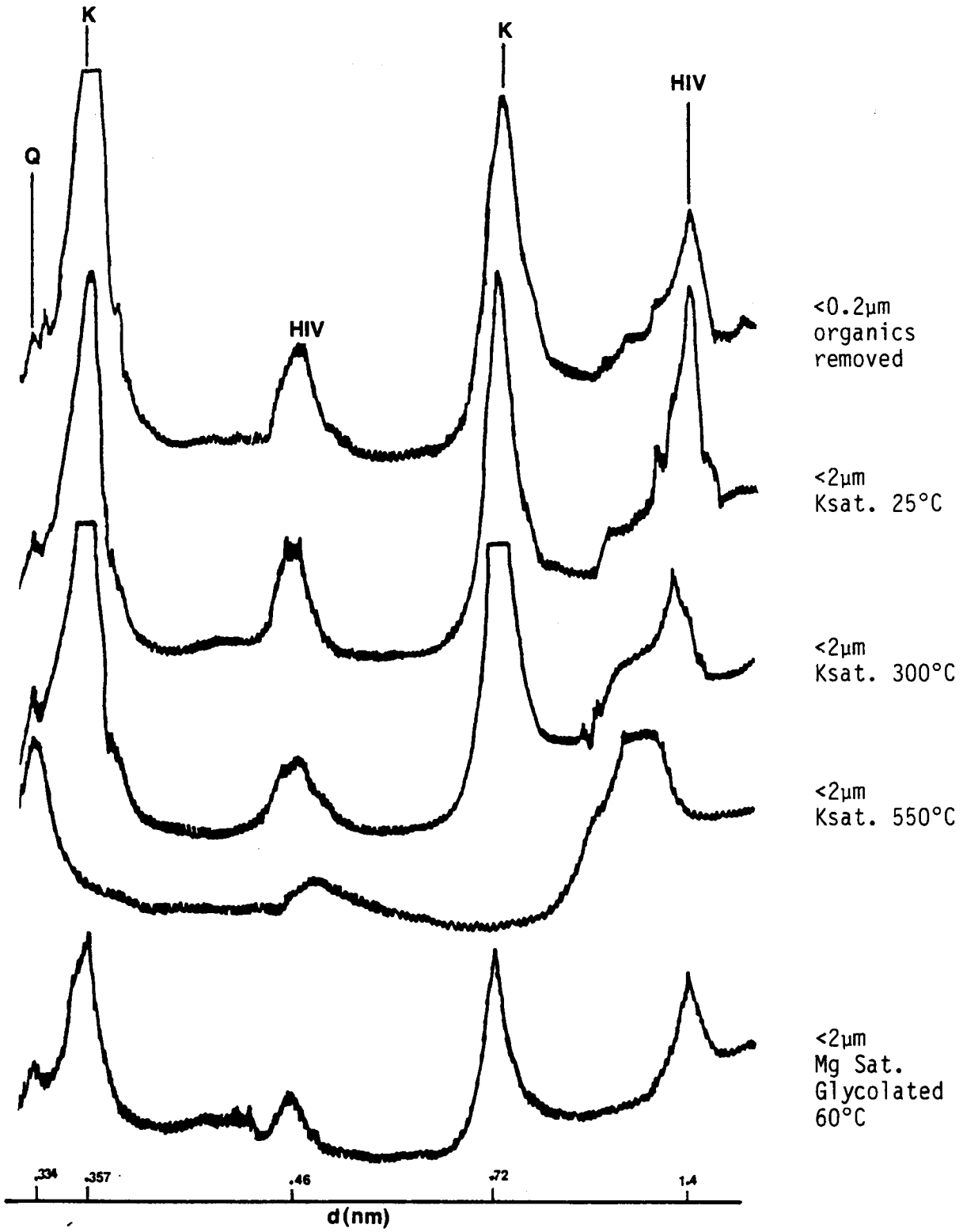

Figure 8. XRD Patterns of Typical Near-Surface Sample (Sample N1-1.8).

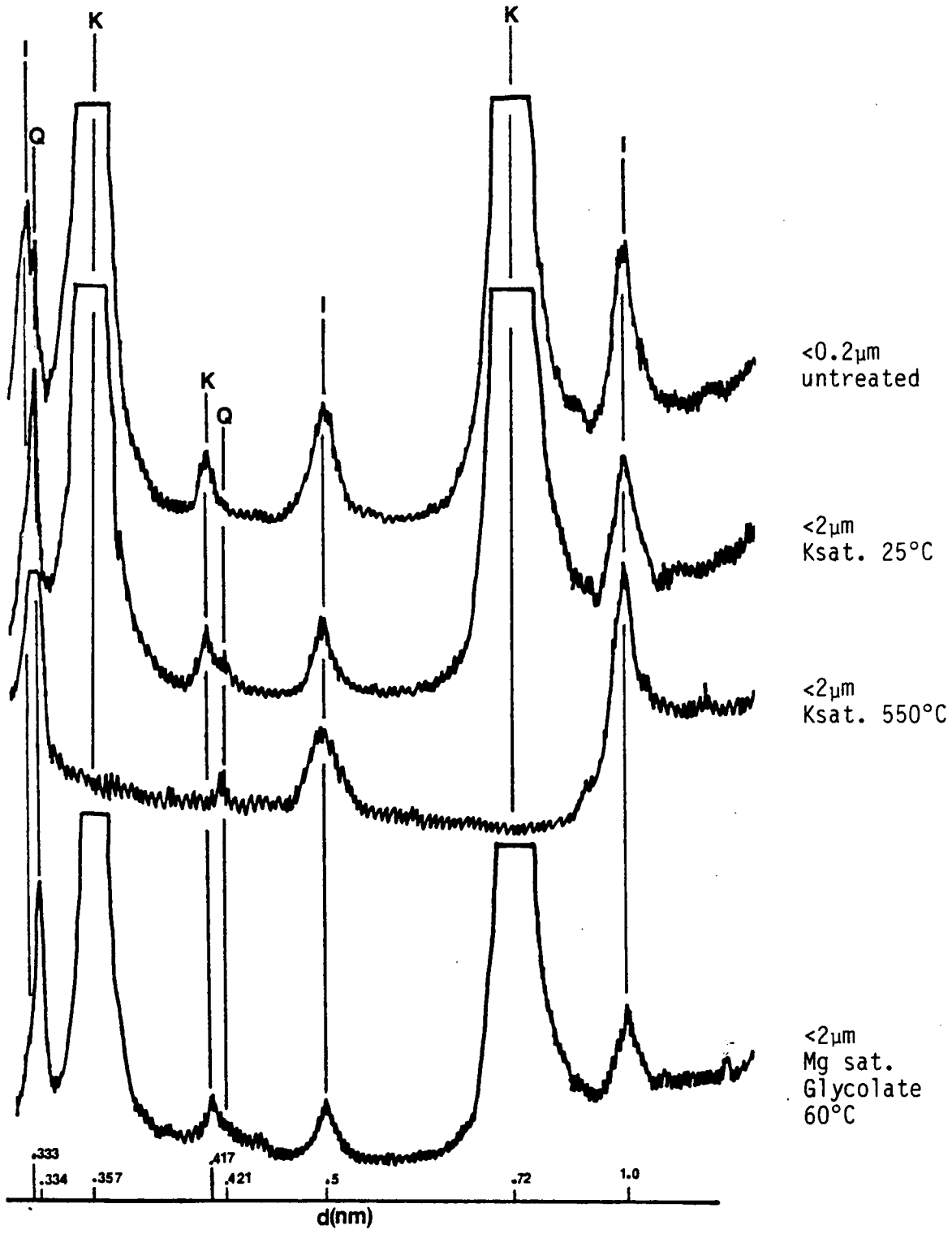

Figure 9. XRD Patterns of a Typical Residuum Sample (Sample A9-13.4).

A series of XRD patterns for the untreated clay fraction of each core is presented with corresponding depths (Figures 10 to 16).

Kaolinite is the dominant minerals in the clay-size fraction based on peak size. Its concentration increases with depth as does clay content in general. The kaolinite in the near-surface samples is poorly crystallized and becomes better crystallized with depth. Evidence for the difference in degree of crystallinity is displayed by peak sharpness: sharper peaks representing more crystalline clays. This is illustrated in Figures 10, 15, and 16, and observations made with a transmission electron microscope which reveals an increase in well-defined pseudo-hexagonal crystals with depth (Lee et al., 1984). Kaolinite, which is present on the walls of macropores, is more poorly crystalline than the kaolinite within an adjacent ped[1] (Khalifa and Buol, 1968). The poorly crystalline kaolinite which lines the macropore walls was most likely derived from the highly weathered surface regolith.

Quartz is present in varying amounts in all samples of <2 μm clay fraction. It commonly shows an increase of peak height with depth (Figures 11, 13, and 15). The increase in peak height with depth may be due to the fact that the abundance of amorphous coatings decreases with depth, while the degree of crystallinity increases. Figure 10 shows an abrupt decrease at

---

[1]A ped is a natural aggregation of individual soil particles.

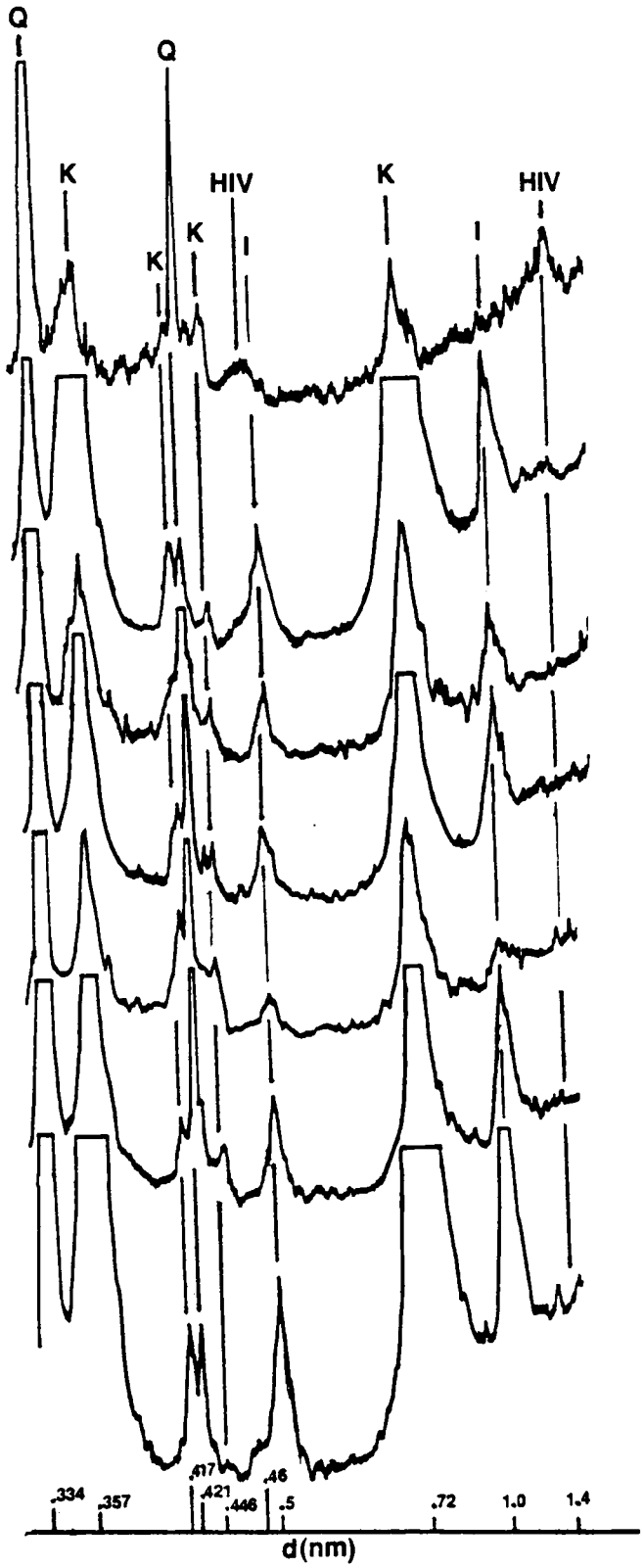

Sample	depth (m)
N1-1.2	0.37
N1-6.25	1.91
N1-9.2	2.80
N1-11.25	3.43
N1-14.2	4.33
N1-18.2	5.55
N1-20.25	6.17

Figure 10. XRD Patterns of Untreated Samples from Core N1 (<2μm).

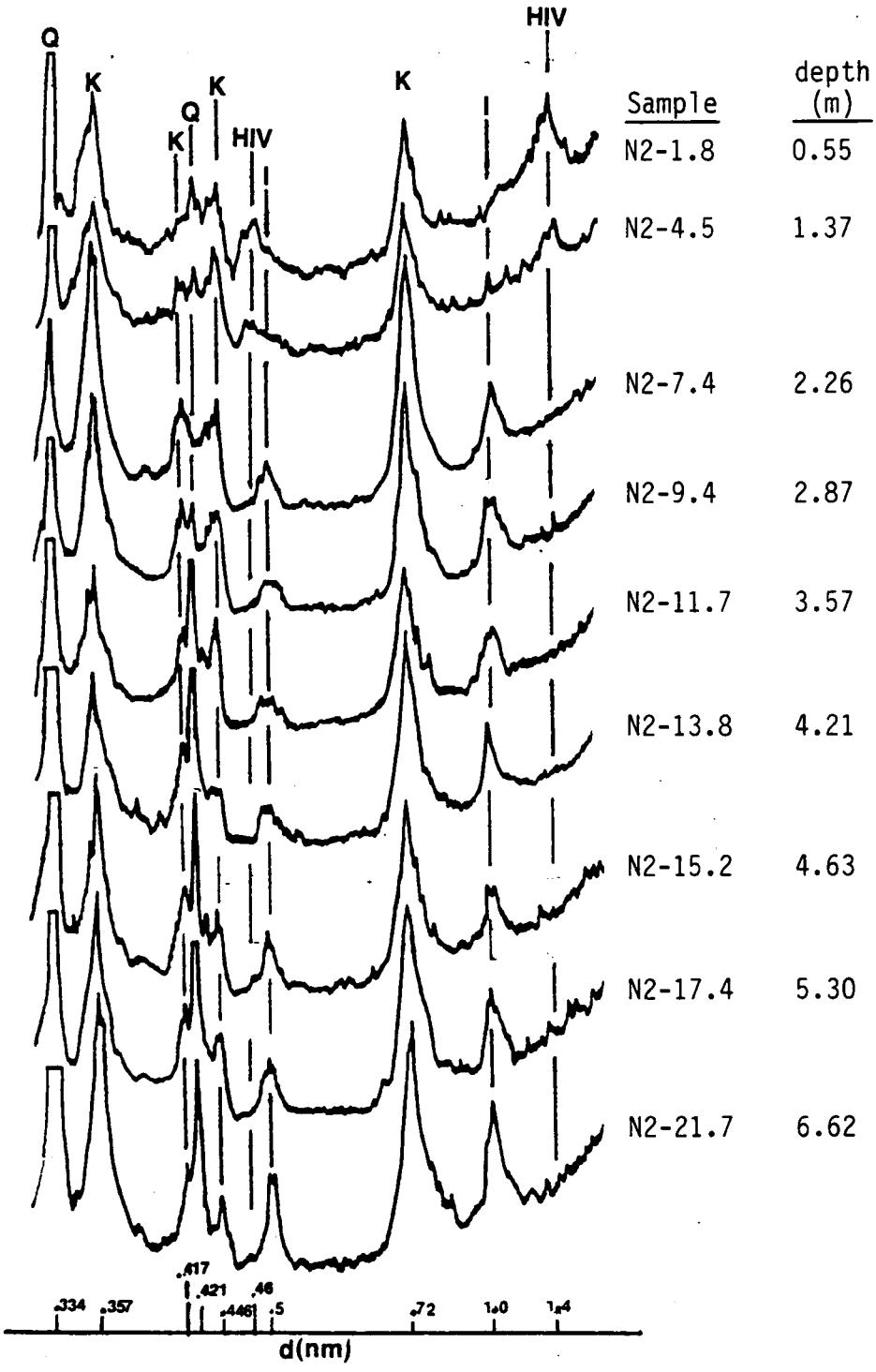

Figure 11. XRD Patterns of Untreated Samples from Core N2 (<2μm).

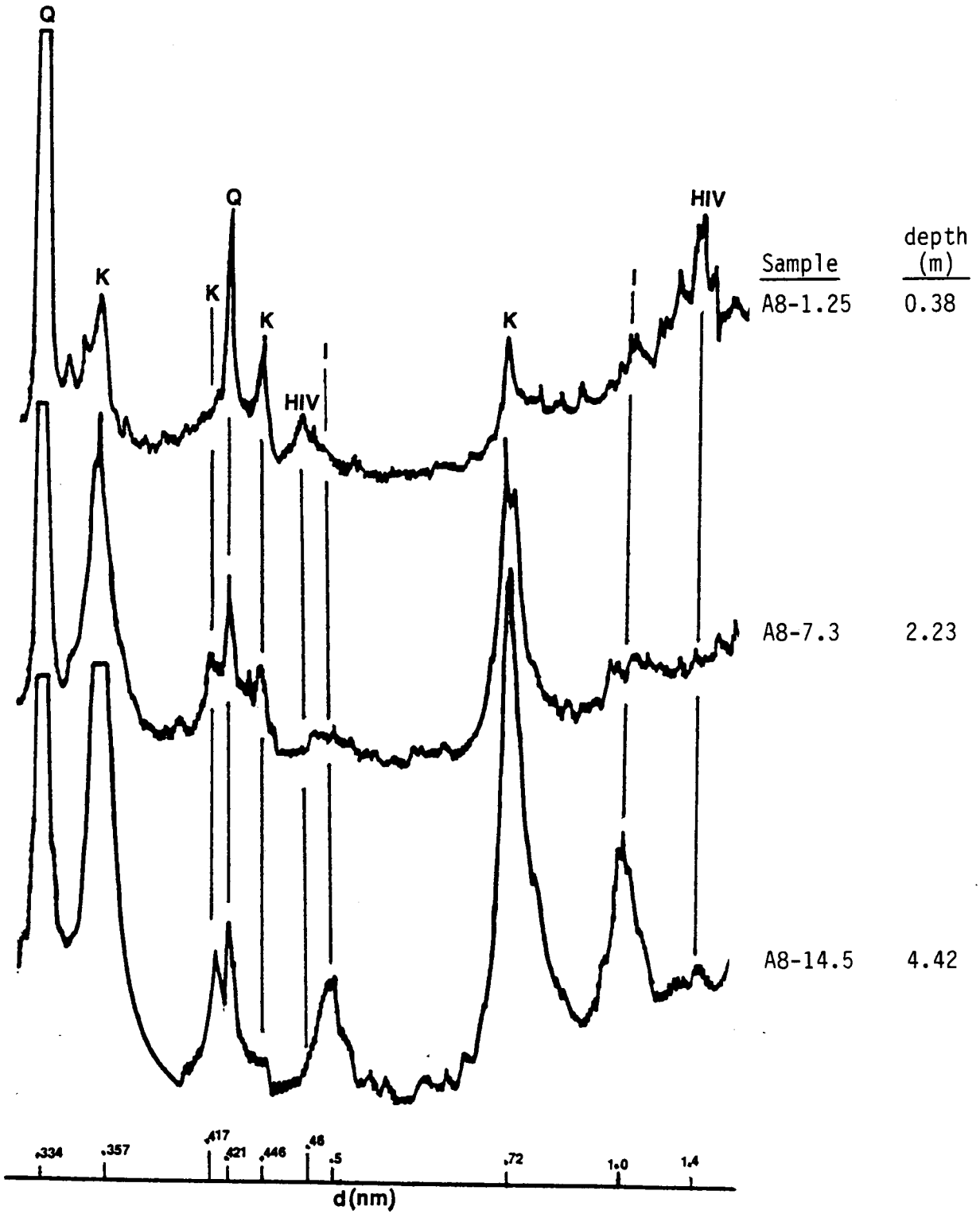

Figure 12. XRD Patterns of Untreated Samples from Core A8 (<2μm).

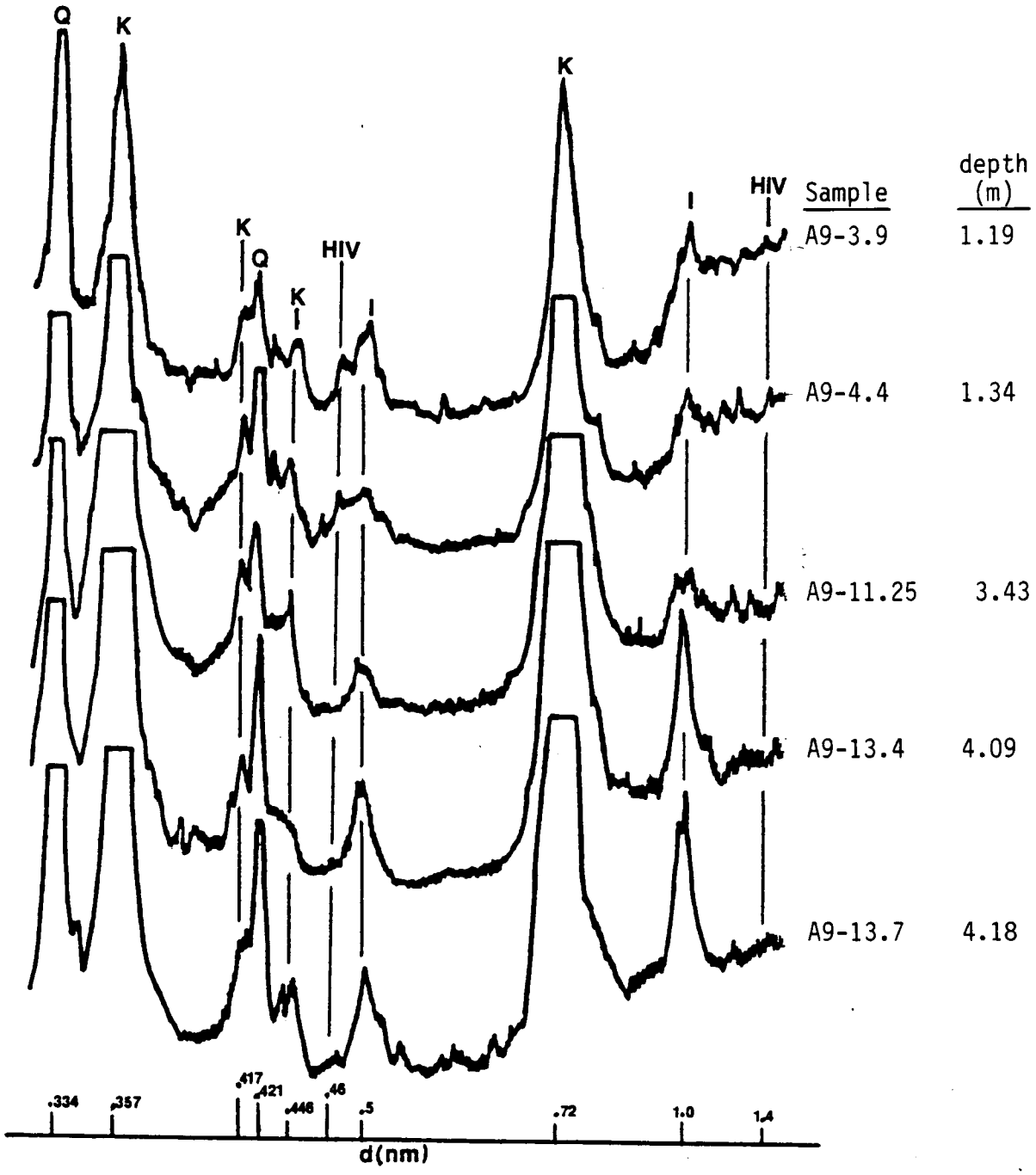

Figure 13. XRD Patterns of Untreated Samples from Core A9 (<2μm).

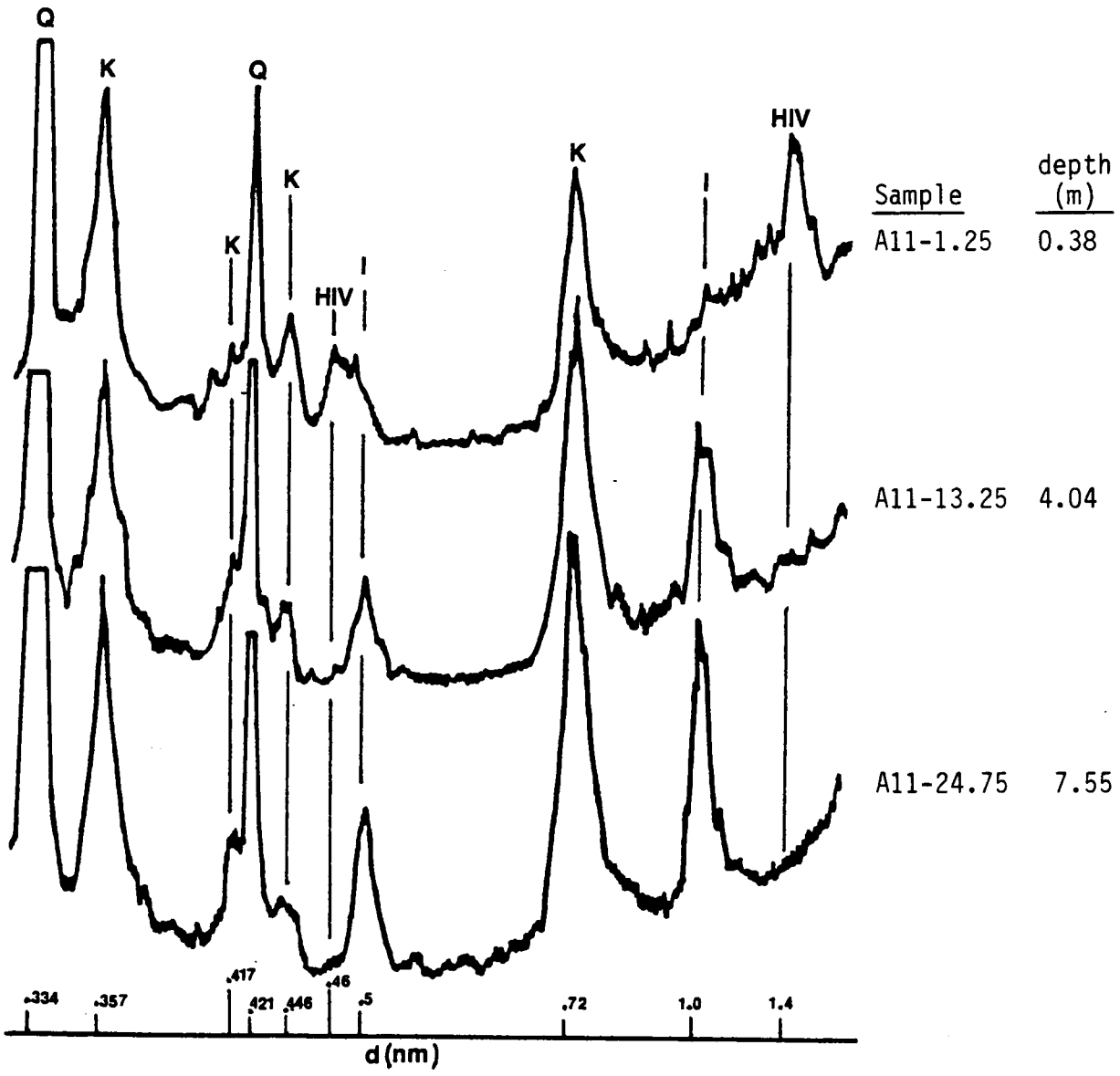

Figure 14. XRD Patterns of Untreated Samples from Core A11 (<2μm).

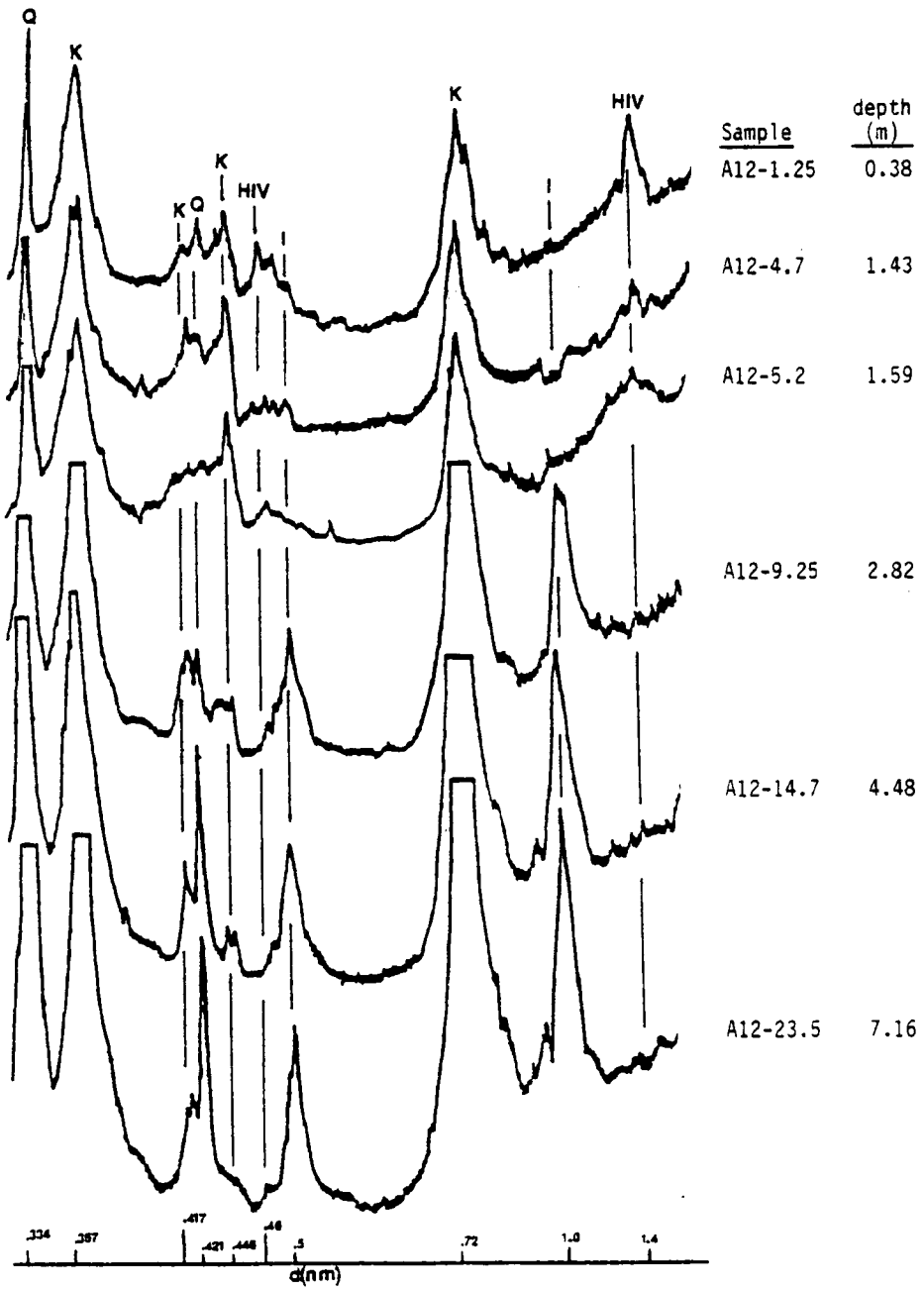

Figure 15. XRD Patterns of Untreated Samples from Core A12 (<2μm).

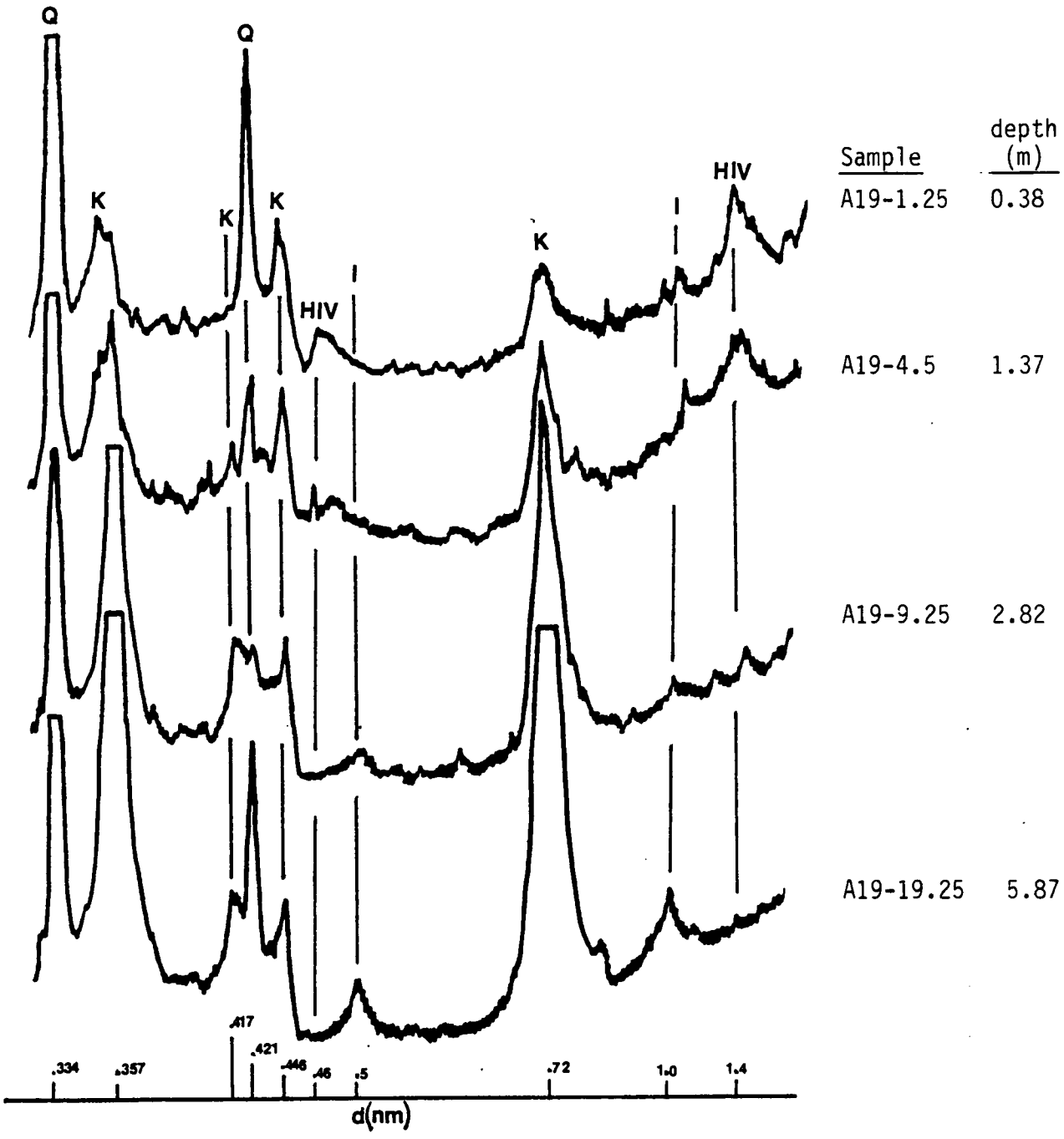

Figure 16. XRD Patterns of Untreated Samples from Core A19 (<2μm).

1.91 m which may indicate a discontinuity in the parent material, possibly an ancient alluvial deposit. Quartz content decreases as particle size decreases below 0.2 m (Figure 9). This trend is in agreement with what is commonly observed (Brady, 1974, p. 44) and was also observed by Miller (1972, p. 121) for similar regolith material.

Illite concentration increases with depth, based on XRD peak intensity, indicating less extremely weathered environments. The illite contained in the regolith is detrital, weathered from the carbonate bedrock. Miller (1972, p. 149) dissolved similar carbonates with HCl and analyzed the residue and found illite to be the major phyllosilicate (often the only phyllosilicate) in the insoluble residue. Illite is a common detrital constituent of residual soils and is usually concentrated in the coarse clay and fine silt fraction (Buol et al., 1973, p. 276).

HIV (or pedogenic chlorite as it is sometimes called) is most abundant, based on peak size, in the upper soil horizon (Figures 10, 11, 12, 14, 15, and 16). It is regarded as a product of intense weathering. Illite is commonly the precursor material which alters to a vermiculite-type mineral and then to HIV as the K^+ ion is stripped from the interlayer sites by weathering (Buol et al., 1973, p. 85). It can be seen in all seven cores that as HIV content increases, illite content decreases. Miller (1972) and Lee et al. (1984) also described a decrease of HIV with depth and a corresponding increase of illite. An $Al(OH)_x$ polymer commonly occupies interlayer sites in vermiculite which has been

exposed to weathering (Rich and Obenshain, 1955; Tamura, 1957; Huang and Lee, 1969). The interlayer spaces serve as a sink for Al in solution (Jackson, 1963). The source of the interlayered Al is kaolinite which is being destroyed by weathering (Lee et al., 1984). Miller (1972, p. 152) describes the weathering sequence by which illite is transformed into an intermediate stage of interstratified mica and then into soil-vermiculite and HIV:

$$\text{illite} \rightarrow \text{interstratified mica} \rightarrow \text{soil-vermiculite} \xrightarrow[\text{soils}]{\text{acidic}} \text{HIV}.$$

Mineralogy: Magnetic Sand-Sized Nodules

Black, brown, and red nodules are common in the sand-sized fraction of samples taken in the upper soil horizons of all seven cores with Cores A9 and A12 containing the most. A portion of the sand-sized fraction was magnetic and was isolated with a hand magnet. After being isolated with a hand magnet, the magnetic nodules were ground to a fine powder using a porcelain mortar and pestle and analyzed using XRD. The resulting XRD pattern (Figure 17) revealed the nodules to be composed of maghemite, hematite, and quartz. The largest concentration of magnetic nodules is in the upper soil horizons and quickly decreases with depth, indicating their weathering related formation (Table 4).

Bulk Chemical Element Distribution

Analysis of 16 elements for each sample was conducted on the <2 mm fraction using X-ray fluorescence. Five soluble elements

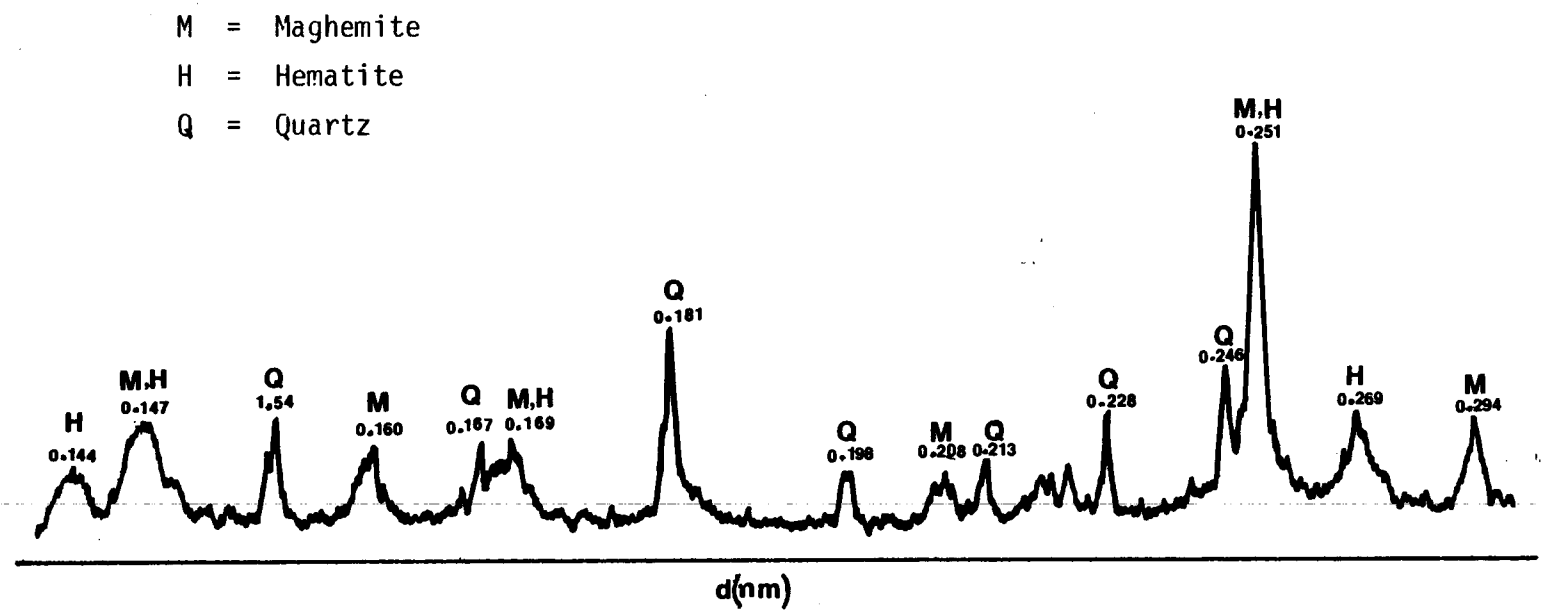

Figure 17. XRD Pattern of Magnetic Nodules (2mm-63μm).

Table 4. Samples Containing Magnetic Nodules (2mm-63μm) and Their Concentrations in wt. %.

Sample	Magnetic Nodules wt. %
N1-1.2	9.09
N2-1.8	2.15
N2-4.5	2.82
A8-1.25	2.11
A8-7.3	0.38
A9-3.9	3.03
A9-11.25	2.27
A9-13.4	1.69
A9-13.7	1.18
A11-1.25	2.27
A12-1.25	2.02
A12-4.1	4.44
A12-4.7	1.45
A12-5.2	1.18
A19-1.25	7.25
A19-4.5	3.65
A19-9.25	0.60

(Na, Mg, K, Ca, and Rb) and five elements which tend to accumulate in weathered residua (Al, Si, Fe, Mn, and Ti), as described by Goldschmidt (1937), are presented in graphical form as concentration versus depth (Figures 18 to 23). The graphical representation is designed to indicate concentration trends within individual cores and does not have the same weight percent scales for the same elements in different cores. For example, the scale for Na_2O in Core N1 ranges from 0 to 0.5 weight percent, while the scale for Na_2O in Core N2 ranges from 0 to 1.4 weight percent.

The soluble elements, Mg, K, and Ca, tend to decrease in concentration from the ground surface downward until a depth of about 2 meters where their concentrations tend to become erratic (Figures 18, 19, and 22). This is probably due to biogenic cycling by plants which extend roots down through 2 meters, extract nutrient elements and re-deposit them on the surface as constituents of plant debris (Buol et al., 1973, p. 276). Also, high concentrations of K, Ca, and Mg may be related to agriculture since these soils were farmed until the 1940's. Rubidium, though it is not recognized as an essential nutrient for plant growth, behaves similarly to K. Since Rb is found in minute concentrations (<0.15 wt. %), it is possible it was relocated in the soil profile by plants as well. Sodium, however, is not recognized as an essential nutrient element which is reflected by the fact that it does not appear to have been concentrated in the upper soil horizons as extensively as K, Ca, and Mg (Figures 18, 19, and 22).

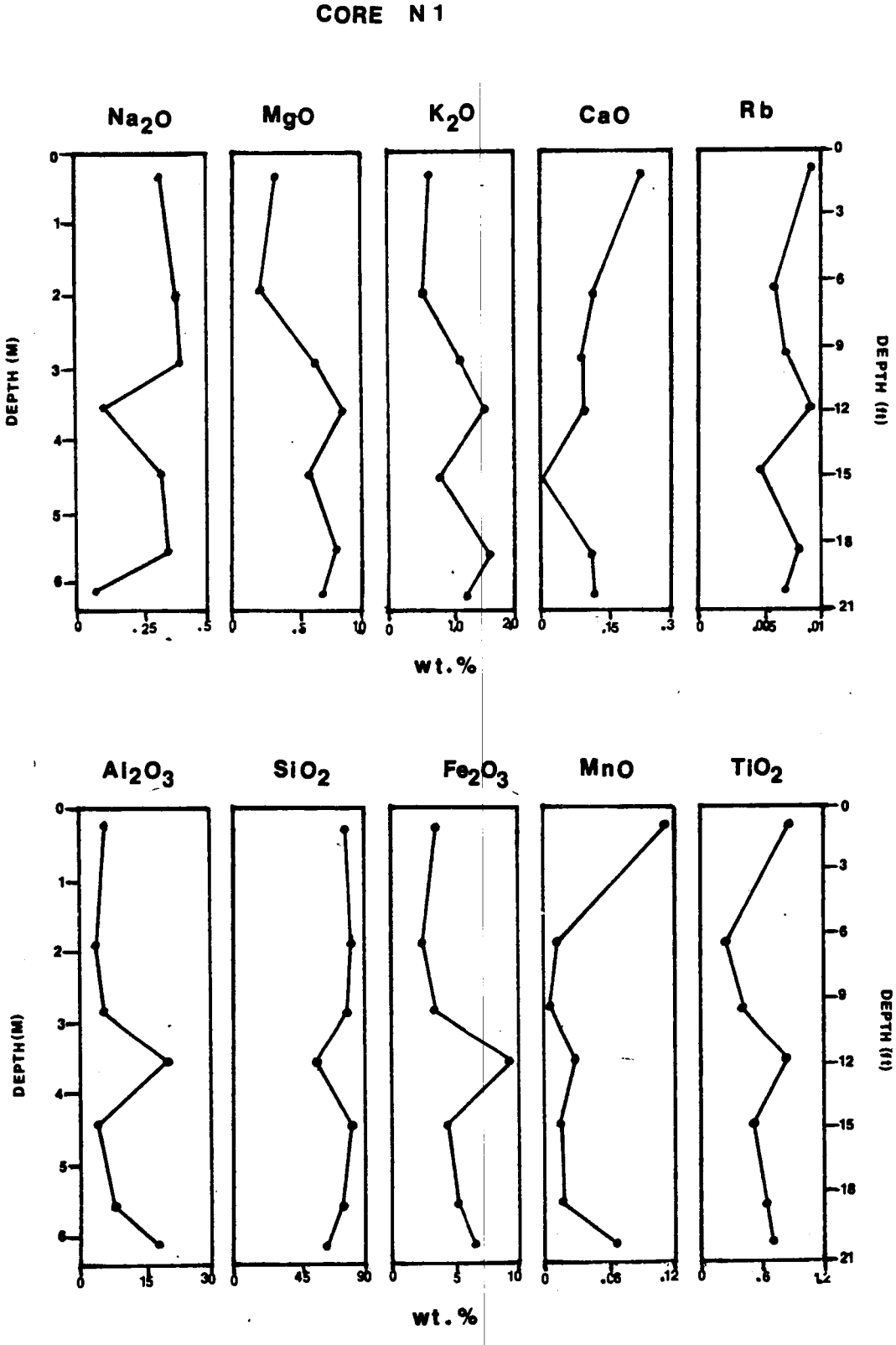

Figure 18. Elemental Distribution as a Function of Depth, <2mm, XRF Bulk Analysis, Core N1.

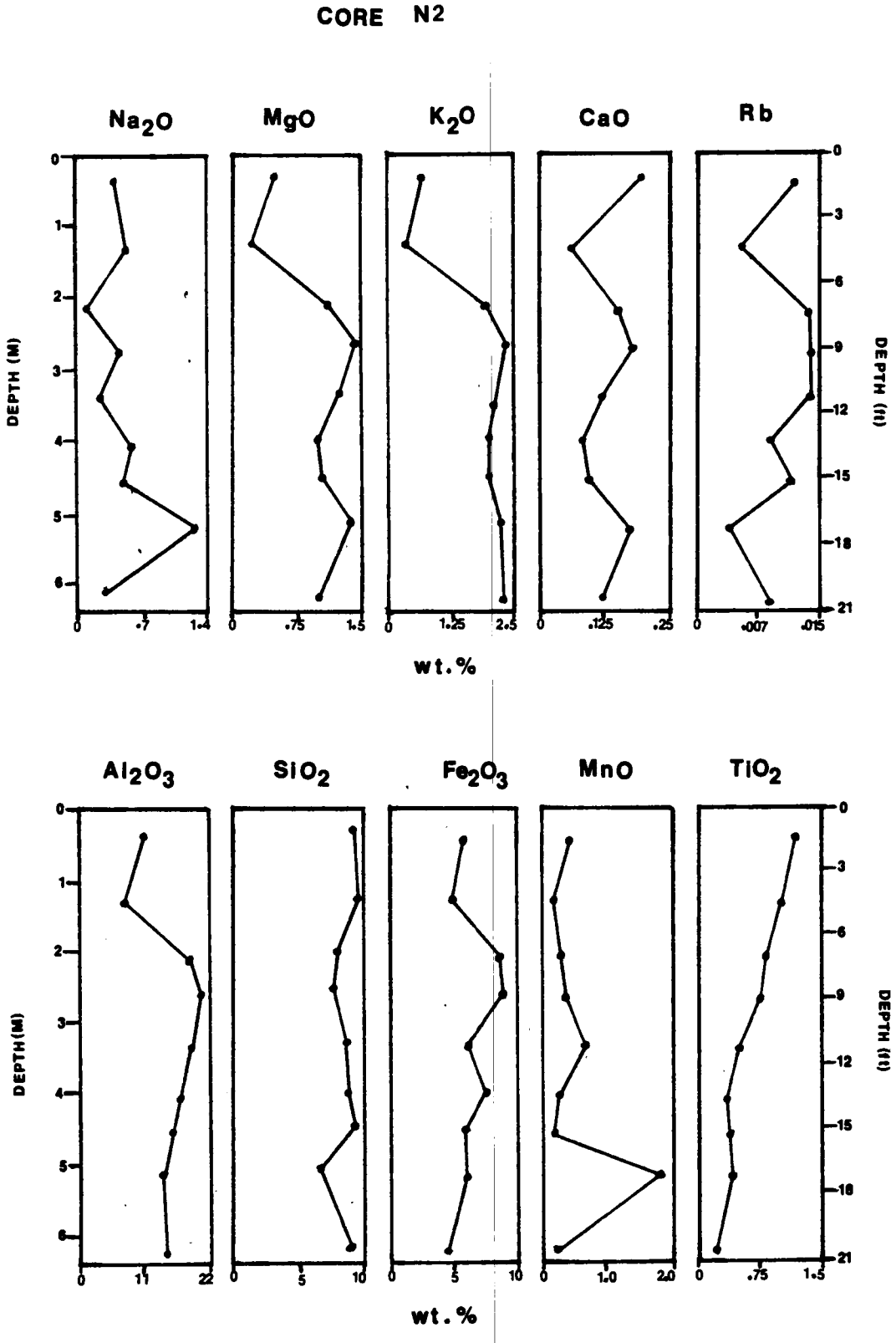

Figure 19. Elemental Distribution as a Function of Depth, <2mm, XRF Bulk Analysis, Core N2.

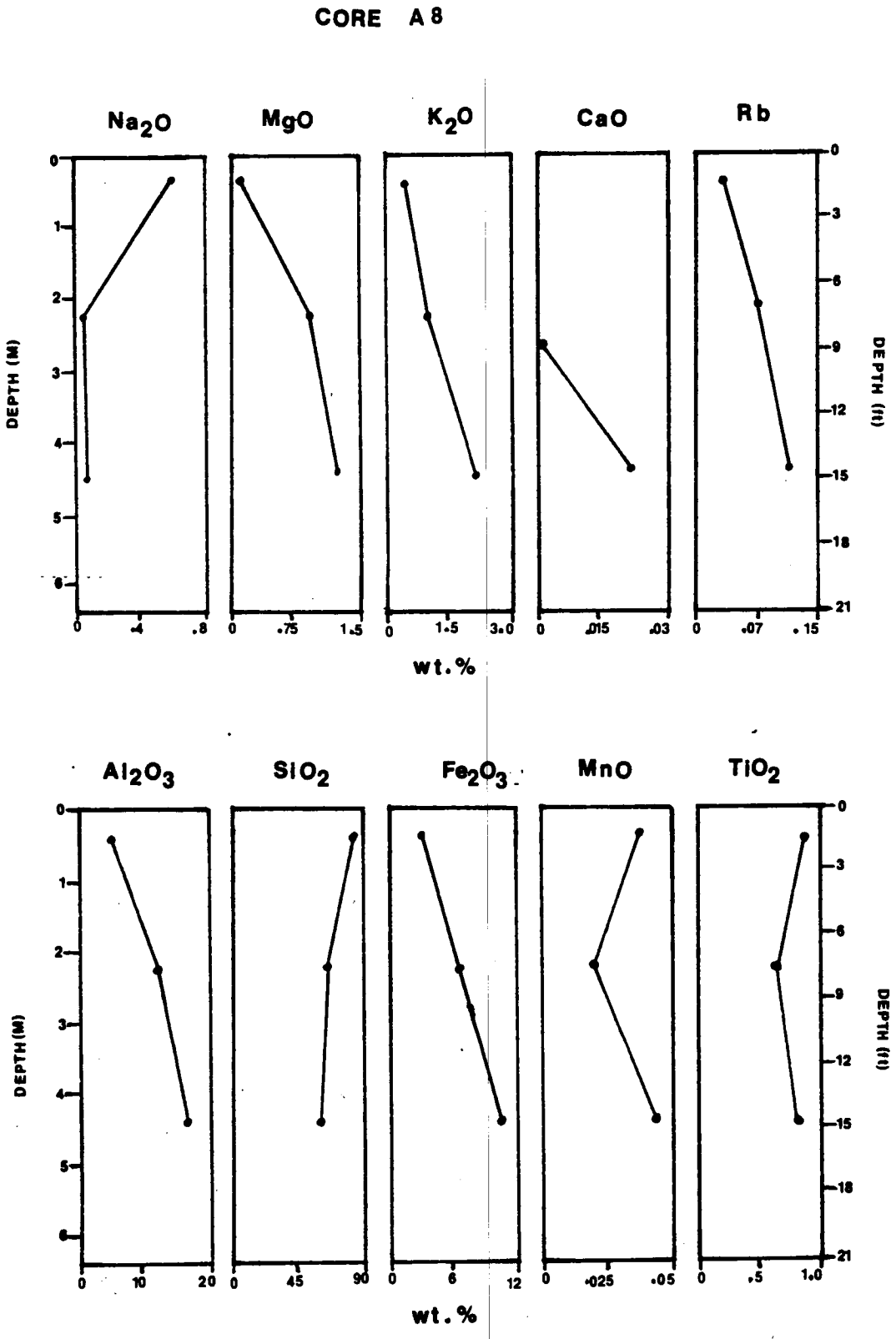

Figure 20. Elemental Distribution as a Function of Depth, <2mm, XRF Bulk Analysis, Core A8.

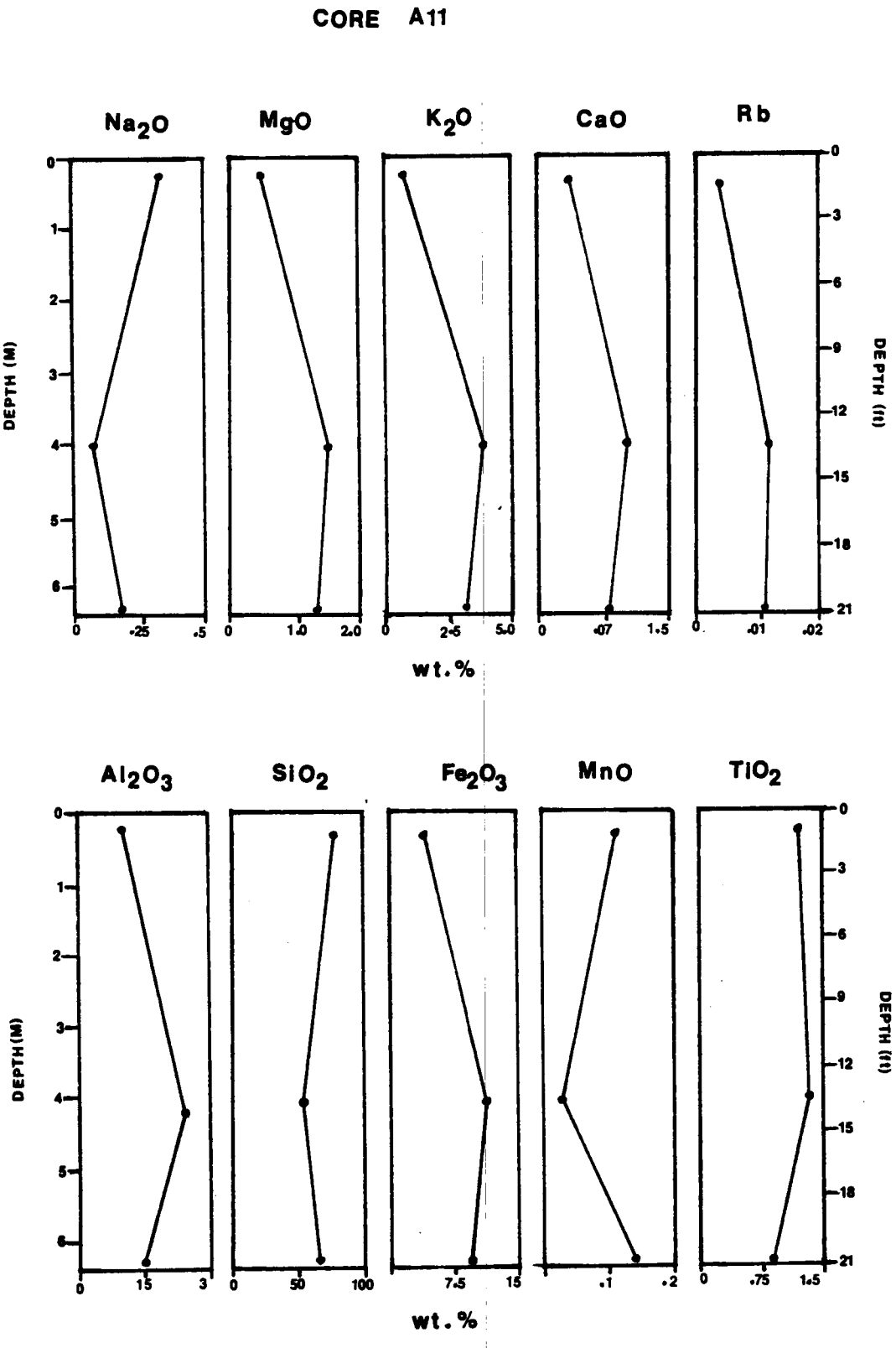

Figure 21. Elemental Distribution as a Function of Depth, <2mm, XRF Bulk Analysis, Core A11.

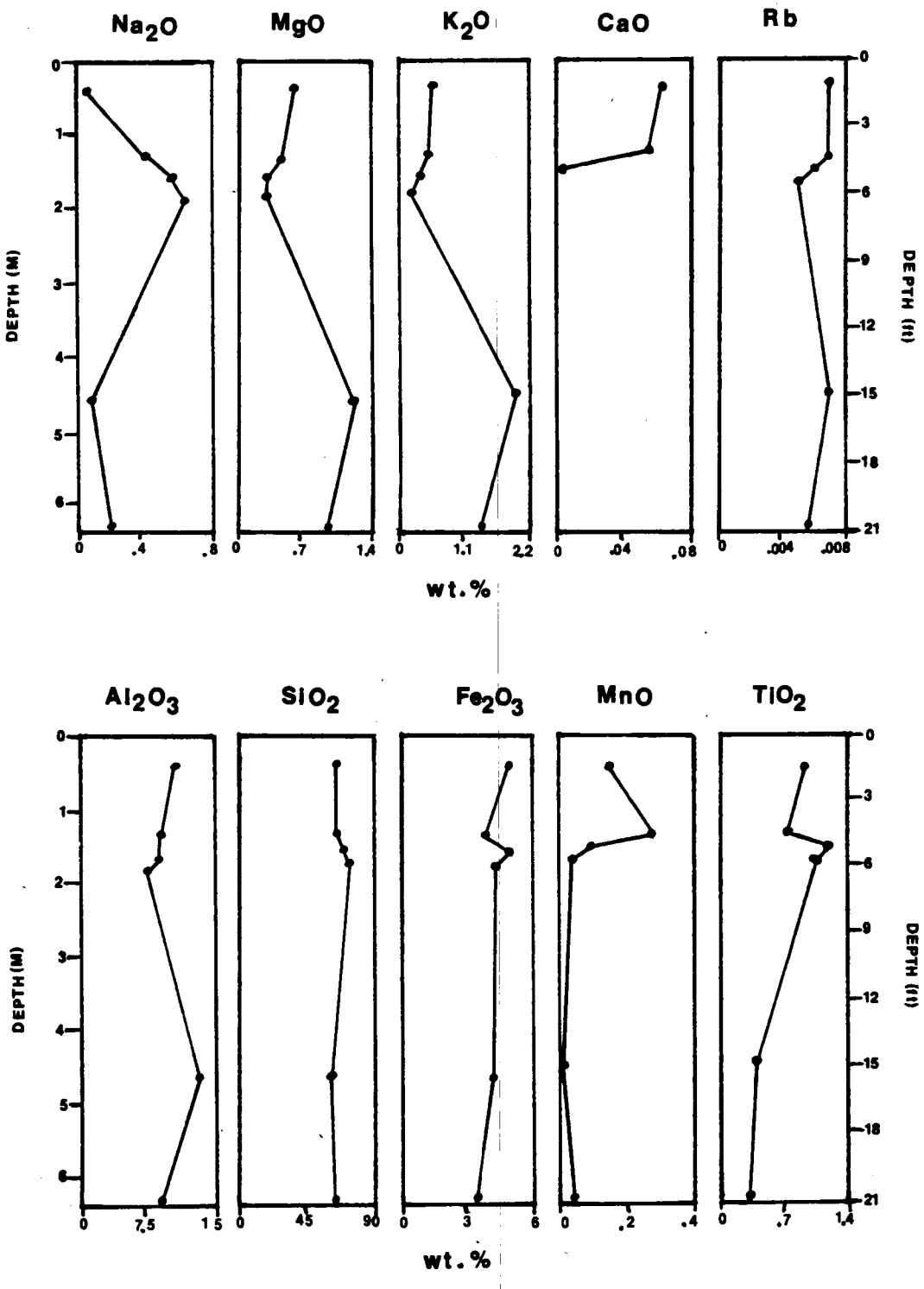

Figure 22. Elemental Distribution as a Function of Depth, <2mm, XRF Bulk Analysis, Core A12.

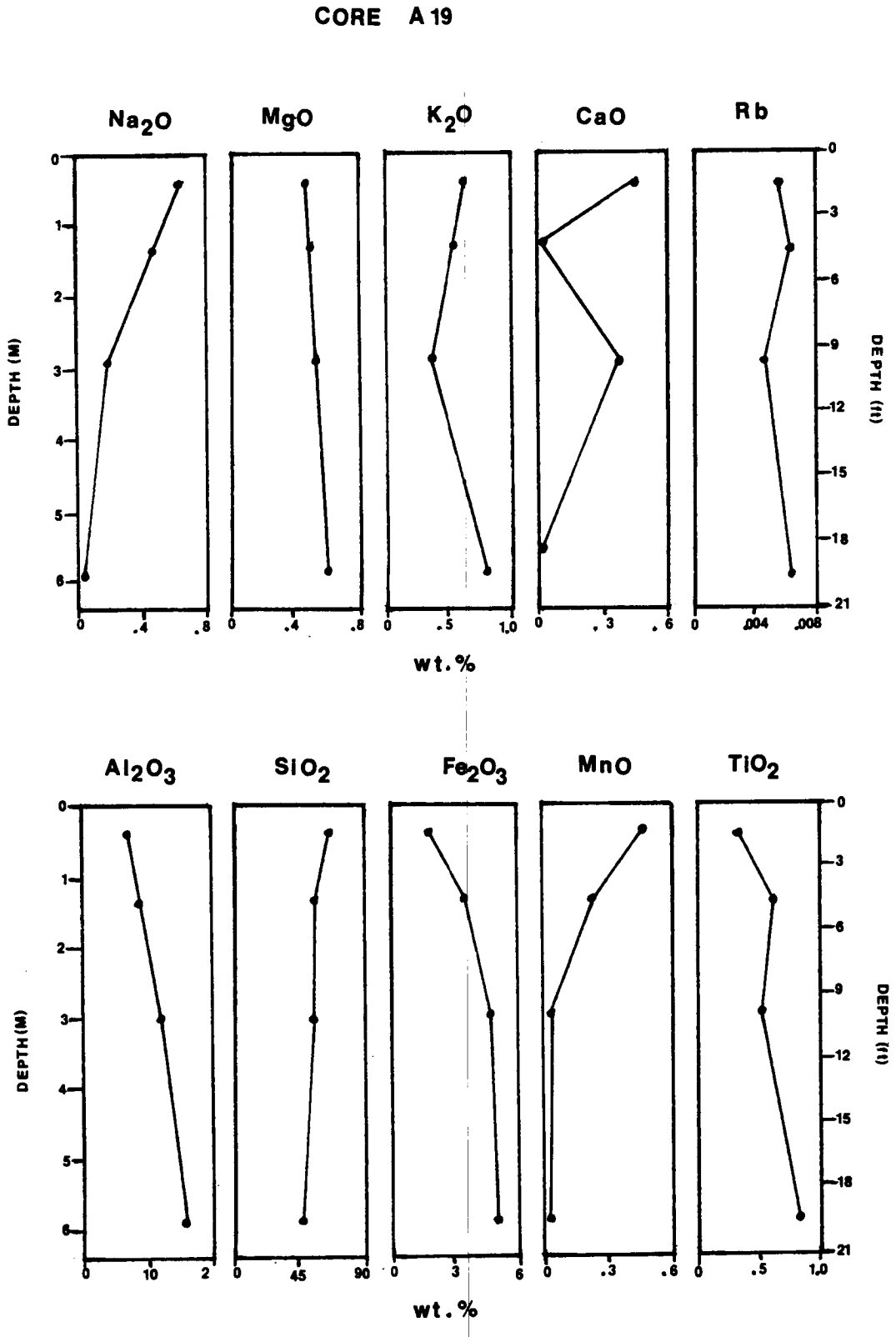

Figure 23. Elemental Distribution as a Function of Depth, <2mm, Bulk Analysis, Core A19.

Other noticeable trends include the correlation between Al content and clay content. Fe and Ti display similar trends (Figures 18, 22, and 23). Si and Al show inverse concentration trends (Figures 18, 19,1 20, 21, and 23).

Complete chemical data, including the other six elements which are not presented graphically (P, S, Cr, Ba, Sr, and Zr), are given for each sample in Appendix C.

Ion Exchange Capacity

The ion exchange capacity for the < 2 mm-size fraction of samples from Cores N1, N2, A8, and A9 were determined using Ba^{2+} and Cl^{-} to saturate the exchange sites and then analyzing for adsorbed Ba and Cl using XRF. The exchange sites adsorb ionic pollutants leached from waste sites. Possible ionic pollutants at WCRS include radioactive I^{-}, TcO_4^{-}, UO_4^{2+}, Sr^{2+}, Ca^{2+}, and Cs^{2+}.

The cation exchange capacity (CEC) ranged from 30 to 200 mmol ($\frac{1}{2}Ba^{2+}$) kg^{-1} (3 to 20 meq/100g, Table 5). In general, the CEC parallels the clay content and amount of extractable amorphous phases. The results are illustrated in Figure 24. Lee et al. (1984) reported CEC values of samples from WCRS to range from 85 mmole Ca/kg to 40 mmole Ca/kg which converts to 17 meq/100 g and 8 meq/100 g. Miller (1972), working with regolith similar to WCRS, found CEC values which ranged from 25.4 meq/100 g to 7.8 meq/100 g. Miller used the summation of cations extracted plus acidity measured by the $BaCl_2$-triethanolamine method.

Table 5. Cation Exchange Capacity Values.

Sample	Ba Conc. in Wt. %		Entrained .002 M	Dehydrated	CEC	
	Untreated	Treated	$BaCl_2$ (grams)	Sample wt.	meg/100g	mmol($\frac{1}{2}Ba^{2+}$)·kg^{-1}
N1-1.2	0.03	0.60	13.44	4.99	9	90
N1-6.25	ND	0.33	11.87	5.00	6	60
N1-9.2	ND	0.31	19.39	4.99	3	30
N1-11.2	ND	1.44	18.67	4.97	20	200
N1-14.2	0.02	0.35	16.71	4.89	6	60
N1-18.2	ND	0.42	16.48	4.98	6	60
N1-20.2	ND	1.09	17.90	4.97	15	15
N2-1.8	ND	1.03	36.89	4.85	13	130
N2-4.5	ND	0.66	49.28	4.96	6	60
N2-7.4	ND	1.39	43.52	4.99	17	170
N2-9.4	ND	0.91	32.40	4.97	9	90
N2-11.7	0.03	1.06	37.96	4.97	12	120
N2-13.8	ND	0.88	33.04	4.96	9	90
N2-15.2	ND	0.97	61.32	4.98	9	90
N2-17.4	0.05	0.77	29.96	5.00	9	90
N2-21.7	ND	0.70	41.48	4.97	6	60
A8-1.25	0.04	0.33	13.85	4.98	6	60
A8-7.3	0.04	0.74	15.34	4.97	12	120
A8-14.5	0.08	0.74	18.68	4.97	12	120
A9-3.9	0.05	0.83	17.77	4.94	12	120
A9-11.25	ND	0.65	15.79	4.98	9	90
A9-13.4	0.05	0.17	14.14	4.95	3	30

ND = Not detected, concentrations below the detection sensitivity of the XRF as indicated by: [-0.xxxx] on the printout.

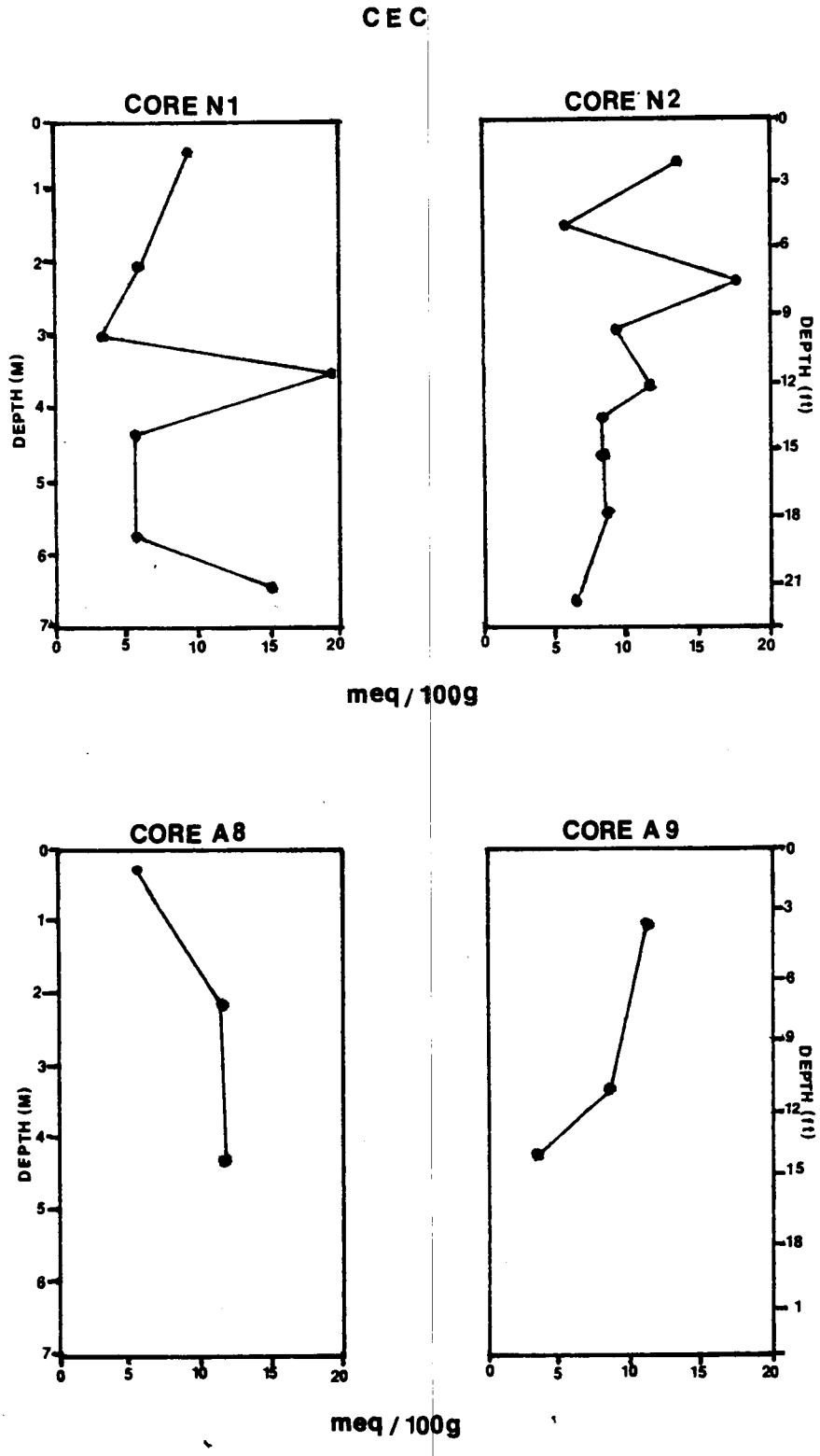

Figure 24. Cation Exchange Capacity as a Function of Depth, Cores N1, N2, A8, and A9.

Analysis of anion exchange capacity was attempted using the same method by measuring adsorbed Cl^-. The adsorbed Cl^- was below the detection sensitivity of this method, which indicates the small anion exchange capacities for these samples. Seeley and Kelmers (1984, p. 9) reported very low anion sorption ratios for regolith material at WCRS. Using technetium and iodine, both anionic species in solution, the measured sorption ratios were 1.6 and 1.8 L/kg compared to 61,000 L/kg for the cation europium (Eu^{3+}). Cation exchange capacity is dependent upon the amount of clay particles (colloidal surface), clay mineral type, amount and type of organic material, pH, and amount and type of amorphous oxhydroxides. In Core N1, at a depth of 3.43 meters, there is an abrupt increase in CEC (Figure 24) which parallels an increase in clay content and an increase in Fe and Mn oxyhydroxide amorphous material (Figure 25). Presumably, this common increase represents a shale-rich layer which has weathered from the bedrock. The correlation coefficient between the CEC of Core N1 and the clay content of Core N1 is 0.77; between CEC and total extractable oxyhydroxides is 0.89. Core N2 has a correlation coefficient of 0.54 between CEC and clay content and 0.24 between CEC and total extractable oxyhydroxides. Core A8, having only three samples, gave a correlation coefficient of 0.98 between the CEC and clay content and 0.99 between the CEC and total extractable oxyhydroxides. Core A9, the final core for which CEC data were obtained, had a low correlation coefficient of 0.22 between CEC and clay content. Correlation between CEC and total oxyhydroxides

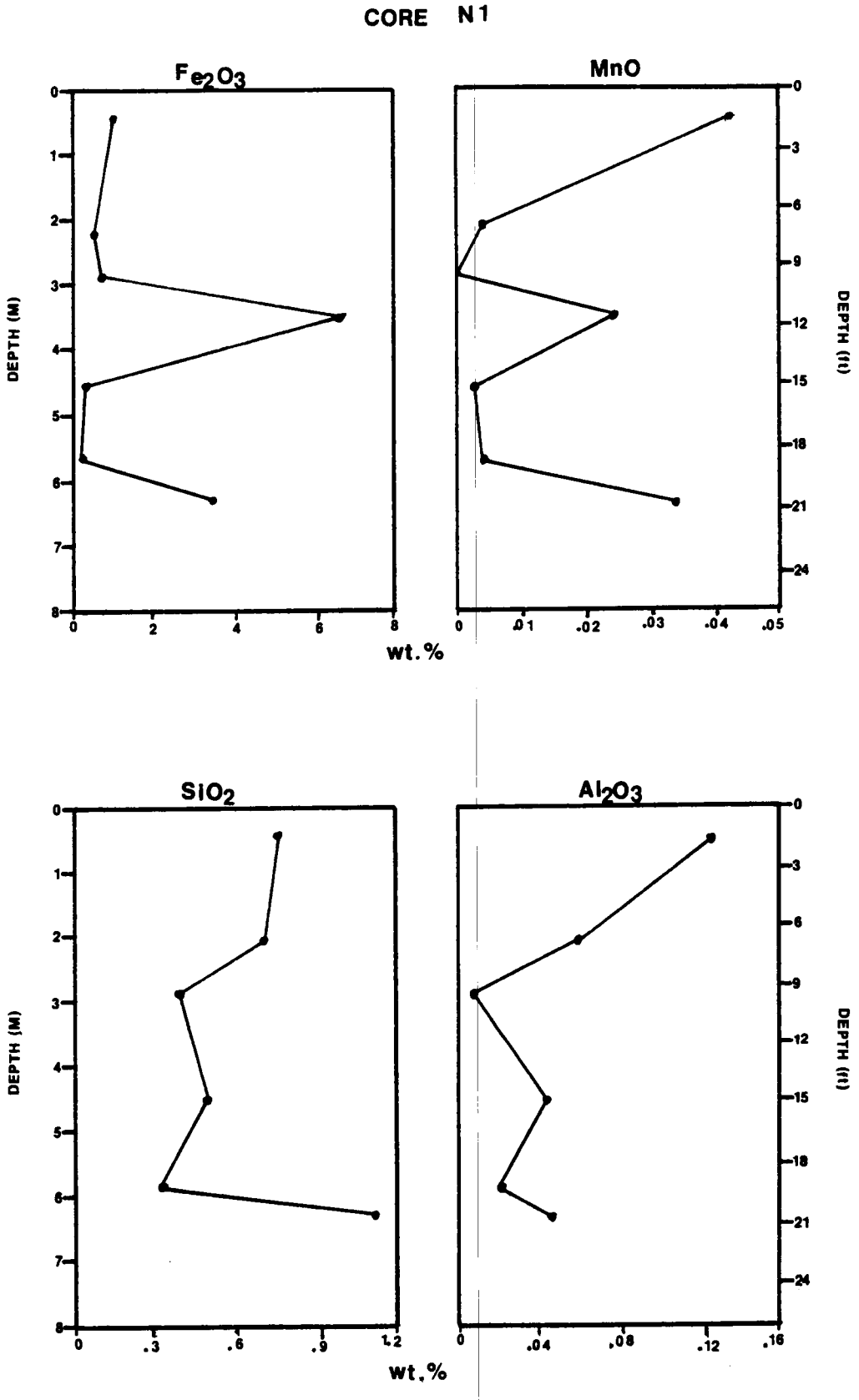

Figure 25. Total CBD and NaOH Extractable Fe, Mn, Si, and Al Oxyhydroxides as a Function of Depth, Core N1. Wt. % Scales Differ.

was not obtained for Core A9 because only two samples were analyzed for both CEC and extractable oxyhydroxides.

Extractable Fe, Mn, Si, and Al Oxyhydroxides of <63 µm-Size Fraction

The extractable oxyhydroxides of Fe, Mn, Si, and Al exist as amorphous coatings on minerals and as discrete particles (Jenne, 1977, p. 456-465). The Fe and Mn were mostly removed by the CBD extraction, whereas the Si and Al were mostly removed by the NaOH extraction (Tables 6 and 7).

The CBD extractable Fe ranged from 0.10 to 5.89 weight % as Fe_2O_3. Lee et al. (1984) observed a range of 2.7 to 9.2 weight % Fe_2O_3 for regolith material at WCRS. An important distinction is that Lee et al. examined the <2 µm-size fraction, a larger weight % Fe_2O_3 for the <2 µm-size fraction is expected due to its larger surface area. For one sample, Jenne (1977) records a 11.2 weight % Fe_2O_3 for the <2 µm-size fraction for limestone soils in the Appalachians, though the extraction technique is not given. Miller (1972, p. 71) observed a range of 2 to 6 weight % free iron oxide (assumed to be Fe_2O_3) for regolith similar to regolith at WCRS.

Manganese extracted by CBD ranged from minute amounts below the detection level of the AA to 0.43 weight % MnO. Silicon in the CBD extract ranged from trace amounts (<0.0095 wt. %) to 0.36 weight % SiO_2. CBD extractable aluminum ranged from trace amounts to 0.03 weight % Al_2O_3.

Table 6. CBD Extractable Fe, Mn, Si, and Al.

Sample	Fe_2O_3 (wt%)	MnO (wt%)	SiO_2 (wt%)	Al_2O_3 (wt%)
N1-1.2	1.08	0.43	0.01	Tr
N1-6.2	0.54	0.05	0.03	Tr
N1-9.2	0.83	Tr	0.02	Tr
N1-11.2	5.89	0.25	NA	NA
N1-14.2	1.07	Tr	0.02	Tr
N1-18.2	0.12	Tr	Tr	Tr
N1-20.25	3.62	0.03	0.06	Tr
N2-1.8	3.22	Tr	0.03	Tr
N2-4.5	3.55	Tr	0.03	Tr
N2-7.4	2.53	0.02	0.04	0.01
N2-11.7	3.21	Tr	0.05	Tr
N2-13.8	3.31	0.02	0.04	Tr
N2-15.2	2.68	Tr	0.05	Tr
N2-17.4	2.63	0.13	0.04	Tr
N2-21.7	0.83	0.07	0.03	Tr
A8-1.25	0.10	Tr	0.01	Tr
A8-7.3	3.36	Tr	0.36	Tr
A8-14.5	3.16	0.03	0.05	0.03
A9-3.9	0.98	0.03	0.05	Tr
A9-4.4	0.73	0.04	0.03	0.02
A9-13.7	2.34	Tr	0.04	Tr
A19-1.25	0.34	0.12	0.02	Tr
A19-4.5	0.88	0.19	0.03	Tr
A19-9.25	0.34	Tr	0.04	0.01
A19-19.25	0.78	Tr	0.03	0.01

Tr = Trace (<0.0095 wt%).

NA = Sample Not Analyzed.

Table 7. 0.5 N NaOH Extractable Fe, Mn, Si, and Al.

Sample	Fe_2O_3 (wt%)	MnO (wt%)	SiO_2 (wt%)	Al_2O_3 (wt%)
N1-1.2[a]	0.02	Tr	0.08	0.13
N1-6.2	Tr	Tr	0.05	0.07
N1-9.2[a]	Tr	Tr	0.02	Tr
N1-11.2	0.16	Tr	NA	NA
N1-14.2	0.01	Tr	0.04	0.04
N1-18.2[a]	0.02	Tr	0.03	0.02
N1-20.25	0.01	Tr	0.05	0.06
N2-1.8	0.03	Tr	0.12	0.40
N2-4.5	Tr	Tr	0.05	0.11
N2-7.4	0.04	Tr	0.09	0.16
N2-11.7	0.03	Tr	0.10	0.15
N2-13.8	0.03	Tr	0.08	0.13
N2-15.2[a]	0.01	Tr	0.03	0.04
N2-17.4[a]	0.02	Tr	0.04	0.07
N2-21.7[a]	0.02	Tr	0.04	0.06
A8-1.25	0.01	Tr	0.05	0.11
A8-7.3	0.02	Tr	0.10	0.14
A8-14.5	0.01	Tr	0.05	0.17
A9-3.9	0.02	Tr	0.05	0.07
A9-4.4	0.01	Tr	0.06	0.11
A9-13.7	Tr	Tr	0.06	0.10
A19-1.25	Tr	Tr	0.11	0.20
A19-4.5	0.01	Tr	0.11	0.19
A19.9-9.25	Tr	Tr	0.06	0.13
A19-19.25	Tr	Tr	0.07	0.11

[a] Developed a rust-colored precipitate.

Tr = Trace (<0.0095 wt%).

NA = Sample Not Analyzed.

The NaOH extractable iron ranged from trace amounts to 0.16 weight % Fe_2O_3. Manganese in the NaOH extract was essentially undetectable with AA. Silicon in the NaOH extract ranged from 0.02 to 0.12 weight % SiO_2. Aluminum extracted by the NaOH treatment ranged from trace amounts to 0.40 weight % Al_2O_3. Weight % amorphous oxyhydroxides versus depth diagrams are illustrated in Figures 25 to 29.

The amorphous oxhydyroxides tend to be most concentrated in the near-surface samples, due to the effects of weathering, as illustrated by the most completely sampled cores, N1 and N2 (Figures 25 and 26).

The fact that amorphous oxhydroxides of Fe, Mn, Si, and Al can be extracted illustrates their vulnerability to chemical alteration which might occur if regolith is used in landfill construction. Examples include an increase in solubility of Fe and Mn due to reduction, the susceptibility of Fe and Mn to be chelated by organic substances, and the formation of soluble sodium silicates and sodium aluminates (Jackson, 1965). Fuller (1978) explains that the chemical nature of regolith used in the construction of landfills often changes when exposed to a wide variety of waste chemicals. It is therefore recognized that though certain amorphous oxhyhydroxides may have the ability to adsorb selective metals, even to a greater degree than aluminosilicate clays (Jenne, 1977), their chemical nature is subject to alteration when exposed to changes in chemical environments.

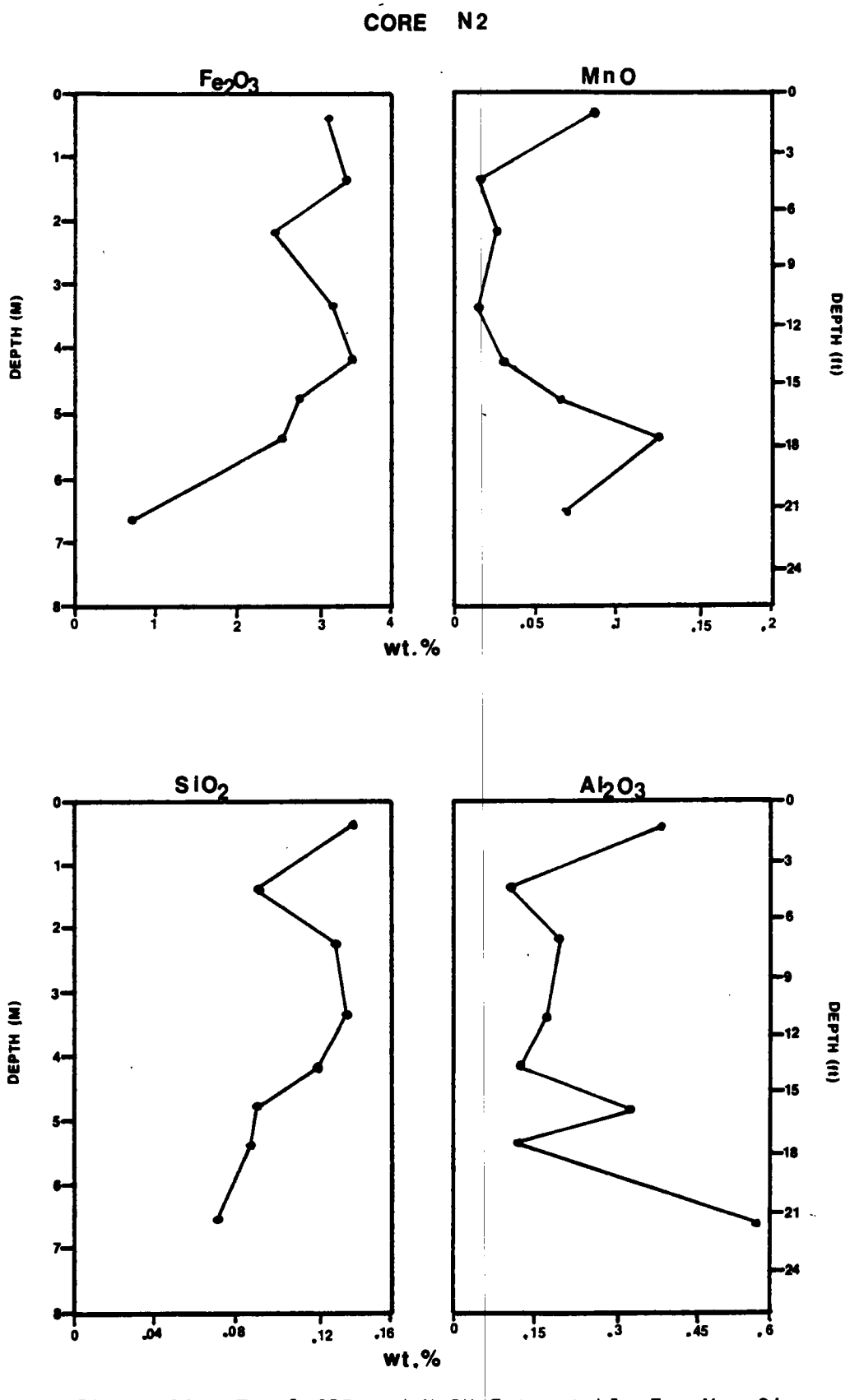

Figure 26. Total CBD and NaOH Extractable Fe, Mn, Si, and Al Oxyhydroxides as a Function of Depth, Core N2.

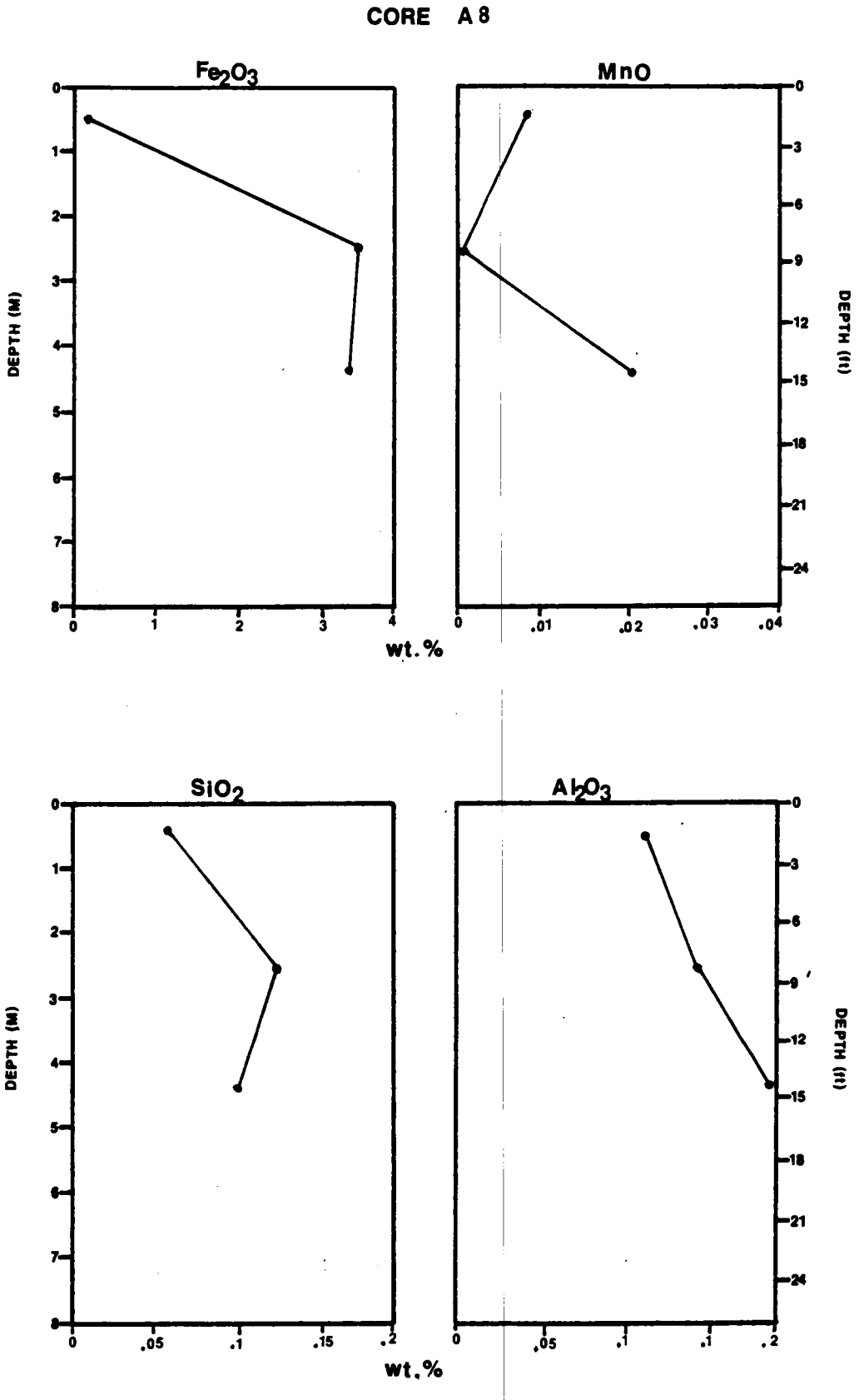

Figure 27. Total CBD and NaOH Extractable Fe, Mn, Si, and Al Oxyhydroxides as a Function of Depth, Core A8.

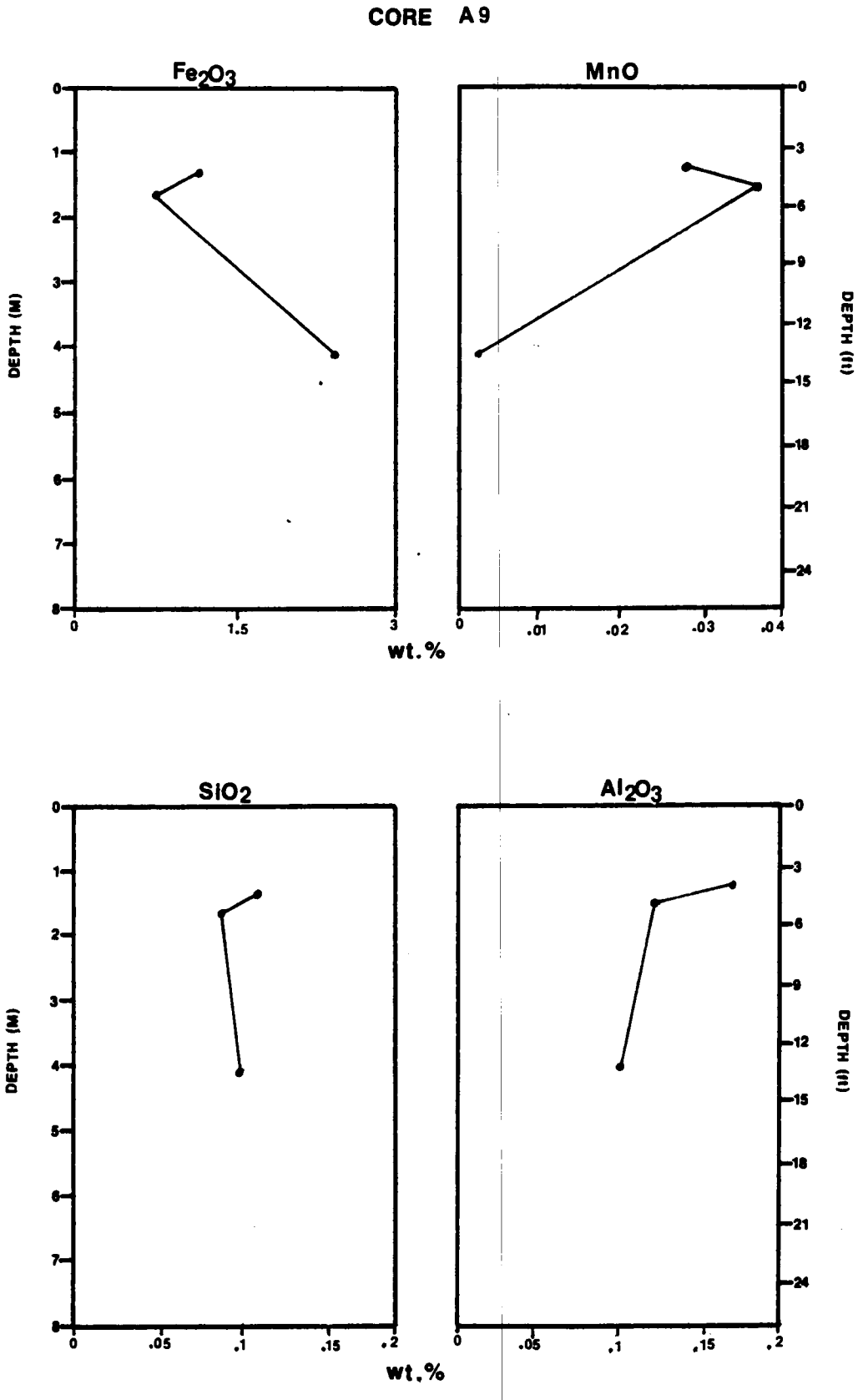

Figure 28. Total CBD and NaOH Extractable Fe, Mn, Si, and Al Oxyhydroxides as a Function of Depth, Core A9.

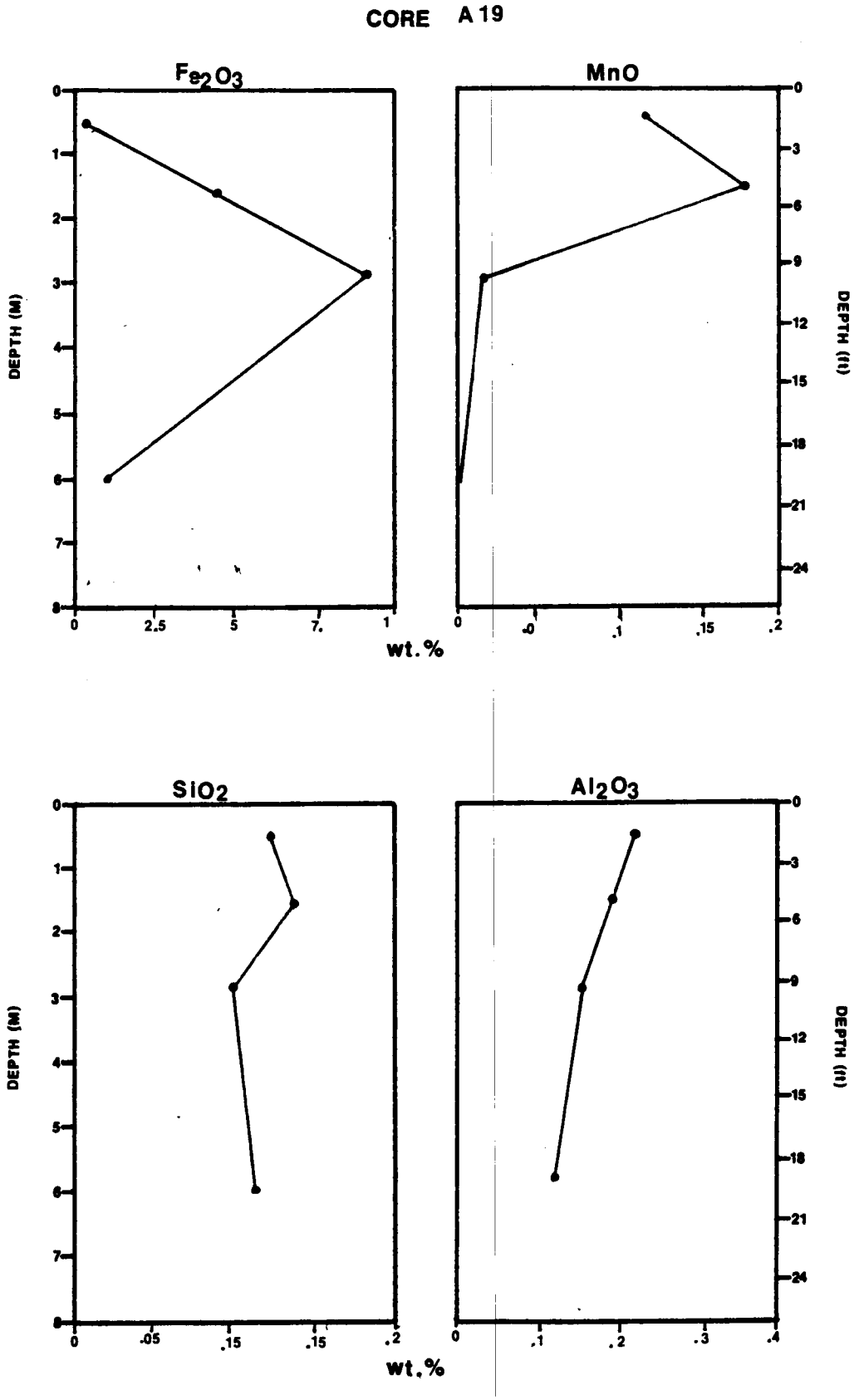

Figure 29. Total CBD and NaOH Extractable Fe, Mn, Si, and Al Oxyhydroxides as a Function of Depth, Core A19.

Insoluble Rust-Colored Precipitate in NaOH Extracts

Six samples out of the total 24 which were treated with NaOH developed a noticeable rust-colored precipitate (Table 7). The Fe-rich precipitate was isolated, dried, and weighed. The samples, which contained the precipitates and their comparative amounts, are given in Table 8.

Table 8. Rust-Colored Insoluble Precipitates in 0.5 N NaOH Extracts.

Sample	Precipitate wt. (g)	Precipitate wt. %
N1-1.2	0.06	1.2
N1-9.2	0.01	0.5
N1-18.2	0.02	0.4
N2-15.2	0.01	0.5
N2-17.4	0.01	0.5
N2-21.7	0.04	2.0

CHAPTER IV

SUMMARY AND CONCLUSIONS

Summary

Samples from the WCRS were taken at various depths from seven cores which were drilled through three soil types: Dewey, Decatur, and Fullerton variants. The soils are predominately Ultisols (Typic and Rhodic Paleudults). The soils manifest themselves in a spatially complicated pattern due to a combination of heterogeneous bedrock parent material and various geomorphic processes.

Standard analytical methods were used in this study with the exception of the method for determining ion exchange capacity using $BaCl$ and analyzing for adsorbed Ba and Cl with XRF.

Results of particle size analysis indicates clay concentration generally reaches a maximum near a depth of 3 meters. Sand and silt fractions tend to be most concentrated near the surface except for an occasional abrupt increase which represents a siliceous layer in the parent carbonate bedrock. The gravel-size fraction shows the most concentration variation with depth, again due to inherited stratigraphy from the bedrock. Field observations at WCRS reveal large concentrations of gravel, cobble, and boulder-size chert on the land surface which has accumulated as smaller particles have been washed away.

The pH in distilled water and salt pH was determined on samples from cores N1, N2, A8, and A9. The pH measurements

ranged from 5.7 to 4.5. Salt pH, in general, decreased by about 1 pH unit relative to pH in distilled water, except for the near-surface samples which only decreased a few tenths of a unit due to the buffering effects of organic matter.

X-ray bulk mineralogy (<2 mm) was determined for 16 randomly chosen samples, with at least one sample from each core, using the pack mount method. There was little variation among samples and all samples were predominately quartz with minor clay peaks of kaolinite, illite, and HIV.

The clay-size fraction was further analyzed using XRD and a smear mount technique. The major minerals (based on peak size) were kaolinite, quartz, illite, and HIV, respectively. The content of kaolinite and its degree of crystallinity increases with depth. Quartz is present in varying amounts in all samples and becomes less abundant as particle size decreases. Illite concentration increases with depth and has been shown by Miller (1972) to be a major phyllosilicate constituent of the unweathered carbonate rock. HIV is most abundant in the upper soil horizons and its concentration decreases with depth as illite, correspondingly, increases.

Magnetic sand-sized nodules were revealed by XRD to be composed of maghemite, hematite, and quartz. The magnetic nodules were found to be most concentrated in the upper soil horizons and their abundance quickly decreased with depth.

Analysis of 16 elements for each sample was conducted on the <2 mm fraction using XRF. Concentrations of the soluble elements,

Mg, K, Ca, and Rb, were high at the surface due to biocycling by plants and introduction as fertilizers. These soluble elements decrease with depth in the tree-rooting zone until their concentrations again increase in the residua, thereafter showing irregular variation most likely due to inherited stratigraphy. The insoluble elements show no clear trend with depth except Al tends to closely follow the weight % clay content, Fe and Ti often have similar trends, and Si and Al are inversely correlated.

Ion exchange capacity was calculated for cores N1, N2, A8, and A9 using Ba^{2+} and Cl^{-} as index ions using an XRF method. Cation exchange capacities ranged from 30 to 200 mmol $(\frac{1}{2}Ba^{2+})\cdot kg^{-1}$. Anion exchange capacities were very low, below the detection sensitivity of the XRF method. Correlation coefficients for CEC versus clay content were 0.77 for Core N1, 0.54 for Core N2, 0.98 for Core A8, and 0.22 for Core A9. Correlation coefficients for CEC versus total extractable oxyhydroxides were 0.89 for Core N1, 0.24 for Core N2, and 0.99 for Core A8. Oxyhydroxide data were obtained on different samples than CEC data for Core A9.

Oxyhydroxides of Fe, Mn, Si, and Al were extracted using CBD and NaOH treatments. Extractable Fe ranged from 0.10 to 5.89 weight % Fe_2O_3 in the CBD extracts and trace amounts (<0.0095 wt. %) to 0.16 weight % in the NaOH extracts. Mn extracted by CBD ranged from trace amounts to 0.43 weight % MnO and was essentially undetectable in the NaOH extracts. Si extracted by CBD ranged from trace amounts to 0.36 weight % SiO_2 and 0.02 to 0.12 weight

% in the NaOH extracts. Al extracted by CBD ranged from trace amounts to 0.03 weight % Al_2O_3 and from trace amounts to 0.40 weight % in the NaOH extracts.

Amorphous oxyhydroxides were most concentrated in the highly weathered, near-surface samples as illustrated by the most thoroughly analyzed cores, N1 and N2. Extractable amorphous phases of cores of N1 and N2 show concentration versus depth trends similar to those of CEC. Abrupt variability of the extractable oxhydroxides is presumed to be due to chemical heterogeneity of the bedrock which is preserved in the residuum or to discontinuities representing ancient alluvium.

Insoluble rust-colored precipitates developed in six of the 24 NaOH extracts which were dried and weighed to provide information on which samples may contain more Fe than was measured by the AA.

Conclusions

The adsorption capacity of the regolith is likely to change after it has been subjected to chemical waste. The fact that oxyhydroxides of Fe, Mn, Si, and Al can be extracted by CBD and NaOH demonstrates their vulnerability to chemical alterations. Also, the regolith displays very little ability to buffer its acidity (Seely and Kelmers, 1984) which may affect the exchange characteristics of the amphoteric amorphous phases. This is important since certain amorphous oxyhydroxides may have a greater ability to adsorb selective metals than aluminosilicate clays (Jenne, 1977).

Anionic species, such as I^- and TcO_4^-, are not significantly attenuated by regolith at WCRS compared to cations such as UO_2^{2+} (Seely and Kelmers, 1984). This observation was corroborated by the inability to measure significant anion exchange capacity using the XRF method.

HIV is a weathering product of illite in the regolith at WCRS. Illite is commonly the precursor material which alters to HIV upon weathering (Buol et al., 1973). Miller (1972) describes the process by which illite is transformed into HIV. In all seven cores a decrease in HIV and proportional increase of illite with depth was observed.

The heterogeniety of the Knox Group, as described by Milici (1973), is preserved in the regolith. Bulk chemical analyses, amorphous oxyhydroxides, particle size distribution, CEC, and physical appearance all display erratic trends. Those in Core N1 are the best examples.

Mineral destruction due to weathering is greatest in the samples nearest the surface. In the surface samples there is the highest concentration of amorphous oxyhydroxides, poorly crystallized kaolinite which becomes more crystallized with depth, and an absence of weatherable minerals such as illite.

Paradoxically, the soluble base cations of Mg, K, Ca, and Rb tend to be relatively concentrated in the samples nearest the surface and decrease in concentration with depth until about 2 meters (out of reach of most plant roots). The elements then exhibit variable concentration trends. Biocycling, i.e., the

extraction of nutrient elements from the soil by plants and their subsequent redeposition on the soil surface as plant debris, is most likely the main process. Agricultural fertilization until the early 1940's may also have contributed to the high surface concentrations of Mg, K, Ca, and Rb.

Suggestions for Future Research

In future studies, it would be beneficial if ion exchange capacities were measured using columns of intact regolith rather than crushed samples. This would more closely simulate natural conditions because macropores would not be destroyed and artificially high surface areas would not be created. Known concentrations of index ions could be applied in measured intervals to the top of the column and corresponding measurements made of the index ion in the leachate.

When measuring the anion and cation exchange capacities of regolith with high concentrations of kaolinite and amorphous oxyhydroxides, it is important to record the pH values of the samples at which the exchange capacities are measured. Kaolinite and amorphous oxyhydroxides are amphoteric, meaning their ability to adsorb and exchange ions varies with pH.

The regolith under investigation in this study often changes characteristics in short distances. Cores N1 and N2, which had the most thorough coverage, demonstrated the limited information obtainable from cores with few and widely spaced samples, such as A8, A9 and A11. Future studies of this type of geomedia should

sample the material at small intervals (approximately 0.5 meters) if accurate mineralogical and chemical trends are to be obtained.

The AA was used to determine Fe and Mn in the CBD and NaOH extracting solutions. Because these extracting solutions have such a high Na content, they tend to salt-up the AA which reduces the accuracy and precision. In the future, other techniques should be used for the determination of elemental concentrations. The possibilities include XRF and colorimetric methods.

The dissolution of parent rock by laboratory techniques and the identification of insoluble minerals would provide valuable information which would allow for an estimate of the degree of secondary mineral formation, i.e., whether the minerals comprising the residua have merely weathered out of the parent rock or whether there has been significant secondary mineral formation. Also, chemical analysis of the parent rock which can then be compared to chemical analysis of residua, especially of insoluble elements like zirconium and titanium would give an estimate of the amount of material that would have to be weathered in order to accumulate a certain amount of residua.

Information about the rust-colored precipitates which developed in the NaOH extracts has been provided in case some interested party should desire to explain why only particular samples developed the precipitates and what exactly is the composition of the precipitate, i.e., Fe^{2+}, combinations of Fe^{3+}, and combinations of Fe^{2+} with reduced forms of Mn, etc.

LIST OF REFERENCES

LIST OF REFERENCES

Allman, M. and D. F. Lawrence, 1972. Geological Laboratory Techniques. Arco Publishing Co., Inc. New York: 186-191.

Aubertin, G. M., 1971. Nature and extent of macropores in forest soils and their influence on subsurface water movement. Forest Service Res. Pap. NE (U.S.) 192PS, 33 pp.

Beasly, R. S., 1976. Contribution of subsurface flow from the upper slopes of forested watersheds to channel flow. Soil Sci. Soc. Am. J., 40:955-957.

Beven, K. and P. Germann, 1982. Macropores and water flow in soils. Water Resources Research, Vol. 18, No. 5, 1311-1325.

Brady, N. C., 1974. The Nature and Properties of Soils (8th Edition). MacMillan Publishing Co., Inc. New York.

Bretz, J. H., 1965. Geomorphic history of the Ozarks of Missouri. State of Mo. Dept. of Business and Admin., Division of Geol. Survey and Water Resources, Rolla, Mo.

Bridge, Josiah, 1956. Stratigraphy of the Mascot-Jefferson City zinc district, Tennessee. U.S. Geol. Survey Prof. Paper 277:31-48.

Buol, S. W., F. D. Hole, and R. J. McCracken, 1973. Soil Genesis and Classification. The Iowa State University Press, Ames, Iowa.

Clark, G. M., 1973. Some Geomorphic Aspects and Problems Related to the Knox County Area, Tennessee. Tennessee Division of Geology, Bulletin 70.

Dokuchaev, V. V., 1883. Russian Chernozem (Russkii Chernozem). (Transl. from Russian by N. Kaner.) Israel Prog. for Sci. Trans., Jerusalem, 1967. Available from U.S. Dept. Commerce, Springfield, Va.

Follet, E. A. C., W. J. McHardy, B. D. Mitchell, and B. F. L. Smith, 1965. Chemical dissolution techniques in the study of soil clays: Parts I and II. Clay Minerals, 6:23-43.

Fuller, W. H., 1977. Movement of Selected Metals, Asbestos, and Cyanide in Soil: Application to Waste Disposal Problems. EPA-600/2-77-020, U.S. EPA Municipal Environmental Research Laboratory, Cincinnati, Ohio 45268.

Fuller, W. H., 1978. Investigation of Landfill Leachate Pollutant Attenuation by Soils. EPA-600/2-78-158, U.S. EPA Municipal Environmental Research Laboratory, Cincinnati, Ohio 45268.

Gamble, E. E., R. B. Daniels, and W. D. Nettleton, 1970. Geomorphic surfaces and soils in the Black Creek Valley, Johnson County, North Carolina. Soil Sci. Soc. Am. Proc., 34:276-281.

Grim, Ralph E., 1968. Clay Mineralogy (2nd Edition). McGraw-Hill Book Co., New York.

Goldschmidt, V. M., 1937. The principles of distribution of chemical elements in minerals and rocks. J. Chem. Soc., 139:655-675.

Govett, G. J. S., 1961. Critical factors in the colorimetric determination of silica. Anal. Chim. Acta, 25:69-80.

Harris, L. D., 1969. Kingsport Formation and Mascot Dolomite (Lower Ordovician) of East Tennessee. Tenn. Div. Geology Rept. Invs., No. 23:1-39.

Hashimoto, I. and M. L. Jackson, 1960. Rapid dissolsution of allophane and kaolinite-halloysite after dehydration. Clays and Clay Minerals, 7:102-113.

Hsu, P. H., 1963. Effect of initial pH, phosphate, and silicate on the determination of aluminum with aluminon. Soil Sci., 96:230-238.

Huang, P. M. and S. Y. Lee, 1969. Effect of drainage on weathering transformations of mineral colloids of some Canadian prairie soils. Proc. Int. Clay Conf.--Tokyo, Japan. 541-551.

Jackson, M. L., 1963. Aluminum bonding in soils: A unifying principle in soil science. Soil Sci. Soc. Am. Proc., 27:1-10.

Jayman, T. C. Z. and S. Sivasubramaniam, 1974. The use of ascorbic acid to eliminate interference from iron in the aluminon method for determining aluminum in plant and soil extracts. Analyst (London), 99:296-301.

Jenne, E. A., 1977. Trace element sorption by sediments and soils--Sites and processes. Molybdenum in the Environment: Chappell, W. R. and K. K. Petersen, eds. Marcel Dekker, New York. 425-465.

Ketelle, R. H. and D. D. Huff, 1984. Site characterization of the West Chestnut Ridge Site. ORNL/TM-9229. Oak Ridge National Laboratory, Oak Ridge, Tennessee.

Khalifa, E. M. and S. W. Buol, 1968. Studies of clay skins in a Cecil (Typic Hapludult) soil. I. Composition and genesis. Soil Sci. Soc. Am. Proc., 32: 857-861.

Kopp, O. C. and S. Y. Lee, 1985. An unusual occurrence of maghemite in soils developed on Knox Group dolostone. Abstract presented at the 1985 International Clay Conference, Denver, CO, July 28-August 2, 1985.

Kunze, G. W., 1965. Pre-treatment for mineralogical analysis. Methods of Soil Analysis, Part I. American Society of Agronomy. Madison, Wisconsin. 574-576.

Lee, S. Y., O. C. Kopp, and D. A. Lietzke, 1984. Mineralogical characterization of West Chestnut Ridge Soils. ORNL/NFW-84/25. Oak Ridge National Laboratory, Oak Ridge, Tennessee.

McLean, E. O., 1982. pH measurements. Methods of Soil Analysis, Part 2 (2nd edition). American Society of Agronomy, No. 9. Madison, Wisconsin. 208-209.

Mehra, O. P. and M. L. Jackson, 1960. Iron oxide removal from soils and clays by a dithionite-citrate system buffered with sodium bicarbonate. Clays and Clay Minerals, 7:317-327.

Milici, R. C., 1973. The Stratigraphy of Knox County, Tennessee. Tennessee Division of Geology Bulletin 70, p. 15.

Miller, B. J., 1972. Relationship of soil properties to transformation of carbonate rocks into soil. University of Tennessee, Doctoral dissertation.

_____. 1983. Ultisols. pp. 283-318. In L.P. Wilding, N.E. Smeck, and G.F. Hall (eds.). Pedogenesis and Soil Taxonomy (Developments in Soil Science, IIB, The Soil Orders). Elsevier, New York.

Mosley, M. P., 1982. Subsurface flow velocities through selected forest soils, South Island, New Zealand. J. Hydrol., 55:65-92.

Rhodes, J. D., 1982. CEC Determination. Methods of Soil Analysis, Part 2 (2nd edition). American Society of Agronomy, No. 9. Madison, Wisconsin. p. 150.

Rich, C. I. and S. S. Obenshain, 1955. Chemical and clay properties of a red-yellow- Podizolic soil derived from musconite schist. Soil Sci. Soc. Am. J., 19: 334-339.

Ristvet, B. L., 1978. Reverse weathering reactions within recent nearshore marine sediments, Kaneohe Bay, Oahu. Defense Nuclear Agency, Test Directorate Field Command, Kirtland AFB, New Mexico 87115.

Schwertmann, U., 1959. Die fraktionierte Extraktion der freien Eisenoxyde in Boden, ihre mineralogischen Formen und ihre Entstehungsweisen. Z. Pflanz, Dung. Boden, 84:194-204.

Seeley, F. G. and A. D. Kelmers, 1984. Geochemical information for the West Chestnut Ridge Central Waste Disposal Facility for low-level radioactive waste. ORNL-6061. Oak Ridge National Laboratory, Oak Ridge, TN 37830.

Simonson, R.W., 1949. Genesis and classification of red-yellow Podzolic soils. Soil Sci. Soc. Am. Proc., 14:316-319.

Sledz, J. G., 1980. Petrologic, mineralogic, and ion exchange characteristics of the Rome Formation and Pumpkin Valley Shale on the Oak Ridge National Laboratory Reservation, Oak Ridge, Tennessee. Appendix 2. Masters Thesis, The University of Tennessee.

Springer, M. E. and J. A. Elder, 1980. Soils of Tennessee. Bull. 596, U.T. Agricultural Experiment Station and the USDA Soil Conservation Service. p. 46.

Swingle, G. D., 1959. Geology, Mineral Resources, and Ground Water of the Cleveland Area, Tennessee. Tenn. Div. of Geology, Bulletin 61:33-38.

Tamura, T., 1957. Identification of the 14 A clay mineral component. Am. Mineral, 42:107-110.

Triegel, E. K., 1980. Attenuation by soils of selected potential contaminants from coal conversion facilities: A literature review. ORNL/TM-7249, Oak Ridge National Laboratory, Oak Ridge, Tennessee.

Tweneboah, C. K., D. J. Greenland, and J. M. Oades, 1967. Changes in charge characteristics of soils after treatment with 0.5 M calcium chloride at pH 1.5. Aust. J. Soil Res., 5:247-261.

U.S. Department of Agriculture, 1975. Soil Taxonomy, Handbook 436, Soil Conservation Service, Washington, D.C.

Woodward-Clyde Consultants, 1984. Subsurface characterization and geohydrologic site evaluation, West Chestnut Ridge Site. ORNL/Sub/83-647641/IvI2. Prepared by Woodward-Clyde Consultants, Wayne, New Jersey, for Oak Ridge National Laboratory, Oak Ridge, Tennessee.

APPENDICES

APPENDIX A

EXPLANATION AND KEY TO SOIL MAPPING UNIT CLASSIFICATION USING THE COMPREHENSIVE SOIL SURVEY SYSTEM

Soils are classified in the United States using the comprehensive Soil Survey System. This system was developed by the Soil Survey Staff of the U.S. Department of Agriculture through several stages or "approximations." The seventh approximation evolved into the 1975 edition of Soil Taxonomy through a couple of intermediate stages. Soils are placed in six categories: order, suborder, great group, subgroup, family, and series. An example will be used to explain the method using the soil series Decatur (Cores N2 and A12) which is classified as clayey, kaolinitic, thermic Rhodic Paleudult. The following discussion is based on Soil Taxonomy (1975), Springer and Elder (1980), and Brady (1975). The reader is referred to Soil Taxonomy (1975) for detailed specifications for each of the subdivisions.

Order

Decatur belongs to the Ultisol order as indicated by the "ult" ending of Paleudult. Ultisols (Latin ultimus, last) are usually moist soils developed under warm to tropical climates. They are highly weathered and acidic, but may still have some weatherable minerals such as illite. They have argillic horizons

with base saturation lower than 35 weight percent. Ultisols mostly form on old land surfaces under forest vegetation.

Suborder

Decatur belongs to the Udult suborder. Each suborder name has two syllables. "Ud" (Latin udus, humid) indicates a humid moisture regime and is combined with the order syllable "ult."

Great Group

The great group is formed by adding a prefix to the suborder. The prefix groups soils with similar degrees of development, moisture and temperature regimes, and base saturation. Decatur is a Paleudult. "Pale" (Greek paleos, old) indicates excessive development by having properties such as a thick argillic horizon, plinthite, low base saturation, and a small amount of weatherable minerals.

Subgroup

Each subgroup is identified by one or more adjectives preceding the great group. Decatur is a Rhodic Paleudult. Rhodic (Greek rhodon, rose) means dark-red color, usually due to large amounts of free iron oxide and has more total phosphorus than soils of the Typic suborder.

Family

Family is a subdivision of the subgroup, made on the basis of physical and chemical properties such as particle size, mineralogy, pH, temperature, and thickness of rooting zone. Decatur

belongs to the family clayey, kaolinitic, thermic. Clayey meaning $\geq$ 35 weight percent clay, kaolinitic meaning the >2 μm-size fraction is more than half kaolinitic; and thermic meaning annual soil temperature is between 15°C and 22°C.

Series

All soils in a series have horizons that are similar in composition, thickness, and arrangement. A series generally takes on the name of a place where the soil was first described, such as Decatur, Tennessee.

Table A1. Names and Formative Elements Used in This Report.

Names and Formative Elements	Derivation or Significance	Connotations
Clayey	particle size class	<35 vol. % >2mm; ≥35 wt. % clay
Clayey-skeletal	particle size class	<35 vol. 5 >2mm; ≥35 wt. % clay
Entisol	"ent" from recent	soil order, young soil
Fine-loamy	particle size class	>15 wt. % 50μm; 18-34 wt. % clay
Fragic	L. fragilis, brittle	brittle pan
Inceptisol	L. inceptum, beginning	young, but more advanced than Entisols
Mixed	mineralogy class	contains <40 wt. % of any one mineral other than quartz or feldspar
Oxidic	mineralogy class	(iron oxide + gibbsite: clay ratio ≥0.2
Pale	Gr. paleos, old	excessive development
Rhodic	Gr. rhodon, rose	dark-red color
Siliceous	mineralogy class	90 wt. % SiO_2
Thermic	soil temperature regime	mean annual soil temp. between 15° - 22°C
Typic	subgroup adjective	signifies most common properties
Ud	L. udus, humid	suborder moisture regime
Ultisol	L ultimus, last	soil order; stable, mature, highly weathered soil

APPENDIX B

DESCRIPTIONS OF SOIL MAPPING UNITS[1]

This appendix describes the soil mapping units which are presented in Figure 2.

Soil No. 1 (Copper Ridge and Chepultepec Colluvium, Shack or Tasso Series)

This soil is moderately-well to somewhat poorly drained due to fragic properties in subsurface horizons. This soil formed in colluvium which has collected on footslopes, saddles, sinkholes, and on the gently sloping sides of ridges. It has, except for some minor areas, a high chert content throughout the soil profile. The fragipan, usually formed in the lithologic discontinuity, has an advanced degree of development where this soil occurs on low toeslopes. This soil grades into soils No. 2 and No. 5, where side slopes meet ridge tops and where slopes become too steep for colluvium to collect.

Soil No. 2 (Longview Soil, Fullerton Series)

This well-drained soil is mostly underlain by the Chepultepec and Kingsport formations. It is very cherty throughout the entire profile, which distinguishes it from soil No. 5. It has a gray E horizon which begins just below the leaf litter and a red clayey subsoil beneath containing abundant chert gravels and cobbles. Chert boulders are visible on the surface in many areas.

1 After Lee et al., 1984.

Soil No. 3 (Ancient Alluvium, Dewey-Decatur Series)

This soil has a dark-brown A horizon and a deep dark-red silty clay loam subsoil with low chert content. It occupies the ridge top and southeastern sideslope of the northeasternly-most ridge in the study area. It is adjacent to soils No. 5 and 1, having relatively abrupt boundaries. In some level and depressed areas, a fragipan has formed but these are minor in extent. The chert in the profile is pebble-size, and iron/manganese nodules are common.

Soil No. 4 (Chepultepec Soil, Dunmore Series)

This soil is underlain by the Chepultepec Dolomite. It forms on a few island-type areas where the Chepultepec has not been covered by colluvium or alluvium. This soil is characterized by a strong brown clayey subsoil. It has a high lag chert content, especially in the upper two feet (0.6 meters).

Soil No. 5 (Copper Ridge Soil, Fullerton and Collegedale Series)

This soil is underlain by the Copper Ridge Dolomite. It is characterized by an abrupt loss of chert below a chert lag zone which is usually at the top of the Bt_2 horizon. It occurs on ridge tops and steep side slopes. It is well drained with an E horizon beginning just below the leaf litter and has a red clayey subsoil with common yellow mottles. The chert is commonly oolitic as well as large massive and small chalky types.

Soil No. 5a (Copper Ridge-North Aspect, Dunmore Series)

This soil is distinguished from Soil No. 5 because of its noticeably lower chert content. Like Soil No. 5, it is well-drained, has an E horizon extending to the surface, and has a clayey subsoil. The chert present is the pebble-sized oolitic type.

Soil No. 6 (Undifferentiated Modern and Holocene Alluvium)

This unit consists of undifferentiated alluvial soils. The soils are Entisols and Inceptisols. Most Entisols are underlain by a buried soil with 1.5 meters.

Soil No. 7 (Kingport Soil and Colluvium over the Kingsport Formation, Dunmore Series)

This soil is underlain by the Kingsport Formation and occupies the eastern side of the most southerly ridge of the study site. It has a brown silty A horizon and a clayey subsoil which gradually becomes redder with depth. It has a low chert content; however, in many places Longview chert has moved downslope and covered its surface. The chert in the profile is white and pebble-size and quite highly weathered. The included colluvial soils typically do not have a subsoil horizon with fragipan properties.

Soil No. 8 (Late Pleistocene Alluvium, Holston Series)

This soil formed in an alluvial fan which occurs near the New Zion Cemetery. It has a loamy brown A horizon with a brown clay loam subsoil.

Soil No. 9 (Late Pleistocene Terrace, Etowah Series)

This soil formed in toe slope colluvium and alluvium. It has a dark-brown A horizon and a reddish silty clay grading to clay loam subsoil. Most of it lies adjacent to soil No. 8 on the southwestern side of the survey area.

APPENDIX C

Bulk Chemical Analysis

Table C1. Bulk Chemical Analysis Using XRF.

Sample	Na_2O	MgO	Al_2O_3	SiO_2	P_2O_5	S	K_2O	CaO	TiO_2	MnO	Fe_2O_3	Ba	Cr[1]	Rb[1]	Sr[1]	Zr[1]	Total[2]
	wt. %												µg/g				
N1- 1.2	.31	.39	9.36	78.66	.05	ND	.68	.20	1.06	.12	3.90	.03	102	89	67	47	94.81
N1- 6.25	.41	.27	7.84	84.25	.00	ND	.53	.12	.27	.02	2.87	ND	92	60	39	31	96.57
N1- 9.2	.44	.83	8.84	83.48	.00	ND	.17	.08	.35	.00	3.54	ND	9	92	45	114	90.96
N1-11.25	.11	.94	25.46	52.54	.07	ND	1.50	.09	.73	.04	9.50	ND	6	92	45	114	90.96
N1-14.2	.34	.58	7.17	85.26	.01	ND	.91	ND	.47	.02	4.55	.02	7	43	44	ND	99.25
N1-18.2	.38	.81	11.73	76.00	.06	ND	1.55	.12	.60	.02	5.26	ND	1029	83	41	95	96.43
N1-20.25	.10	.76	19.77	63.04	.09	ND	1.29	.12	.65	.06	6.94	ND	1049	77	46	100	92.81
N2- 1.8	.40	.54	12.85	73.03	.06	ND	.67	.20	1.25	.36	5.07	ND	8	86	64	453	94.45
N2- 4.5	.60	.26	8.58	79.73	.07	ND	.39	.06	1.06	.05	4.64	ND	9	69	53	517	95.45
N2- 7.4	.18	1.11	18.00	61.40	.06	ND	1.67	.12	.88	.10	8.30	ND	7	101	44	179	91.79
N2- 9.4	.49	1.48	20.51	60.03	.08	ND	2.22	.14	.80	.26	8.38	ND	8	100	40	122	94.37
N2-11.7	.26	1.29	18.31	65.42	.04	ND	1.99	.12	.69	.54	5.85	.03	1081	97	40	104	94.57
N2-13.8	.53	.97	15.75	67.60	.08	ND	1.66	.11	.52	.09	6.69	ND	8	78	36	71	93.97
N2-15.2	.45	1.04	14.48	71.83	.06	ND	1.66	.11	.52	.04	5.40	ND	9	87	39	84	95.58
N2-17.4	1.30	1.43	12.26	53.82	.19	ND	1.84	.15	.54	1.97	5.45	.05	ND	60	36	18	79.01
N2-21.7	.33	1.11	13.14	71.44	.07	ND	1.88	.13	.51	.52	4.30	.00	10	83	39	78	93.43
A8- 1.25	.65	.38	4.23	89.51	.03	ND	.46	ND	.95	.04	2.73	.04	9	46	64	782	99.03
A8- 7.3	.01	.88	13.81	70.70	ND	ND	1.10	ND	.72	.02	6.29	.04	10	72	49	72	93.51
A814.5	.07	1.37	16b.56	59.78	.11	ND	1.98	.02	.94	.05	11.20	.08	3	105	44	16	92.18
A9- 3.9	.30	1.39	19.92	55.45	.20	.01	4.61	1.11	.51	.16	6.75	.05	10	119	72	110	90.52
A9-13.4	.04	7.90	23.38	59.92	.02	ND	1.34	ND	.82	.02	5.17	.05	12	66	57	138	91.50
A11- 1.25	.36	.43	2.27	80.82	.03	ND	.60	.04	1.03	.10	3.87	.03	10	61	75	618	95.65
A11-13.25	.05	1.63	25.48	51.28	.06	ND	3.57	.11	1.34	.03	10.22	.06	8	129	47	126	93.87
A11-24.75	.12	1.53	15.17	63.53	.06	ND	2.94	.08	.91	.14	8.38	.07	9	117	45	107	92.96
A12- 1.25	.39	.62	12.25	73.51	.05	ND	.58	.07	1.07	.18	5.18	.05	9	73	73	62	94.01
A12- 4.1	.39	.53	10.67	74.85	.03	ND	.55	.07	.73	.32	4.27	.05	11	68	73	64	92.52
A12- 4.7	.49	.46	10.29	75.93	.04	ND	.41	ND	1.31	.08	5.54	.05	11	62	66	61	94.63
A12- 5.2	.67	.46	7.36	82.76	.05	ND	.36	ND	1.24	.05	4.40	.04	10	53	64	65	97.39
A12-14.7	.02	1.30	14.10	72.81	.03	ND	2.12	ND	12.00	.02	4.31	.04	1201	71	50	100	95.32
A12-23.5	.13	.90	10.52	79.04	.02	ND	1.51	ND	.47	.06	3.73	.03	11	58	48	74	96.38
A19- 1.25	.72	.43	7.23	82.89	.04	ND	.62	.06	.45	.51	2.19	.04	12	54	77	781	95.27
A19- 4.5	.44	.49	7.75	80.81	.04	ND	.56	ND	.79	.28	3.56	.04	10	57	70	724	94.77
A19- 9.25	.18	.49	11.40	75.79	ND	ND	.43	.04	.73	.02	5.24	.04	12	49	57	128	94.38
A19-19.25	.06	.64	17.54	66.38	ND	.03	.98	ND	.97	.02	5.63	.04	11	65	60	186	92.25
Standard Error of Calibration	(15)	(4)	(8)	(24)	(1)	(1)	(2)	(5)	(1)	(40)	(2)	(1)	(76)	(6)	(7)	(23)	

[1] Expressed in ppm as ug per gram of sample.

[2] Total doesn't always equal 100% because organics, carbonate, and water are not analyzed.

ND = Not Detected.

Table C2. XRF **Replicate Analyses.** Values given in Wt. % unless otherwise indicated by a "p", which indicates ppm given as µg/g.

Element	Standard SC01[1]			Standard S02[2]			Standard S03[3]			Standard S04[4]			Standard DKTB[5]		
	STD Value	$\bar{X}$	SX	STD Value	$\bar{X}$	SX	STD Value	$\bar{X}$	SX	STD Value	$\bar{X}$	SX	STD Value	$\bar{X}$	SX
Na_2O	0.78	0.71	0.21	2.35	2.45	0.27	1.00	0.89	0.09	1.31	1.36	0.20	1.32	1.15	0.14
MgO	2.32	2.45	0.09	0.90	0.90	0.04	8.47	8.84	0.32	0.93	0.92	0.02	1.93	1.67	0.07
Al_2O_3	13.80	13.93	0.17	15.52	15.16	0.09	5.76	5.94	0.20	10.32	9.62	0.11	20.64	20.75	0.21
SiO_2	62.80	63.19	0.53	53.46	53.36	0.10	33.93	34.60	0.51	68.46	70.40	0.43	60.23	58.79	0.40
P_2O_5	0.19	0.18	0.02	0.69	0.65	0.02	0.11	0.09	0.01	0.21	0.20	0.01	0.10	0.09	0.01
S	0.06	0.06	0.01	0.03	0.03	0.01	0.02	0.06	0.01	0.04	0.04	0.01	NA	NA	NA
K_2O	2.65	2.69	0.02	2.95	2.93	0.01	1.40	1.40	0.01	2.08	2.08	0.01	3.87	3.88	0.02
CaO	2.56	2.55	0.02	2.74	2.74	0.02	20.71	20.77	0.25	1.55	1.57	0.01	0.31	0.26	0.01
TiO_2	0.60	0.64	0.02	1.44	1.41	0.03	0.32	0.31	0.01	0.57	0.57	0.01	0.93	0.91	0.03
Cr	NA	120p	9	16p	51p	3	26p	52p	6	155p	5	82p	82p	112p	6
MnO	600p	537p	14	930p	962p	7	670p	508p	15	770p	791p	3	520p	534p	18
Fe_2O_3	5.23	5.21	0.03	7.95	7.86	0.05	2.16	1.46	0.01	3.39	3.42	0.03	6.90	7.07	0.06
Ba	622p	569p	18	1010p	992p	15	280p	198p	17	1780p	522p	12	780p	778p	23
Rb	122p	119p	4	81p	85p	2	41p	35p	1	75p	76p	1	180p	187p	5
Sr	193p	183p	2	340p	342p	3	217p	224p	4	170p	208p	4	160p	156p	2
Zr	178p	182p	5	790p	784p	16	150p	166p	3	310p	434p	7	180p	187p	7

[1] Number of analyses = 4.
[2] Number of analyses = 5.
[3] Number of analyses = 5.
[4] Number of analyses = 4.
[5] Number of analyses = 4.
NA = Not Analyzed.

APPENDIX D

ABSORPTION VALUES AND THEIR STANDARD DEVIATIONS, MEAN ABSORBANCE, AMOUNT OF SAMPLE TREATED AS DETERMINED BY AA

Table D1. Fe in CBD Extract.

Sample	Absorbancy Run 1	Run 2	Run 3	Run 4	$\bar{X}$[a]	σ[b]	Amount treated (grams)
N1- 1.2	.019	.019	.003	.015	.014	.008	5
N1- 6.25	.002	.011	.025	.018	.014	.010	2
N1- 9.2	.052	.019	.006	.002	.020	.023	2
N1-11.25[c]	---	---	---	---	---	---	4
N1-14.2	.016	.029	.023	.031	.025	.007	5
N1-18.2	.002	.008	.002	.003	.004	.003	5
N1-20.25	.035	.048	.027	.048	.040	.010	5
N2- 1.8	.017	.051	.040	.037	.036	.014	2
N2- 4.5	.056	.055	.096	.095	.076	.023	1
N2- 7.4	.041	.039	.072	.066	.005	.017	2
N2-11.7	.060	.078	.065	.073	.069	.008	2
N2-13.8	.064	.081	.076	.062	.071	.009	2
N2-15.2	.048	.043	.070	.069	.058	.014	2
N2-21.7	.031	.029	.011	.009	.020	.012	2
A8- 1.25	.001	.015	.001	.003	.005	.007	2
A8- 7.3	.088	.069	.085	.047	.072	.018	1
A8-14.5	.071	.049	.072	.080	.068	.013	2
A9- 3.9	.058	.016	.007	.011	.023	.024	2
A9- 4.4	.011	.006	.048	.005	.018	.021	2
A9-13.7	.065	.049	.040	.048	.051	.010	2
A19-1.25	.014	.020	.003	.001	.010	.009	2
A19-4.5	.028	.021	.015	.021	.021	.005	2
A19-9.25	.005	.002	.000	.031	.010	.014	2
A19-19.25	.021	.020	.013	.023	.019	.004	2

[a] Mean absorbancy

[b] Standard deviation of absorbancy

[c] Determined with AA by Dr. R. Lewis, Plant and Soil Science Dept., University of Tennessee.

Table D2. Mn in CBD Extract.

Sample	Absorbancy Run 1	Run 2	Run 3	Run 4	$\bar{X}$	σ	Amount treated (grams)
N1- 1.2	.651	.735	.555	.713	.664	.081	5
N1- 6.25	.130	.096	.050	.159	.109	.047	2
N1- 9.2	.020	.042	.041	.017	.030	.013	2
N1-11.25	---	---	---	---	---	---	4
N1-14.2	.067	.079	.072	.098	.079	.014	5
N1-18.2	.095	.078	.088	.084	.089	.007	5
N1-20.25	.047	.050	.051	.063	.063	.007	5
N2- 1.8	.014	.012	.016	.026	.017	.006	2
N2- 4.5	.160	.047	.107	.089	.101	.047	1
N2- 7.4	.364	.255	.201	.250	.268	.069	2
N2-11.7	.013	.004	.008	.016	.010	.005	2
N2-13.6	.295	.251	.273	.336	.289	.036	2
N2-15.2	.011	.011	.012	.019	.013	.004	2
N2-17.4	.236	.251	.223	.208	.230	.016	2
N2-21.7	.137	.140	.104	.155	.134	.021	2
A8- 1.25	.248	.180	.121	.102	.163	.066	2
A8- 7.5	.056	.012	.013	.034	.029	.021	1
A8-14.5	.623	.453	.420	.415	.478	.098	2
A9- 3.9	.109	.070	.072	.064	.079	.020	2
A9- 4.4	.666	.592	.707	.514	.620	.085	2
A9-13.7	.059	.069	.079	.065	.073	.011	2
A19-1.25	.228	.224	.228	.193	.218	.017	2
A19-4.5	.347	.287	.296	.332	.316	.029	2
A19-9.25	.077	.047	.075	.100	.075	.022	2
A19-19.25	.032	.025	.042	.046	.036	.010	2

Table D3. Fe in NaOH Extract.

Sample	Absorbancy Run 1	Run 2	Run 3	Run 4	$\bar{X}$	σ	Amount treated (grams)
N1- 1.2	.060	.045	.043	.062	.053	.010	5
N1- 6.25	.039	.032	.020	.013	.026	.012	2
N1- 9.2	.016	.018	.009	.011	.014	.004	2
N1-11.25	---	---	---	---	---	---	4
N1-14.2	.055	.024	.032	.030	.035	.014	5
N1-18.2	.063	.035	.044	.036	.045	.013	5
N1-20.25	.022	.037	.048	.027	.034	.012	5
N2- 1.8	.065	.060	.058	.053	.059	.005	2
N2- 4.5	.009	.004	.018	.023	.014	.009	1
N2- 7.4	.079	.067	.064	.072	.071	.007	2
N2-11.7	.050	.056	.066	.071	.061	.010	2
N2-13.8	.056	.054	.044	.060	.054	.007	2
N2-15.2	.049	.022	.030	.040	.035	.012	2
N2-17.4	.038	.038	.047	.043	.042	.004	2
N2-21.7	.054	.036	.044	.034	.042	.009	2
A8- 1.25	.045	.020	.022	.032	.030	.011	2
A8- 7.3	.042	.037	.039	.039	.039	.002	1
A8-14.5	.028	.031	.037	.043	.035	.007	2
A9- 3.9	.032	.040	.049	.057	.045	.011	2
A9- 4.4	.044	.032	.024	.047	.037	.011	2
A9-13.7	.027	.019	.024	.032	.026	.005	2
A19-1.25	.030	.023	.029	.026	.027	.003	2
A19- 4.5	.031	.032	.026	.028	.029	.003	2
A19-9.25	.027	.014	.014	.020	.019	.006	2
A19-19.25	.023	.032	.029	.019	.023	.004	2

APPENDIX E

PHYSICAL DESCRIPTIONS OF SAMPLES

Table E1. Physical Descriptions

	Sample Number			
	N1-1.2	N1-6.25	N1-11.25	N1-11.25
Color	7.5YR(5/6)matrix	2.5YR(4/8)clay skins 10YR(6/6)matrix	10YR(7/6)matrix 2.5YR(4/6)clay skins	2.5YR(4/6) 10YR(7/6)-(7/4)
Texture	SiL	SCL	Si clay skins	SiL matrix Clay skins
Structure	Gr-SBK	SBK	SBK	---
Consistency	Fr	Fi	Fr	Fi
Roots	Few	---	---	---
Chert	Few	---	---	---
Nodules	Few	---	---	---
Coatings	---	Many	Prominent	Clay skins prominent
Comments	---	---	---	Mostly massive clay

Abbreciations include: Si = silt, SiL = silt loam, SCL = silty clay loam, SiC = silty clay, SiCL = silty clay loam, CL = clay loam, Fr = friable, Fi = firm, Gr = grandular, SBK = subangular blocky, ABK = angular blocky.

Table E1. (continued)

	Sample Number		
	N1-14.2	N1-18.2	N1-20.25
Color	10YR(7/6)	2.5YR(5/8) 10YR(7/4)	5YR(5/8) 2.5YR(4/6)clay skins 2.5YR(3/0)layer
Texture	SiL matrix Clay skins	SiC clay skins	SiC
Structure	---	---	SBK
Consistency	Fr	---	Fr
Roots	---	---	---
Chert	---	---	Abundant
Nodules	---	---	---
Coatings	Prominent skins in fractures	Crossed yellow material	---
Comments	Crisscrossing flow zones	Alternating silty and clayey layers	

Table E1. (continued)

	Sample Number N2-1.8	N2-4.5	N2-7.4
Color	2.5YR(3/4)	5YR(5/6)mottles 2.5YR(3/6)	10YR(6/4)clay skins 2.5YR(4/6)clay
Texture	SiL	CL	SiC
Structure	Gr	Gr-SBK	ABK
Consistency	Fr	Fr	Fi
Roots	Few	Few	---
Chert	---	Small chalky chert	Small 2cm oolitic chert
Nodules	Few black, 2cm	---	Few black
Coatings	A horizon	Smashed sample	Prominent peds good sample

Table E1. (continued)

	Sample Number		
	N2-9.4	N2-11.7	N2-13.8
Color	2.5YR(4/7)clay skins 5YR(5/6) 7.5YR(5/8)	2.5YR(5/8) 10YR(6/8) 10YR(8/2)	10YR(8/1) 10YR(8/8) 2.5YR(4/6)clay skins
Texture	Clay	SiC	SiCl
Structure	ABK	Massive	ABK
Consistency	Fi	Fi	Fi
Roots	---	---	---
Chert	Massive chalk 3 cm	Massive chalk 1 cm	Massive chalk 3 cm
Nodules	Common black	Large black	Few black
Coatings	Ped faces	Fracture flows	Chert and ped faces
Comments	Strong structure	Mixed-mottled material	Very cherty

Table E1. (continued)

	Sample Number N2-15.2	N2-17.4	N2-21.7
Color	10YR(8/1) 10YR(6/6) 2.5YR(4/6)clay skins	10YR(7/8) 10YR(8/1) 2.5YR(4/6)	2.5YR(4/6) 5YR(5/8) 10YR(7/6)
Texture	SiCL	CL	SiCL
Structure	ABK	ABK	ABK
Consistency	Fi	Fi	Fi
Roots	---	---	---
Chert	Massive 3 cm	Massive 5 cm	Oolitic
Nodules	Few black	Common red and black	Many black
Coatings	Chert and ped faces	Chert and ped faces	Few clay skins
Comments	Very fractured	Very cherty w/layers of Fe-Mn concretions	Localized concretions

Table E1. (continued)

	Sample Number A8-1.25	A8-7.3	A8-14.5
Color	10YR(7/4)	2.5YR(4/8)	2.5YR(4/6)clay skins 10YR(6/8) 10YR(7/4)
Texture	SiL	Clay	SiC
Structure	Gr	SBK	Platy-massive
Consistency	Fi	Fi	Fi
Root	Common	---	---
Chert	---	White chalky	Gray massive
Nodules	Few red/black	---	Few black
Comments	E horizon	Homogeneous mixture of red soil w/small (3cm) banded chalky chert/ sand size dust	Silty banded residuum w/gravel sized chert (massive) black streaks

Table E1. (continued)

	Sample Number			
	A9-3.9	A9-11.25	A9-13.4	A9-13.7
Color	7.5YR(4/4)	7.5YR(5/6) 10YR(8/2)	10YR(8/4) 7.5YR(6/6) 2.5YR(5/8)	10YR(8/4) 7.5YR(6/6)
Texture	SiL	SiC	SiC	SiC
Structure	Platy	ABK	Platy-ABK	ABK
Consistency	Fi	Fi	Fi	Fi
Root	---	---	---	---
Chert	5mm(chalky)	Banded gray/white	3mm, Stained	Several 2.5cm
Nodules	---	---	---	---
Coatings	Yellow stains	---	Common	Common
Comments	---	Intermixed red clay, yellow type material	Mixed, jumbled layers	Intermixed orange and white material

Table E1. (continued)

	Sample Number A11-1.25	A11-13.25	A11-24.75
Color	5YR(5/6)	10YR(4/6)clay skins 10YR(7/8) 10YR(8/1)	2.5YR(6/8)clay skins 10YR(7/6) 10YR(2/1)black layer
Texture	SiCL	SiCL	SiCL
Structure	SBK	SBK	SBK
Consistency	Fi	Fr	Fi
Roots	Common	---	---
Chert	Chalky type	---	Small, few
Nodules	Uniformly disseminated, black 1cm	---	---
Comments	Abundant sand sized and small gravel sized chert, homogeneously mixed	Silty material w/clay coated fractures very abundant	Prominent black layers
Coatings	---	Abundant	Abundant

Table E1. (continued)

	Sample Number A12-1.25	A12-4.1	A12-4.7	A12-5.2
Color	2.5YR(4/6)	5YR(3/4) 2.5YR(4/6)	2.5YR(4/6)matrix 2.5YR(3/6)skins	2.5YR(4/6)skins 5YR(5/6)matrix
Texture	SiL	Si	SiL	SiL
Structure	SBK	Gr-SBK	Gr-SBK	ABK
Consistency	Fi	Fr	Fr	Fi
Roots	Few	---	Few	Few
Chert	Small chalky type	Small chalky type	Chalky type	Very common, small chert
Nodules	Black, common	Black, common	Black, common	---
Comments	A horizon	Visible abrupt soil horizon boundry	Relatively homogeneous	Abundant angular chert 5 cm
Coatings	---	---	Weakly developed clay skins	Ped faces

Table E1. (continued)

	Sample Number A12-9.25	A12-14.7	A12-23.5
Color	5YR(5/8)	2.5YR(4/6)clay skins 10YR(8/2) 10YR(8/8)	10YR(7/6) 7.5YR(5/8)matrix
Texture	Clay	SiL	SiCL
Structure	ABK	SBK	Platy-SBK
Consistency	Fi	Fi	Fi
Root	---	---	---
Chert	Very common, small chert	Massive gray and oolitic	Massive gray and oolitic
Nodules	Small black	---	Few black
Coatings	Minor on ped faces	Abundant	---
Comments	Very cherty, oolitic type small sample	Abundant flow zones	Layered

Table E1. (continued)

	Sample Number A19-1.25	A19-4.5	A19-9.25	A19-19.25
Color	7.5YR(3/4)	7.5YR(4/6)	2.5YR(4/8)	5YR(6/8) 10YR(8/6)
Texture	Si	SiL	CL	SiL
Structure	Gr	Gr	ABK	ABK
Consistency	Fr	Fr	Fi	Fi
Roots	Many	Few	---	---
Chert	---	---	Chalky type	Small angular massive type
Nodules	---	---	---	---
Coatings	---	---	---	---
Comments	A horizon	Ap-Bt with fragic properties	Abundant chert	Intermixed

VITA

Hugh Curtis Monger was born in Lenoir City, Tennessee on September 24, 1957. He attended elementary schools in that city and was graduated from Lenoir City High School in June 1975. Upon graduation from The University of Tennessee in March, 1981 with a B.S. in Plant and Soil Science, he accepted a position as a county soil scientist, which involved mapping soils for the USDA-SCS in West Tennessee. In September, 1982 he entered the Master of Science program in Geology at The University of Tennessee. In August 1985, he began further graduate study at New Mexico State University. In June 1986, he received the M.S. degree in Geology.